CHEMICAL REVIEWS

Review

Boosting Rechargeable Batteries R&D by Multiscale Modeling: Myth or Reality?

Alejandro A. Franco,[*,†,‡,§,‖] Alexis Rucci,[†,‡] Daniel Brandell,[§,⊥] Christine Frayret,[†,‡,§] Miran Gaberscek,[§,@] Piotr Jankowski,[§,#,▽] and Patrik Johansson[§,#]

[†]Laboratoire de Réactivité et Chimie des Solides (LRCS), CNRS UMR 7314, Université de Picardie Jules Verne, Hub de l'Energie, 15 Rue Baudelocque, 80039 Amiens Cedex 1, France

[‡]Réseau sur le Stockage Electrochimique de l'Energie (RS2E), CNRS FR 3459, Hub de l'Energie, 15 Rue Baudelocque, 80039 Amiens Cedex 1, France

[§]ALISTORE-European Research Institute, CNRS FR 3104, Hub de l'Energie, 15 Rue Baudelocque, 80039 Amiens Cedex 1, France

[‖]Institut Universitaire de France, 103 boulevard Saint Michel, 75005 Paris, France
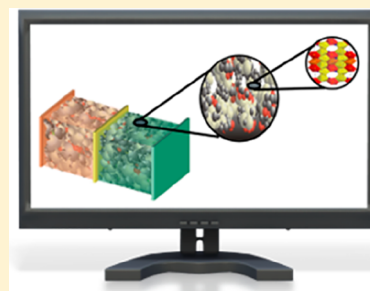
[⊥]Department of Chemistry − Ångström Laboratory, Box 538, SE-75121 Uppsala, Sweden

[@]Department for Materials Chemistry, National Institute of Chemistry, Hajdrihova 19, SI-1000 Ljubljana, Slovenia

[#]Department of Physics, Chalmers University of Technology, SE-412 96 Göteborg, Sweden

[▽]Faculty of Chemistry, Warsaw University of Technology, Noakowskiego 3, 00-664 Warsaw, Poland

ABSTRACT: This review addresses concepts, approaches, tools, and outcomes of multiscale modeling used to design and optimize the current and next generation rechargeable battery cells. Different kinds of multiscale models are discussed and demystified with a particular emphasis on methodological aspects. The outcome is compared both to results of other modeling strategies as well as to the vast pool of experimental data available. Finally, the main challenges remaining and future developments are discussed.

CONTENTS

1. INTRODUCTION

During the last decades, very significant efforts have been carried out to find alternatives to the depleting fossil fuels resources. For
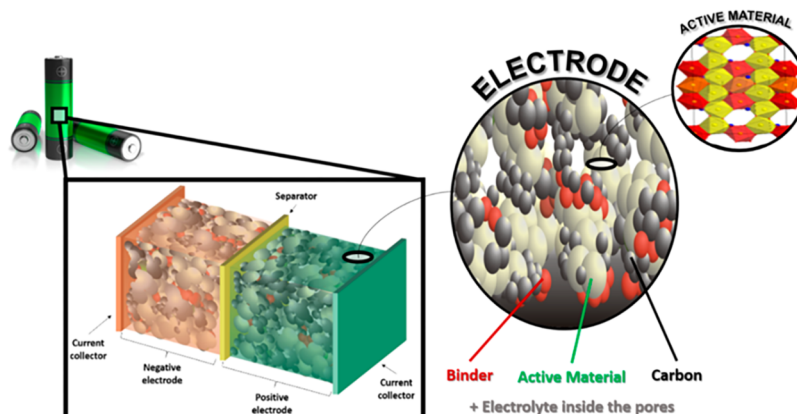
Figure 1. Schematic representation of a LIB cell.

the design of any new energy technology, the amount of energy that can be stored/converted, the accompanying cost at all levels of implementation, and the overall environmental impact all constitute major concerns. Within the spectrum of devices suggested in order to develop a more sustainable energy ecosystem, rechargeable batteries are likely to play a very significant role as energy storage devices. Battery technology has great potential to become competitive in terms of cost in particular with respect to nomadic applications; it is highly efficient (e.g., > 90% electric efficiency) and environmentally benign with zero-emission and low noise in the usage stage. The development of portable personal electronic devices and electric vehicles (EVs) has resulted in a rapidly growing demand for lithium-ion batteries (LIBs) with high energy density. Currently, >10 billion cells are made annually and at much lower prices per energy stored than previously believed possible, down by 24% even from 2016 levels.[1,2] For further market segment penetration, for example, for heavy vehicles and large energy storage for the electricity grid, advanced, possibly postlithium batteries must be designed in order to achieve even higher efficiencies, lower production costs, little or no maintenance, and great safety.

Since their invention, the development of rechargeable batteries has mainly been driven by trial-and-error experimental approaches. For example, Volta invented the first (non-rechargeable) battery to store electricity in 1800, before the electron was discovered by Thomson in 1896 (i.e., almost 100 years later).[3] Being a new technology with a high potential for further development, modern rechargeable batteries (hereafter, referred to as batteries) saw a relatively fast penetration in the market without the need for a deep theoretical understanding of their operation principles. In stark contrast, today, when significant cost reductions and performance improvements are required, the situation is rapidly changing and the development of physical theories to guide and to rationalize the design is urgently needed.

A theory is a supposition or a set of ideas intended to explain something, especially on the basis of general principles independent of what is to be explained.[4−6] Physical theories aim to explain experimental observations. In the battery field, they usually take the form of mathematical models constituted by a set of (generally coupled) mathematical equations. Mathematical models (hereafter called models) are the natural choice to achieve a greater fundamental understanding of existing designs and to predict properties and performance of new designs. The advantage is a comparatively limited cost as

compared to extensive experimental investigations, which is why modeling can catalyze innovation and technology breakthroughs and ultimately reduce the time-to-market of new designs. In the battery field, mathematical models can be useful for the discovery and use of new materials/combinations thereof.

In this review, we address modern battery cells (i.e., we disregard Pb-acid, NiMH, or NiCd technologies). The physical system here addressed (i.e., the battery cell) is centrally made of a negative and a positive electrode, separated by an electrolyte, the latter often contained in a membrane (separator). The negative and positive electrodes are where the electrochemical reactions take place. For example, in the case of a LIB, the electrodes are porous composites fabricated from particle-based laminates comprising mixtures of materials with various sizes and physicochemical properties. Usually, the active materials, ~1−10 μm particle size, and the electronically conductive additives (e.g., carbon particles), 50−100 nm size, are held together by an organic polymer binder (e.g., polyvinylidene fluoride, PVdF) and altogether deposited on a current collector (e.g., Cu) (Figure 1). The porous electrodes and the separator are both filled with the electrolyte, often an organic solvent based liquid, which is responsible for the cell internal ion transport between the electrodes, needed to match/balance the electrons transported in the outer circuit. Similar electrode textures can be found for metal, metal−sulfur, and metal−air batteries.

Over the last 40 years both the models describing properties of materials in general and the models describing battery operation principles have been considerably improved, to become faster, more accurate, and predictive of materials, mechanisms, and processes at various length and timescales. Examples of typical battery models include (i) electronic models for simulating atomistic structures and properties, providing fundamental insights into the processes governing local properties of electrolytes as well as energy densities and stabilities of active materials; (ii) atomistic models such as molecular dynamics (MD) for the simulation of structure and dynamics of electrolytes and active materials, to address ionic transport, defect formations, and evolution in the active materials, or models based on stochastic and kinetic Monte Carlo (kMC) methods for the simulation of electrochemical reactions at active material/electrolyte interfaces; (iii) meso-scopic models based on kMC, discrete element method (DEM), and coarse-grained MD (CGMD), for simulating particles self-organization during the fabrication of composite electrodes; and (iv) a range of continuum models, for example those based on

lattice Boltzmann techniques to investigate the wettability properties of porous electrodes, phase field methods for simulation of phase separation in active materials, and full cell models supported on coupled sets of partial differential equations (PDEs) addressing spatiotemporally varying quantities, such as concentration of species, temperature, and stress/strain.

Within the realm of battery modeling, some of these models have already been the subject of numerous comprehensive review papers.[7−19]

Due to the complexity of materials employed and the operation principles of a modern battery cell, it is often disadvantageous to stick to a single modeling method: to adequately model the battery materials and processes, a combination of at least two of these methods is frequently needed, which hence leads to the application of multiscale modeling (MSM) approaches.[6,9,20]

This review has three major objectives. (i) To review the latest progress within MSM, illustrated with examples for battery materials and processes, including also the level of components and cells. Some success stories of concrete added value to battery R&D are also provided. (ii) To demystify modeling of battery cells and make the benefits of MSM accessible and understandable for nonspecialists who often perceive modeling as a self-standing, more or less academic activity without clear connection to real experiments; this perception is, among others, reflected in the title of this review paper. MSM strategies are therefore described with a particular emphasis on connections to experiments (both input parameters needed and output obtained are of interest for experimentalists and engineers). (iii) To identify opportunities and challenges of MSM to advance several battery technologies, present and future.

We do acknowledge that some previous battery MSM reviews do exist, but they are far from extensive and do not cover the MSM methodology. In this review, our aim is for readers to get a different perspective to the whole area as we consistently introduce and evaluate a new categorization of MSM which by itself makes this review different and more systematic (in terms of the MSM approach and not merely in terms of subject (e.g., anode, cathode, as usually done).

1.1. Multiscale Complexity in Batteries

At the functional level, the structural, textural, and compositional complexity of the electrodes renders the rate-determining processes of a battery cell during charge and discharge to change. They will depend on the active ion (e.g., Li^+ or Na^+) concentration in the bulk of the electrolyte but also at the electrode active material surface and inside the active material, as well as depend on the potential drop between the active material and the bulk electrolyte. For example, in a LIB, the lithium ion (de)intercalation takes place at the nanoscale in the active material and the electrochemistry strongly depends on both its chemistry and structure. Charge, mass, and heat transport as well as mechanical stresses are important from the materials up to the cell level. The timescales vary from subnanoseconds (electrochemical reactions) to seconds (transport) up to hours (electrode compositional changes), and days or even months (structural and chemical degradation). All these phenomena and associated mechanisms are strongly and nonlinearly coupled (i.e., processes at the nano and microscale influence the overall battery behavior) (Figure 2).
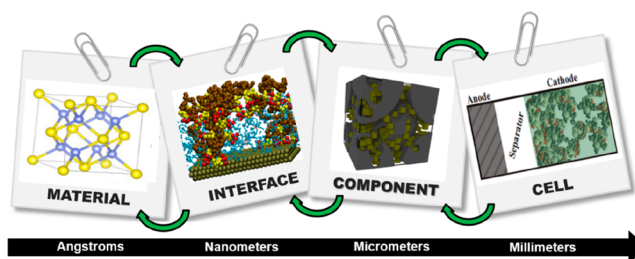

Figure 2. Multiscale character of a battery cell.

The development of a proper understanding of the relationship between these multiple-scale mechanisms constitutes the key to foster the innovation in terms of materials, components, and/or battery cell operation strategies. In view of this complexity, the system under investigation cannot be fully understood using reductionist approaches which assume that the system is made of the simple addition of its parts. For example, the cell performance is not necessarily an addition of phenomena taking place in its individual materials; locally correct descriptions using only one level may lead to erroneous or at least inaccurate predictions. A more complete understanding can only result by viewing the system as a whole, where effects are correlated, then through an holistic viewpoint. In modeling, such holistic approaches crystallize as "multi-scale models" (i.e., using both parametrization and/or mathematical descriptions to capture the interplay of mechanisms occurring at multiple spatiotemporal scales in a single material or component or combinations thereof). MSM aims to considerably reduce the empirical assumptions by explicitly describing mechanisms in scales neglected in simpler models.

1.2. Multiscale Modeling (MSM)

In the following, we will follow the standardized terminology established at the European level[21] and promoted by the European Materials Modeling Council (EMMC).[23] This standarization, being endorsed by several European academic institutions and companies, aims at improving exchanges among experts in the materials modeling field, to foster the understanding between the industry, the software developers, and the scientific communities. Such standards can also facilitate the interoperability between models and databases.

In accordance with these standards, MSM refer to multi-equation mathematical models (i.e., models describing a system by a set of interconnected models applied at different length scales). They have a hierarchical structure; the solution variables of a system of equations defined in a lower hierarchy domain (e.g., an active material particle of an electrode) have a finer spatial resolution than those at a higher hierarchy (e.g., the whole electrode). Consequently, small length-scale phenomena and quantities are evaluated at the corresponding small-scale geometry and the output subsequently homogenized using a coarser spatial resolution, to evaluate properties at larger scales. The overall resulting model architecture separates domains, the characteristic length-scale of each of these domains being "segregated" (the scales can be clearly "distinguished").

MSM is hence inherently different to stand-alone models (Figure 3a) where the input is provided by the user and the output is not used by any other model. There are different flavours of MSM, which are defined in the following three categories.[21] (1) Multiscale models based on sequential linking (MSMSL): these models imply a sequential solution of the governing equations of two or more models, where the
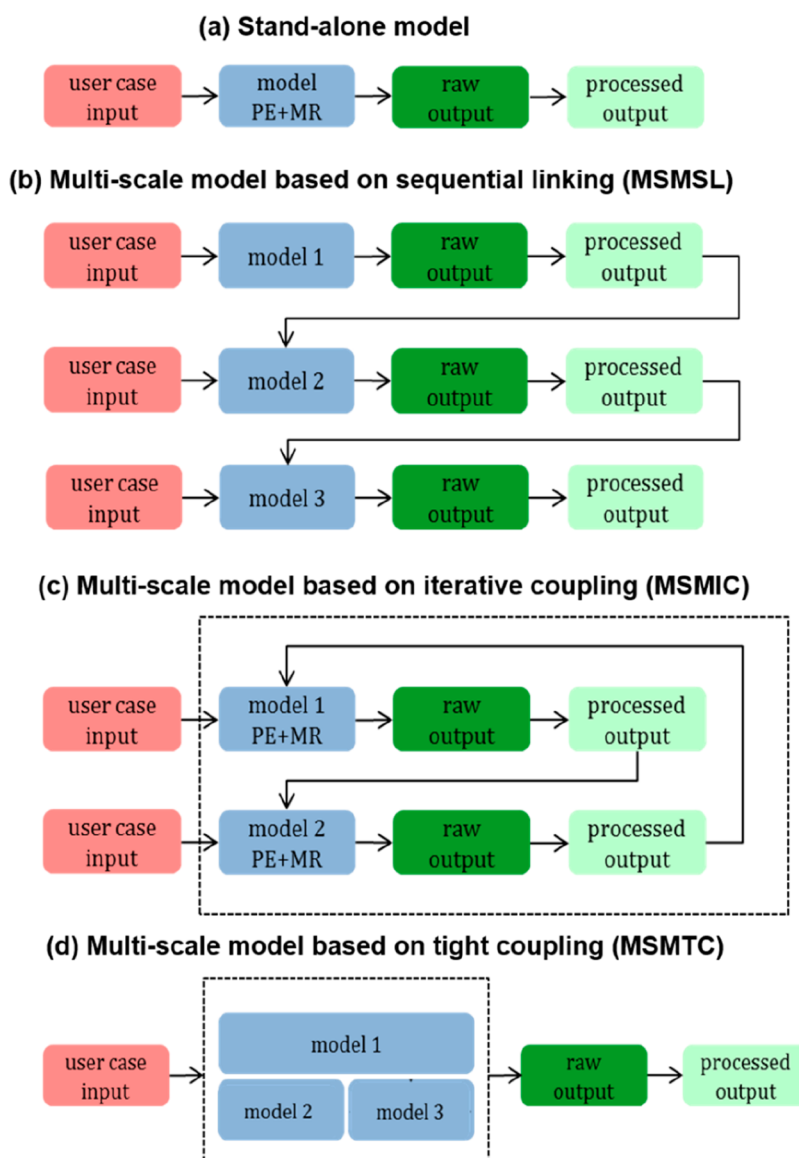
(a) Stand-alone model

user case input → model PE+MR → raw output → processed output

(b) Multi-scale model based on sequential linking (MSMSL)

user case input → model 1 → raw output → processed output

user case input → model 2 → raw output → processed output

user case input → model 3 → raw output → processed output

(c) Multi-scale model based on iterative coupling (MSMIC)

user case input → model 1 PE+MR → raw output → processed output

user case input → model 2 PE+MR → raw output → processed output

(d) Multi-scale model based on tight coupling (MSMTC)

user case input → model 1 / model 2 / model 3 → raw output → processed output

Figure 3. Workflows of (a) stand-alone models, (b) multiscale models based on sequential linking (MSMSL), (c) multiscale models based on iterative coupling (MSMIC), and (d) multiscale models based on tight coupling (MSMTC). "PE" refers to "physical equation" (mathematical equation based on a fundamental physics theory which defines the relations between physics quantities of an entity) and "MR" to material relation (materials specific equation providing a value for a parameter in the physics equation).[21]

processed output[22] of one model is used as an input for the following model (i.e., one-way dependency) (Figure 3b). A typical example is deriving and using a classical atomistic force-field (FF) for a MD simulation based on electronic structure calculations. (2) Multiscale models based on iterative coupling (MSMIC): these models rely on an iterative solution of the (segregated) governing equations of two or more models (each of them for a unique spatial scale). For two spatial scales the processed output of the first model is used as input for the second model and vice versa. Each of these models has its own processed output, and the iterative coupling leads to a closed loop data stream (Figure 3c). The numerical solution requires a number of iterations to eventually reach convergence. An example is using a kMC model resolving a chemical reaction kinetics at an interface from the chemical species concentrations resolved with a continuum model describing these species transport along a porous electrode (the reaction kinetics act as a sink/source term for the PDE describing the transport). (3)

Multiscale models based on tight coupling (MSMTC): these models consist of the concurrent solution of the governing equations of two or more physics-based models (each of them relevant at a single length scale) where the physics equation(s) and materials' relations of each model are collected and solved as a single system of equations (Figure 3d). The models' interdependency is expressed through physical quantities appearing in more than one equation. The tight coupling leads to one single raw or processed output for all models. A typical example is using a continuum model describing electrochemical reactions and transport mechanisms by temperature-dependent parameters at the porous electrode scale coupled with a continuum model describing thermal management in the cell scale.

Furthermore, the mathematical descriptions in a MSM can be performed within a single simulation paradigm (e.g., only on a continuum level) or carried out using different simulation

paradigms (e.g., a discrete model coupled with a continuum level model).[2,6]

1.3. Software for Multiscale Modeling and Identifiability

Governing equations in MSM are frequently nonlinear and coupled PDEs needed to be solved temporally and spatially in one and/or two and/or three dimensions.

MSM methods used to investigate battery materials include *ab initio* Molecular Dynamics (MSMIC approach), ReaxFF (MSMSL approach), and COSMO (MSMSL approach). Such methods are available in softwares such as Gaussian,[24] GAMESS,[25] SIESTA,[26] and COSMO-RS.[27] At the component and cell level, MSMIC and MSMTC methods have been developed within software such as Matlab,[28] Fluent,[29] COMSOL,[30,31] or even combinations of those software. Some of these utilize finite element solvers, making it possible to model complex geometries. Other commercial alternatives which exist can offer a single and integrated solution for LIB simulations, for example CD-adapco's STAR-CCM+[32] and its Battery Simulation Module and Battery Design Studio.[32] Similar tools have been achieved by other research institutes developing in-house software for three-dimensional (3D)-simulations of LIBs.[33] In order to carry out reliable simulations, the numerical solver needs to be properly chosen or designed in view of the problem one wants to solve. Besides the choice, often limited, of numerical solvers and spatial meshing capabilities of commercial software, numerous groups have developed their in house numerical solvers (e.g., PETSc,[34] LIMEX,[35] or FiPy[36]).

It is also possible to imagine the combination through computational workflows of simulation packages dealing with different scales and different simulation paradigms within a MSMSL approach. For instance, electronic structure calculations performed with first-principles softwares such as VASP,[37] CRYSTAL,[38] Wien2k,[39] ADF,[40] Gaussian,[24] BigDFT,[41−43] and NWChem[44] can be combined with the most frequently used MD software of today such as GROMACS,[45] LAMMPS,[46] AMBER,[47] CHARMM,[48] and DL_POLY.[49] In such a case, establishing workflows for automatic data flows between models is very important.[50] Several middleware platforms allowing this are available, including KNIME,[51] AIIDA,[52] ECCE,[53] and UNICORE,[54] and can be used with parallelized programs[55] Workflows within the MSMSL approach have been developed for LIBs[56] and interfaced with scripts devoted to automatic parameter sensitivity analysis and cell design optimization.

Identifiability (i.e., whether parameters can be uniquely retrieved from input-output data) is a crucial aspect of multiscale models.[57−60] This can result in structurally nonidentifiable model parameters and in limited data and/or bad data quality. Altered experimental design or model reduction, such as linearization,[61] are the main remedies. Until recently,[62−67] due to computational restrictions, there were no significant efforts made to develop efficient techniques for estimating parameters for multiscale battery models, but Boovaragavan et al. did report on a numerical approach for real-time parameter estimation using a reformulated LIB model.[68]

In the following, we discuss examples of MSM, with particular emphasis on battery applications, in this order, for active materials, interfaces, components (composite electrodes and separators), and cells. In the case of active materials, due to the large extent/complexity of existing possible approaches, examples are sorted by materials families. The following sections, respectively devoted to interfaces, components, and cells, are sorted by methodology type, including examples of applications.

2. ACTIVE MATERIALS

The knowledge of the materials properties or especially their atomistic structure gained through modelling can be the starting point for the engineering of optimized active materials. Quantum chemical models based on electronic theories that do not rely on any parameters are often referred to as first-principles (or *ab initio*) techniques. They play a significant role by suggesting guidelines to improve well-known active materials or even in helping the discovery of some brand-new ones, with specific functionality. Such *ab initio* methods were used very successfully in recent years for the description of, for example, bulk materials, metal organic frameworks, and molecular entities... Density Functional Theory (DFT)[69,70] is based on the Hohenberg−Kohn theorem which states that ground-state energy is uniquely defined by the electron density. In this formalism, the real system made of many interacting electrons is replaced by a set of noninteracting particles generating the same density that the real system of interacting particles would generate. The formulation is then simplified: instead of explicitly including the real potential of many interacting electrons, the Kohn−Sham equation contains a local effective (fictitious) external potential of these noninteracting particles. Compared to higher level *ab initio* methods based on the complex many-electron wave function, DFT computational costs are thus relatively low. In practice, the properties of a many-electron system are determined by using functionals, which are functions of the spatially dependent electron density. They also need to model the electron exchange, the correlation energy terms, and the difference between the kinetic energy of the fictitious noninteracting system and the real one. The use of an iterative self-consistent approach based on the variational principe allows for solving the corresponding equations. DFT calculations constitute nowadays a standard tool for the accurate description of the individual atomic and molecular processes in many areas.

Predicting physical observables with reasonable accuracy and relatively low computational cost for a large set of systems by calling to DFT even using local or semilocal approximations for the unknown exchange correlation energy [e.g., the local density approximation (LDA)[70] or the generalized gradient approximation (GGA)][71,72] let it become popular. In the specific field of battery devices, it is nowadays very well-established that many key properties can be reachable by making use of this computational tool including the structural and energetic characteristics related to point defects, the estimation of equilibrium voltages,[73,74] the activation energy for atomic jumps, etc. DFT+U methods can be used for open-shell transition metal compounds, U referring to an on-site Coulomb interaction parameter derived either self-consistently or by fitting to experimental data. Use of a suited U term might be critical for getting reliable results, and one known limitation is that U values able to reproduce certain material properties may fail to account for other features. Similarly, different polymorphs may need to be modeled with different U-values. Zhou et al.[75] demonstrated that DFT+U greatly improves predicted lithiation potentials using self-consistently calculated U-values. Apart from the widespread use of DFT+U, it can be outlined that the theory based on the Koopmans' condition represents a significant step toward the correction of electron self-interaction in electronic structure theories (which can be applied to any local, semilocal, or hybrid density-functional approximation).[76] Standard

implementations of DFT is devised to describe correctly strongly bound molecules as well as solids but is not suited to account for long-range van der Waals attractions (vdW), which are related to mutually induced and correlated dipole moments[77] and can be relevant for both electrodes made of layered inorganic compounds and organic crystalline matrices characterized by π-stacking. Contrary to the Hartree–Fock model, which does not consider electron correlation effects, DFT calculations should, in principle, give the exact description of ground state energy, including the vdW energy, if the true functional is known. However, practical implementations relying on either LDA or GGA fail to reproduce the physics of vdW interactions at large separations with little or no overlap of atomic electron densities.[78] As a result, DFT calculations usually overestimate the lattice parameters along the stacking direction for organic crystals or layered materials.[79,80] Recently, a number of semiempirical approaches have been taken to incorporate correction schemes for London-type dispersive interactions into DFT.[81−88] A great interest of first-principles calculations lies in the possibility to get access to electronic structure features, which are sometimes crucial to unravel mechanisms, the computation thus serving as a tool to probe what happens at the scale of atoms and chemical bonding. Beyond the examination of dispersion curves and density of states,[89] other concepts relying for instance on the topology of the electron density as implemented by Bader through the quantum theory of atoms in molecules and crystals[90,91] or also the electron localization function[92] can be investigated to shed light on the phenomena related to chemical bonds, including, for instance, atomic charges/volumes and critical points, which provide rigorous and quantitative information especially on bonds.[93]

For applications in materials science, in general, and notably for LIBs, the DFT calculations along with the above-mentioned post-treatments present an invaluable interest, as they can deepen the understanding of mechanisms at the atomic/bonding scale and thus act as a kind of microscope able to unravel the various structure−property relationships. In the specific field of battery devices, it is nowadays very well-established that many key properties can be reachable by making use of this computational tool including, for example, the structural and energetic characteristics related to point defects, the estimation of equilibrium voltages, the activation energy for atomic jumps, etc. There is indeed a plethora of investigations having used first-principles calculations to describe the crystal structures, the redox potentials, the ion mobility, the possible phase transformation mechanisms, and the structural stability changes of electrochemical systems. All of these properties are key features to the development of advanced high-energy, high-power, low-cost electrochemical systems. However, despite the large scope of applications and the important extent of information that are reachable from "first-principles" quantum mechanics calculations by themselves, some shortcomings might occur as soon as one tries to simulate large macroscopic systems at an atomic level. Many problems at the leading edge of materials science involve collective phenomena. Such processes may occur over a range of time and length scales which are either intrinsically difficult to capture solely from quantum chemistry simulation or even intractable from the current computing resources. Indeed, being computationally very demanding, the simulations using *ab initio* methods are limited to a small number (i.e., a few hundred) of atoms and short simulation times in the range of a few picoseconds. In order to close this "reality gap" and make most efficient use of current computing

capabilities for real materials problems, we must therefore continue to make further methodological developments, in particular the connection of different time and length scales through the coupling of various modeling methodologies. In the context of batteries modeling, one shall also take into account the dependence on the local temperature of many processes, including, for example, the intercalation rate or degradation effects, the thermal behavior of the systems having a very significant impact on the initiation of aging processes and thus on their lifetime. Additionally, treating the electrode as a homogeneous component might be unsuited to get insight into actual features or properties related to the electrode real microstructure. A successful cutting-edge computational strategy has therefore to guarantee that newly developed simulation tools are able to take into account all these parameters and specific conditions. Beyond thermodynamic quantities, which give the opportunity for instance to get an estimation of intercalation voltage, a myriad of kinetic phenomena occurs in both electrodes and electrolytes (Figure 4).
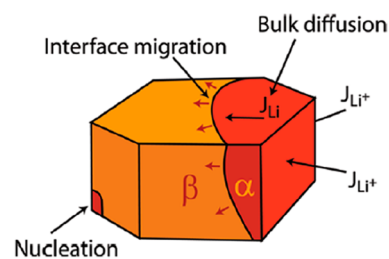

Figure 4. A variety of kinetic phenomena, including Li diffusion and first-order phase transformations involving nucleation and interface migration, occur within individual electrode particles during each charge and discharge cycle of a Li-ion battery. Reproduced from ref 94. Copyright 2013 American Chemical Society.

One of the properties for which MSM may be of relevance corresponds in particular to the migration of lithium from one site to another, which can be seen as an activated process with an associated free energy barrier. The unit steps of ionic conduction occur in the nanometer length scale and picosecond timescale. Being cheaper computational methods because of their dependence to empirical or fitted potentials, classical MD and kMC simulations can be used to probe the diffusion pathway and gain information on mobile carriers (e.g., vacancies or interstitials) on a larger length scale in order to be consistent with experimental observation. The kMC method is a variant of the Monte Carlo (MC) method and enables one to carry out dynamical simulations of stochastic and/or thermally activated processes because time is also updated during the simulation.[95−98] When combined with a spatial coarse-graining procedure, this additionally leads to a method of bridging length scales. More precisely, one of the possible ways of getting properties for battery materials is to perform the following series of calculations[99] (Figure 5): (i) first-principles electronic structure calculations in order to extract the activation energy barriers, (ii) local cluster expansion calculations, which will give access, in any configuration corresponding to partially disordered states, to the activation barrier for migration,[99,100] and (iii) kMC simulation that enables the numerical calculation of the diffusion coefficients by explicit stochastic simulations of the migration of a collection of ions within a host.

In atomic-scale processes, nudged elastic band (NEB) method,[101] which corresponds to an efficient algorithm for the
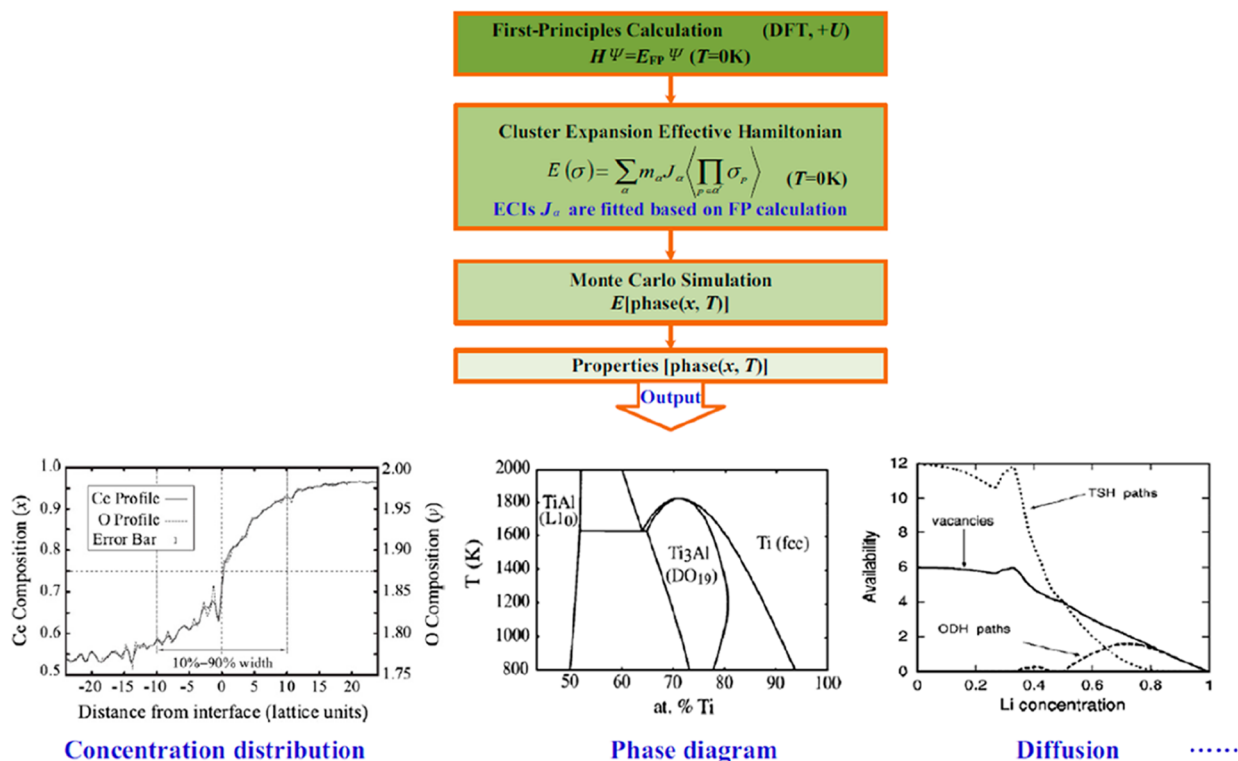
Figure 5. Computation approach integrated by first-principles calculation, cluster expansion, and MC simulation. Reproduced from ref 102. Copyright from IOP Publishing.
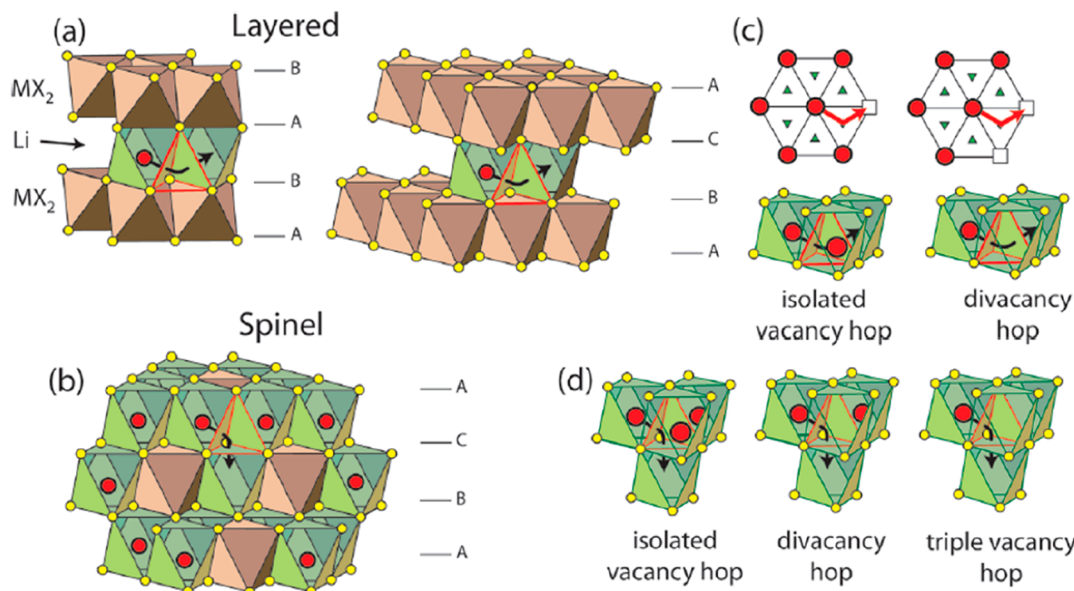

Figure 6. Important crystal structures and Li hop mechanisms in common intercalation compounds. Many intercalation compound chemistries have either (a) a layered crystal structure (with an ABAB or ABC stacking of a close-packed anion sublattice) or (b) a spinel crystal structure characterized by a three-dimensional interstitial network for Li ions. (c and d) Diffusion in these crystal structures is often mediated by vacancy clusters (divacancies in the layered form and triple and divacancies in the spinel form) if Li occupies octahedral sites. Reproduced from ref 94. Copyright 2013 American Chemical Society.

computation of transition-state energies, can be used to determine the maximum energy along the lowest energy pathways between two neighboring atomic sites. The introduction of phase-field modeling can lead to an accurate prediction of the phase transitions both in individual electrode particles and multiparticle systems representing entire electrodes.

Another way to gain insight into lithium ion diffusion through simulations is by calling to the *ab initio* molecular dynamics (AIMD) technique in view of investigating the inherent microscopic diffusion mechanisms. In this method, the atomic forces originating from quantum mechanics treatments are injected in order to propagate the atoms in the system by following the laws of classical mechanics (i.e., the motions of the
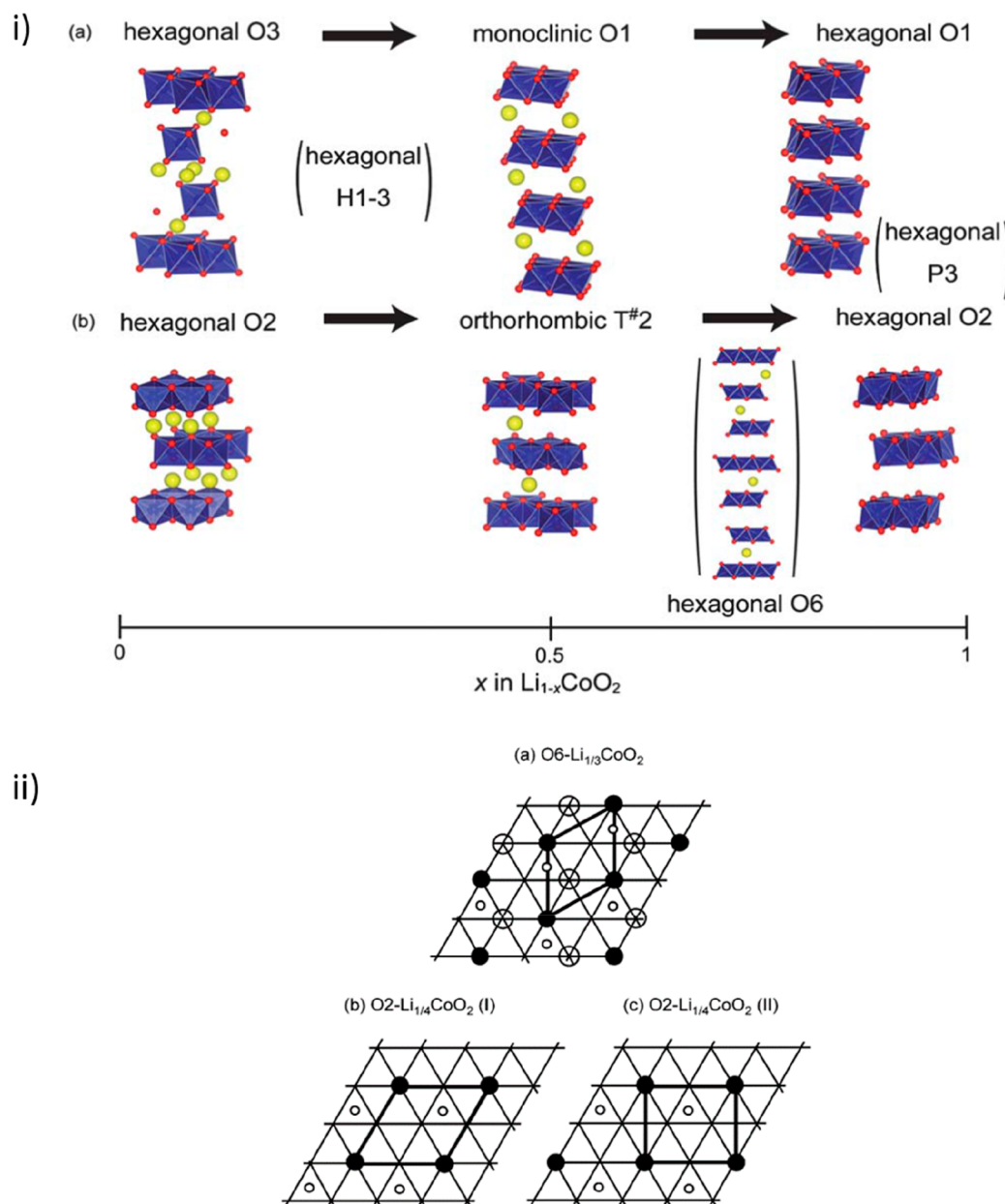
Figure 7. (i) Schematic diagram of phase transition during deintercalation from (a) O3-LiCoO$_2$ and (b) O2-LiCoO$_2$. Blue octahedrons represent CoO$_6$, red balls indicate oxide ions, and yellow balls represent lithium ions. (ii) Ordered (a) O6-Li$_{1/3}$CoO$_2$ and (b, c) O2-Li$_{1/4}$CoO$_2$ phases found to be stable at room temperature by first-principles calculations. The lattice denotes the lithium sites within a Li plane, and the filled circles correspond to Li ions. For the (b, c) O2 host, the unfilled small circle denotes the projection of the Li sites of an adjacent Li plane. For the (a) O6 host, the lithium positions of the two adjacent layers are different: the projection of one is represented by the small unfilled circle, and the projection of the other is represented by the large unfilled circle. Reproduced from ref 105. Copyright 2003 American Chemical Society. Reproduced with permission from ref 106. Copyright 2012 Royal Society of Chemistry.

atoms are computed by applying Newton's second law to the atomic coordinates). Due to the significantly higher computational cost of AIMD simulations compared to classical MD investigations, these calculations are often limited to a small system size of a few hundred atoms and are suitable for short-time-scale phenomena ($\approx 10-100$ ps). Gathering reliable statistics, which require hundreds to thousands of trajectories is thus more time-consuming compared to classical MD, but examples of applications of AIMD to materials modeling abound. In conditions of elevated temperatures, in which the extent of required trajectories are lower, the diffusivity can be

easily estimated, whereas an extrapolation may then be used to get an insight of the values characterizing lower temperatures.

Combining first-principles, phase field and finite element calculations were also applied to active materials as will be exemplified and can cover processes occurring on various dimensions, from atomic- to mesoscale. Such methodology provides information about thermodynamic and kinetic properties, together with strain development during phase separation.

2.1. Layered AMO$_2$ Materials

Layered compounds (e.g., LiTiS$_2$, LiCoO$_2$, LiNiO$_2$, etc.) with an anion close-packed lattice where layers have a structure of

alternating sheets are one of the most famous class of positive electrode materials (Figure 6).

In this structure, the transition metal lies in a position into anion sheets while lithium inserts itself into a free layer between anion sheets. In particular, the layered materials with formula $LiMO_2$ (where M is a transition metal or a mixture of transition metals) correspond to the archetypal positive electrode for LIBs. Within this kind of compounds, the most prominent example is $LiCoO_2$ due to its commercial success in 1992. $NaMO_2$ (M = Ti, V, Cr, Mn, Fe, Co, and Ni) materials also characterized by a layered rock-salt structure show high voltage and capacity and are considered to constitute promising positive material for sodium ion secondary batteries (SIBs). While $LiMO_2$ is synthesized only in the thermodynamically stable O3 phase, the $NaMO_2$ materials can be synthesized in two different polymorphs (i.e., P2 and O3, where P (prismatic) and O (octahedral) denote the shape of the LiO_6 or NaO_6 polyhedra and 2 and 3 stand for the number of alkali layers in the repeat unit perpendicular to the layers). Additionally, the O2-type $LiCoO_2$, which was prepared for the first time by Delmas et al.[103] through a Na^+/Li^+ exchange experiment starting from the P2−$Na_{0.70}CoO_2$ phase, is metastable. Van der Ven, Ceder, et al.[104] were pioneers in investigating the layered Li_xCoO_2 system, through various studies involving a MSM by calling to activation barriers originating from first-principles calculations. The phase diagram of Li_xCoO_2 was calculated for x ranging from 0 to 1 by considering the set of host structures that are likely to be stable as a function of Li concentration and temperature. For this compound (Figure 7), different host structures can be considered for which the oxygen octahedra surrounding the Li sites, LiO_6, share either edges with the oxygen ions surrounding the Co ions, CoO_6 (i.e., the O3 host) or faces (i.e., the O1 host). In the H1−3 host, oxygen octahedra around the Li sites of every other plane between O−Co−O slabs share edges with the octahedra surrounding Co ions as in O3, while in the remaining planes these octahedra share faces as in O1. By using pseudopotential first-principles results as input, cluster expansions of the formation energy of the O3 and H1−3 hosts were generated prior to be implemented in MC simulations in the grand canonical ensemble to investigate the finite temperature thermodynamics of Li and vacancy ordering. Within the Li concentrations interval of 0.05−0.10 centered at x = 0.15, modeling indicated that the H1−3 host is more stable than both O1 and O3. Due to an agreement between the experimental and the calculated XRD, the experimentally observed phase transformation below x = 0.21 was ascribed to the H1−3 host. The calculations also highlighted a trend for Li ordering at x = 0.5 in agreement with experiment. Carlier et al.[105] then focused on the phase stability of the O2-$LiCoO_2$ system in view of elucidating the series of unusual structures experimentally observed during Li deintercalation (i.e., the layered phases, T#2 (where T stands for tetrahedral) and O6). After first-principles calculations, separate cluster expansions were set up for each of the O2, O6, and T#2 hosts then followed by MC simulations. The experimentally observed two-phase O2/T#2 region was accounted for from theoretical prediction only when both tetrahedral sites in T#2 were considered. These results allowed one to clarify the underlying mechanism for this structural phase transformation, which is largely governed by enhanced configurational entropy in the T#2 phase and not by a metal−insulator transition as previously proposed. Calculations performed on O6−$Li_{1/2}CoO_2$ and O6−$Li_{1/3}CoO_2$ by considering several lithium sites and lithium/vacancy orderings

demonstrated that the structures with Li in octahedral sites are more stable by 110 meV compared to the structures with Li in the tetrahedral sites that do not share faces with CoO_6. The calculations also proved that the genesis of the O6 phase is neither linked to Li staging nor driven by Co^{3+}/Co^{4+} ordering in the two different cobalt layers as initially believed. Two ordered compounds, namely $Li_{1/4}CoO_2$ in the O2 structure and $Li_{1/3}CoO_2$ in the O6 structure, were found to be stable at room temperature (Figure 7), and the modeling further indicated that the O_2 structure should remain stable for CoO_2 (with respect to T#2 and O6).

Similar to the work devoted to Li_xCoO_2, a study involving the phase diagram of Li_xNiO_2 (0 < x < 1) was performed using a combination of first-principles calculations, cluster expansion, and MC simulations to account for energy dependence of the Li-vacancy configurational disorder.[107] At room temperature, ordered Li_xNiO_2 phases appeared in the phase diagram at x = 1/4, 1/3, 2/5, 1/2, and 3/4, and the most stable calculated lithium-vacancy arrangements for $Li_{1/4}NiO_2$ and $Li_{1/3}NiO_2$ were consistent with experimental models based on electron-diffraction data. The computational study tends to indicate that Li_xNiO_2 behaves differently from Li_xCoO_2 despite having identical structures and that Co and Ni have similar ionic sizes. Unlike in Li_xCoO_2, the stability of ordered Li_xNiO_2 structures is not solely determined by short-ranged repulsive in-plane Li−Li interactions (which are in both compounds screened by the local oxygen environment). In its Ni-based counterpart, long-range attractive interplane Li−Li interactions due to the Jahn−Teller activity of Ni^{3+} ions constitute the main driving force for the phase ranking in stabilization. Ordering in $Li_x(Ni_{0.5}Mn_{0.5})O_2$ and its relation to charge capacity and electrochemical features was also studied by Van der Ven and Ceder.[108] The proposed energetically competitive ordered structure for the Li, Ni, and Mn ions within $Li_x(Ni_{0.5}Mn_{0.5})O_2$ was found to be compatible with experimental data. Although this material is a layered compound in which lithium resides in octahedral sites, tetrahedral sites tend to emerge as a result of the electrochemical activity of the lithium in the transition metal layers and have a significant incidence on the electrochemical behavior of the material. The phase transformations of this material were then studied by Hinuma et al.[109] who concluded that the cation ordering in $Li(Ni_{0.5}Mn_{0.5})O_2$ is a complex function of the temperature and the heating/cooling history. Their combined first-principles modeling, cluster expansion, and MC calculations coupled with selected experiments led to propose a phase diagram of $Li(Ni_{0.5}Mn_{0.5})O_2$, which was indicative of the phase transition upon heating: a zigzag model, which has very little Li/Ni disorder in the Li layer, first transforms to a partially disordered flower structure with about 8−11% Li/Ni disorder (~550 °C), which upon further heating (~620 °C) transforms to a disordered $\sqrt{3}*\sqrt{3}$ honeycomb structure. The uncommon ordering of this material with temperature was ascribed to the competition between Ni_{TM}-O-Ni_{Li} hybridization and electrostatics. Van der Ven et al.[110] also investigated Li diffusion in Li_xTiS_2, the first lithium insertion compound experimentally investigated, as a function of Li concentration, x, using the well-established simulation approach combining first-principles, cluster expansion, and kMC calculations. Predictions indicated that diffusion is driven by Li ions hopping between neighboring octahedral interstitial sites of the TiS_2 host by passing through an adjacent tetrahedral site. A significant decrease in the migration barriers for these hops was observed when the end points belong to a divacancy. Hinuma et al.[111] studied the temperature−

concentration phase diagrams for Na$_x$CoO$_2$ (for x between 0.5 and 1) by combining either GGA or GGA+U DFT, cluster expansion, and MC simulations. The type of interactions was found to be dependent upon the first-principles treatment: whereas the prevalent interactions correspond to long-range in-plane electrostatics and relaxation effects in GGA, in GGA+U Co—Co interactions were found to dominate. The comparison of calculated and experimental data including c-lattice parameter and the Na1 site/Na2 site ratio revealed that GGA is a better approximation for 0.5 < x < 0.8. Later, Mo et al.[112] made use of AIMD simulations and NEB calculations in view of identifying the Na diffusion mechanisms in Na$_x$CoO$_2$ sodium layered oxide material at nondilute Na concentrations. While it was still unclear from previous investigations what the dominant Na migration mechanism was in the P2 polymorph, some elucidation was provided by this study. Although both P2 and O3 showed good Na conductivities over a wide range of Na concentrations, the presented results highlighted the fact that P2 outperforms O3 for Na migration except at high Na concentrations. They may account for the generally higher achieved capacities in P2 NaMO$_2$ compounds (see, for example, ref 113). The authors were able to indicate that Na diffusion in P2 was not mediated by divacancies, whereas it was the dominant carrier for Na diffusion in O3. Instead, Na ions migrate with a low energy barrier (of approximately 0.1 eV) in a honeycomb sublattice in P2. Such hexagonal network topology for the Na$^+$ diffusion implies alternating transition-metal face-sharing and nonface-sharing prismatic sites. While the drawback of O3 is the drop in diffusion at $x \sim 0.5$, it has been evidenced that P2 is a fast ionic conductor in the same condition and is expected to remain so for x < 0.5. The fast Na conduction at $x \sim 0.5$ may partly explain why P2 can be cycled to the lower half of Na concentrations (x < 0.5) in some experimental studies. The high calculated migration energy barriers account for the sluggish Na diffusion at high Na concentrations in P2, which was ascribed to the strong electrostatic interactions among Na ions.

It was stressed that taking into account the effect of finite temperature for the estimation of thermodynamic quantities may be crucial to exactly describe the performance of the electrode materials in LIBs. It has been recognized that the accurate prediction of cell voltages should be related to the ability to get temperature-dependent Gibbs energy functions of electrode materials. Therefore, an effort to go beyond DFT-like calculation strategies at 0 K has been pursued. A possible methodology relying on the vibrational and related thermodynamic quantities of these electrode materials gained from density functional perturbation theory (DFPT) proved for instance to be helpful to better understand the performance of LIBs at finite temperature.[114] On the other hand (by calling to another MSM than the already presented one using first-principles results as well as cluster expansions and kMC simulations), an approach based on combined *ab initio* calculations and use of CALPHAD (CALculation of PHAse diagrams) was recently proposed by Chang et al.[115] in order to develop a thermodynamic database for multicomponent Li-containing oxide systems (Figure 8). The purpose of such new MSM strategy is to explore the phase diagrams and thus to describe the continuous properties of complete composition coverage for the well-known electrode materials. The flowchart involved in this work first encompasses the estimation of enthalpies of formation (per metal) for the binary oxide, MO$_n$, by using *ab initio* calculations in DFT treatment (without +U correction) and the method suggested by Kubaschewski et al.[116]
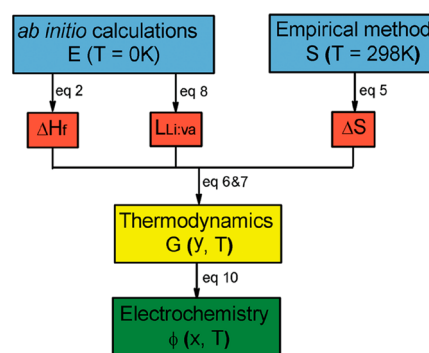

Figure 8. Flowchart of the theoretical approaches used in ref 115. Reproduced from ref 115. Copyright 2012 American Chemical Society.

to get entropy formation data of the oxide, MO$_n$, thanks to the anionic and cationic contributions [i.e., S(MO$_n$) = S(M) + nS(O)]. The Gibbs energy functions of the binary and ternary oxides in the Li—Co—O and Li—Ni—O systems can then be obtained thanks to these accurate data of formation enthalpies by using the empirical entropy. They are subsequently introduced in the calculation of theoretical cell voltage. By observing a good agreement of this methodology with experimental data, Chang et al. claimed that an advantage of this new procedure is to prevent an inappropriate use of U value, as it may arise for the estimation of the phase diagram as well as the thermodynamic and electrochemical properties of any Li—M—O system.

2.2. Spinel AM$_2$O$_4$ Oxide-Based Compounds

Spinel oxides constitute another promising class of LIB positive electrode active material (Figure 6). In particular, LiMn$_2$O$_4$ can be considered as an ideal high-capacity active material because of its low toxicity, the high natural availability of Mn, and its low cost. First, although not directly related to a coupling of theoretical treatments, one can outline that the idea of injecting barriers derived from experimental measurements in the case of Li diffusion modeling in Li$_y$Mn$_2$O$_4$[117] led to Fickian diffusion coefficients (D) versus fractional occupancies (θ) from 0 to 1 (with the fraction of pinned Li ions varying from 0% to 40%) and predicted theoretical open circuit potential, that were both consistent with experiments. Ouyang et al.[118] studied the structural and dynamic properties of spinel LiMn$_2$O$_4$ by calling to DFT-based AIMD simulations. The structural properties and the phase reconstruction of Li$_{0.5}$Mn$_2$O$_4$ were simulated through full AIMD, while the calculation of the Li migration energy barriers was performed by selective MD technique. They proved that in Li$_{0.5}$Mn$_2$O$_4$, lithium tends to be located in one *fcc* sublattice, and that diffusion coefficient for lithium in Li$_{0.5}$Mn$_2$O$_4$ is much lower than that of LiMn$_2$O$_4$, consistent with the experiment. While the migration energy barrier was found to be symmetric along the diffusion pathway for LiMn$_2$O$_4$, the symmetry was broken when the lithium content was extracted to reach the value of 0.5. This latter observation has been ascribed to the associated breaking of the structural symmetry, which could be one of the reasons for the less stability of the compound as cathode material for LIBs. Following a computational study[119] already devoted to the same material, Jiang et al.[120] focused their work on the spinel Li$_{1+x}$Ti$_2$O$_4$ by combining DFT calculations with statistical mechanics methods including cluster expansion/Metropolis MC and kMC. This complete investigation encompassed the prediction of lattice parameters, elastic coefficients, thermodynamic potentials,

migration barriers, as well as Li diffusion coefficients. This set of data was then introduced in continuum scale studies in a framework corresponding to a coupled phase field and finite strain mechanics formulation. The chemo-mechanical evolution of electrode particles was simulated by considering various case studies able to account for either homogeneous or heterogeneous nucleation. The ability of getting insight into the spatial distribution of lithium ion composition as well as on stress profiles and peak stress value evolution through this framework during the lithiation−delithiation processes therefore provided access to a complete vision of the kinetics and mechanics features of this system. The estimation of the stress localization and the potential for crack initiation during lithiation and delithiation can be gained through the temporal evolution of maximum principal stress values. The time evolution of lithium ion composition in the presence of zero, two, and five nucleation sites suggested that in view of avoiding the phase localization within electrode particles the lithiation−delithiation rates has to be carefully controlled (Figure 9).
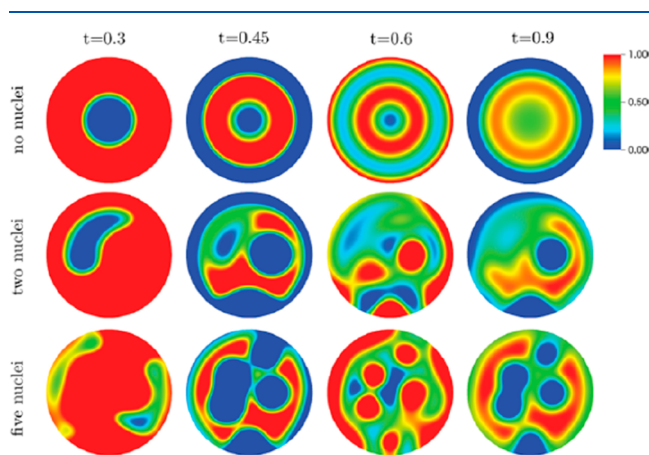

Figure 9. Time snapshots of lithium ion composition during the lithiation−delithiation cycles for the cubic spinel $Li_{1+x}Ti_2O_4$ electrode particles. Shown are the composition fields at time $t = 0.3$ ms, $t = 0.45$ ms, $t = 0.6$ ms, and $t = 0.9$ ms for the problems with no nuclei, two nuclei, and five nuclei. The blue regions with composition close to $x = 0$ are in the α-phase, and the red regions with composition close to $x = 1$ are in the β-phase. Intermediate values of the composition correspond to the two-phase regions. Reproduced with permission from ref 120. Copyright 2016 American Chemical Society.

It was demonstrated that the peak stress profile can be connected to the presence and the density of nucleation sites, whereas its time evolution is related to the rates of the imposed lithiation−delithiation cycles. This MSMSL is based on continuum scale studies parametrized using data extracted from first-principles, MMC as well as kMC calculations. It provides a new way of predicting the incidence of nucleation sites on the mechanical degradation of electrode particles, which is of high interest in view of understanding fracture and voiding.

Additionally, Zhang et al.[121] exploited the potential of combining *ab initio* calculations and a CALPHAD approach (as already mentioned in section 2.1[115]) to systematically probe infinite composition−structure−property−performance relationships under sintered and battery states of spinel cathodes. By calling to this high-throughput computational framework and with the aim to find the overall best performance for 4 V cathode materials, they conducted a systematic search for the best compromise for three key factors: energy density, cyclability,

and safety, within the $LiMn_2O_4$-$Li_4Mn_5O_{12}$-$Li_2Mn_4O_9$ triangle and were able to identify favorable compositions for each of these three properties.

2.3. Polyanion Oxide-Based Frameworks

In the 1990s, Goodenough's group initiated the replacement of simple O^{2-} ions by XO_4^{y-} polyanions in the positive electrode hosts in order to define systems with higher cell voltage (see, for example, ref 122). The principle is based on the fact that the strength of the X−O bond can influence the M−O covalence and thereby the relative position of the $M^{n+}/M^{(n-1)+}$ redox energy. The stronger the X−O bonding, the weaker the M−O bonding and consequently the lower the $M^{n+}/M^{(n-1)+}$ redox energy relative to that in a simple oxide. Polyanion-based frameworks (with general formula XY_4^{y-}: X = P, S, Si, As, Mo, and W) have been widely studied in the past decade as alternative positive active materials for LIBs (see, for example, ref 123). In particular, a specific interest was devoted to PO_4^{3-} and SO_4^{2-} containing materials. These compounds are nowadays renowned thanks to their ability to tune the transition-metal redox potential. From the viewpoint of coupled computational methodologies, Yang and Tse[124] examined the mechanisms inherent to thermal (self) diffusion of Li ions in $LiFePO_4$ (LFP) through spin polarized *ab initio* (GGA+U) MD calculations. In agreement with neutron diffraction experiments, a dominant process was found to correspond to the hopping between neighboring Li sites around the PO_4 groups, leading to a zigzag pathway along the crystallographic b axis (Figure 10a).
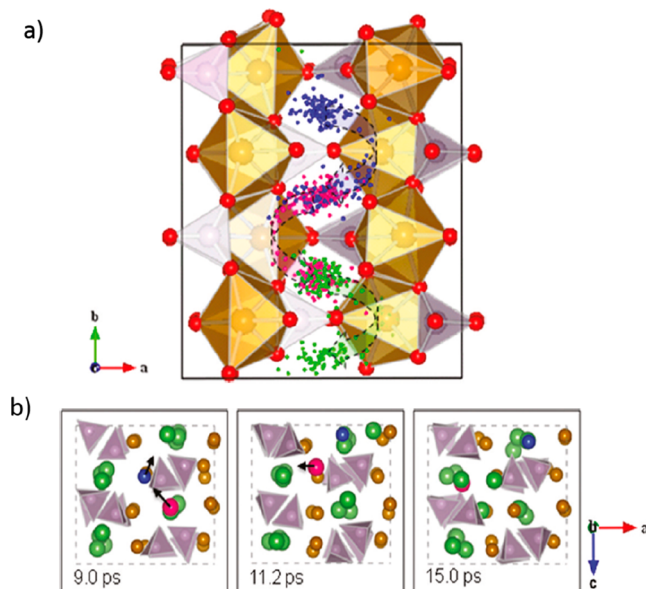

Figure 10. (a) Trajectories of the three Li atoms originally situated in the crystalline $LiFePO_4$ structure along the b axis obtained from the MD simulation at 2000 K. The three specific Li atoms are highlighted with different colors, and all other Li atoms are omitted for clarity. A zigzag diffusion pathway can be clearly identified (shown with the curved arrows) along the b direction and confined in the (ab) plane. (b) Snapshots from the MD simulation of the fully lithiated $LiFePO_4$ at 2000 K showing the second diffusion mechanism involving the formation of Li_Fe antisite. Large (light green) and small (brown) spheres represent Li and Fe atoms, respectively. A pair of Li (pink) and Fe (blue) atoms are highlighted to illustrate this mechanism. Dashed lines indicate the size of the used supercell. Reproduced with permission from ref 124. Copyright 2011 American Chemical Society.
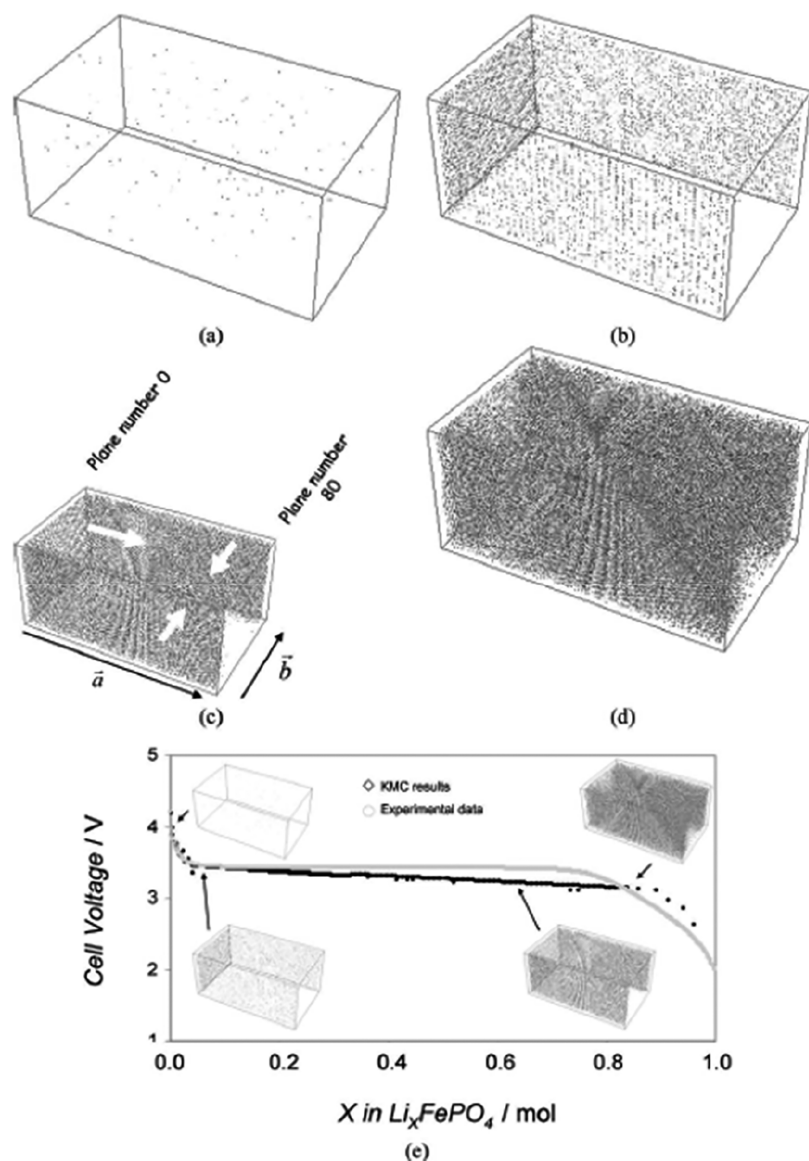
Figure 11. MC simulation of the galvanostatic discharge process performed at room temperature for the Li_xFePO_4 olivine nanocrystals. The gray points represent the lithium atoms in the active particle. The superficial current density is 0.5 Å m^{-2}. The far-field flux of Li ions is perpendicular to the b direction of the cell. Microstructure at (a) 0 s (initial random solid solution), (b) 0.0001 s (two Li-enriched phases have formed and joined together), (c) 0.00056 s (growth of the Li-enriched phase), and (d) 10.81 s (the Li-poor phase is almost consumed). (e) Cell voltage as a function of Li concentration (mol) in the active material. Reproduced with permission from ref 127. Copyright 2011 John Wiley and Sons.

A second process was evidenced, which involves the collaborative movements of the Fe ions resulting in the formation of Li_Fe antisite defects thus promoting Li diffusion across the Li ion channels (Figure 10b). The atomic transport within these [010] channels was found to be consistent with the experimental findings on the propensity to form antisite defects. Evidencing the simultaneous occurrence of such two distinct Li transport processes in this matrix led to the conclusion that Li diffusion cannot be described as a simple linear process but may instead be characterized by a "two-dimensional" diffusion pattern. Another investigation dealing with this kind of material was performed by Ouyang et al.,[125] who applied the adiabatic trajectory method for their AIMD simulations on LFP and Na doped LFP (i.e., $Na_xLi_{1-x}FePO_4$). Their collected energy barriers of Li ions tend to indicate that the Na-doped compound exhibits a higher ionic transport dynamic compared to the undoped one. Recently, Xiao et al.[126] performed kMC simulations based on DFT energetics to study the kinetics of phase evolution and Li intercalation in LFP during the intercalation/deintercalation processes. Atomistic pictures of the phase changes were obtained under realistic charge/discharge conditions. A cluster expansion was employed to rigorously extract the effective Li—Li interactions from hundreds of DFT calculations. These interactions were evidenced as being attractive across the [010] channels and repulsive in the same channel. In agreement with X-ray diffraction experiments showing peaks associated with an intermediate Li phase, the kMC results revealed that an ordered $Li_{0.5}FePO_4$ phase with alternating Li-rich and Li-poor planes along the ac direction forms between the $LiFePO_4$ and $FePO_4$ phases. A nucleation mechanism accounting for the high-rate $LiFePO_4$ was identified. Pre-existing vacant or weakly bound sites, such as lateral surface and defects were identified as serving as nucleation centers that promote the phase transition under both charge and discharge.
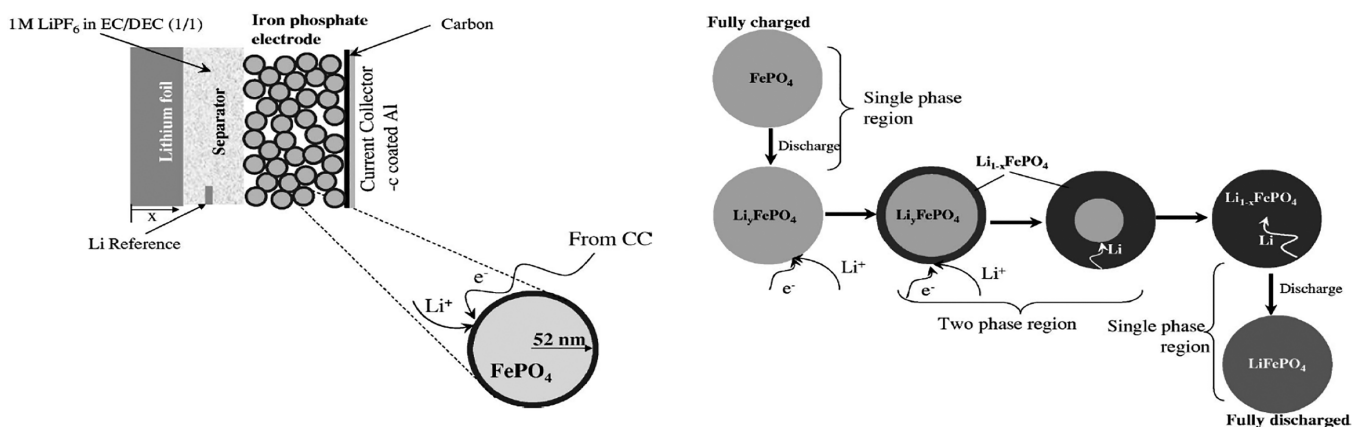
Figure 12. (Left) Schematic of the cell as modeled by Newman et al. Cell consists of a Li-metal negative and a LiFePO$_4$ positive with a separator between them. The cell is filled with electrolyte. The LiFePO$_4$ porous electrode is attached to a carbon-coated aluminum current collector. The electrode is assumed to consist of spherical particles at the surface of which an electrochemical reaction occurs. (Right) Illustration of the shrinking-core model with the juxtaposition of the two phases and the movement of the phase boundary. Both the single-phase and the two-phase regions are shown. Reproduced with permission from ref 130. Copyright 2004 The Electrochemical Society.
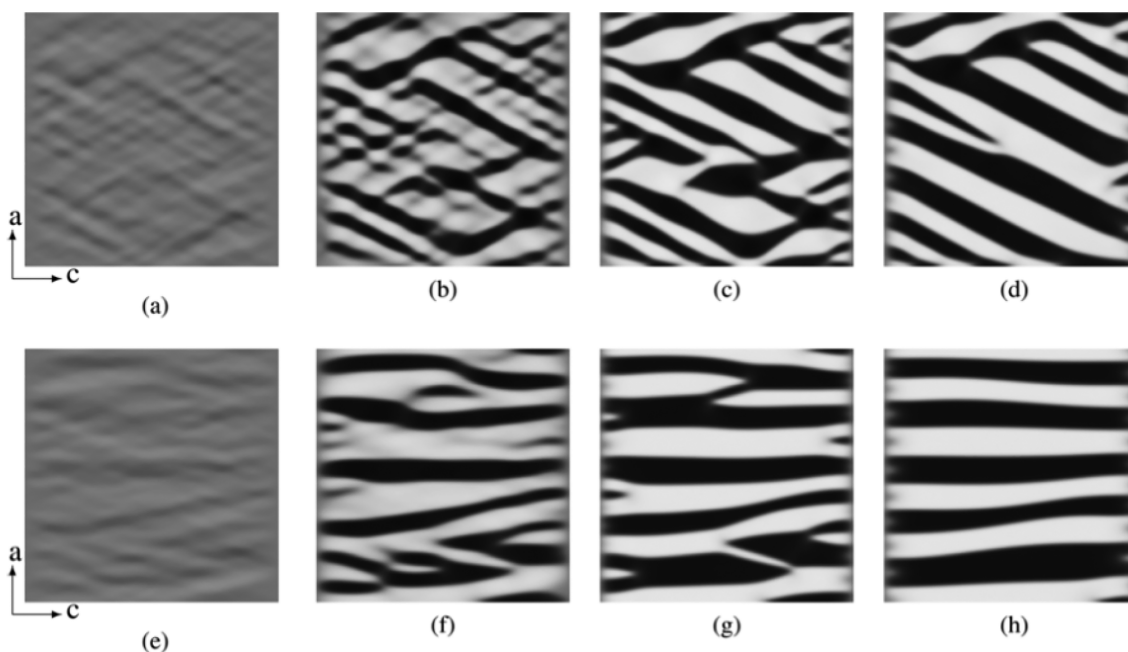

Figure 13. (a−h) Simulations of reaction-limited phase separation of a 500 nm single crystal of Li$_{0.5}$FePO$_4$ into Li-rich (black) and Li-poor (white) phases in an electrolyte bath at zero current and zero pressure, consistent with *ex situ* experiments. (a) Coherent phase separation, where lithium insertion causes contraction along the (c) [001] axis and expansion along the (a) [100] axis, leading to tilted interfaces aligned with {101} planes. (b) Loss of [001] coherency (e.g., due to microcracks) causes the phase boundaries to rotate to align with the [100] planes. Reproduced from ref 131. Copyright 2012 American Chemical Society.

Additionally, Hin[127] developed another methodology based on the use of kMC, by calling to a residence-time algorithm, which has been used in conjunction with a finite-element simulation of Li-ion diffusion into the surrounding electrolyte. Within this approach, kMC algorithm based on a cathode particle rigid lattice was used to simulate the kinetic anisotropy of lithium ion adsorption and lithium absorption for Li$_x$FePO$_4$ olivine nanocrystals. The adsorption kinetics of the electrolyte/electrode interface were treated by coupling the normal flux outside the particle from a continuum numerical simulation of Li-ion diffusion in the electrolyte to the atomistic kMC model within the particle. The atomic potentials for the kMC simulation were derived from empirical solubility limits [originating from open circuit voltage (OCV) measurements],

and the local concentration fields were coupled to particle adsorption via Butler−Volmer (B−V) interface kinetics. Such investigations tend to prove that the galvanostatic lithium-uptake/cell voltage is characterized by (i) a decreasing cell potential for Li-insertion into a Li-poor phase; (ii) after the nucleation of a Li-rich phase Li$_{(1-\beta)}$FePO$_4$, a nearly constant potential; (iii) and after the Li-poor phase has been evolved into a Li-rich phase, a decreasing cell potential (Figure 11).

The behavior in the second regime was found to be sensitive to crystallographic orientation.

With respect to this kind of approach, it is important to stress that the so-called shrinking core methodology and the phase field description of phenomena inside the active matter have to be compared. It seems that the shrinking core model (developed

by Newman, see earliest works[128,129]) already allows for a quite satisfactory description of charge–discharge behavior of various storage chemistries. For example, in the case of LFP, the shrinking core model assumes that the storage proceeds via a two-phase mechanism with the end phases being $LiFePO_4$ and $FePO_4$. During the charge, an initial spherical $LiFePO_4$ particle starts to transform into $FePO_4$ at its surface so that a shell of the latter is created around the core of the former. As the charge proceeds, the shell gets thicker and the core is shrinking until consumed entirely. On discharge, the reverse process occurs (Figure 12).

However, later on it was found that some essential ingredients found in real LFP material were missing. In particular, the spherical nature of the phase transformation is a rather large oversimplification. Thus, although the shrinking model does capture the basic charge–discharge shape, it fails to fit the real measurements at various conditions of interest. On the basis of new experimental discoveries, the shrinking core model was gradually upgraded by taking into account anisotropy of transport paths, particle size distribution, composition-dependent diffusion coefficient, and similar approaches. As even these improvements were unable to describe all the observed features, a completely different approach to phase transformation was introduced: the phase field description. The underlying physical phenomenon is the spinodal decomposition mechanism, well-known from metallurgical investigation of cooled alloys. Phase separation is here directly associated with a double-well energy diagram and the energy minimization principle, with parameters which can be estimated by DFT calculations for solid/solid interfaces (e.g., interphase energies), thus within a MSM framework. This is probably the most important difference with respect to the shrinking core model, which disregards the thermodynamics; in contrast, phase field models predict that phase-boundaries will only form when energetically favorable (Figure 13). Phase field models also allow consistent implementation of anisotropic elastic strain, which improves prediction of special experimentally observed phenomena such as phase-boundary alignment.[131]

Recently, Bazant showed that a consistent development of the phase field approach may lead to a new general theory of transport-reaction mechanism that extends significantly beyond the conventional porous electrode model proposed by Newman. In particular, for charged species, this theory provides a general and unified framework by combining concepts from the Poisson–Nernst–Planck equations describing ion transport, the Butler–Volmer equation describing the electrochemical kinetics, and the Marcus theory describing charge transfer for concentrated electrolytes and ionic solids (Figure 14).[132] In other words, the theory modifies significantly all three ingredients constituting the conventional average volume models (the electrode level, the intracrystal level, and the junction between these two levels). The theory allows simulating intercalation mechanisms in phase-separating LIB active materials and captures complex phenomena such as wavy intercalation in anisotropic nanoparticles at low currents. Rather unexpectedly, the author found that below a critical particle size and above a critical current value, the phase transformation is suppressed and homogeneous insertion/deinsertion is favored. This seems consistent with experimentally observed very high rates for LFP.[133]

Among others, this generalized model successfully explained the dynamics of the Li composition and insertion rate in Li_xFePO_4 as measured using advanced operando X-ray
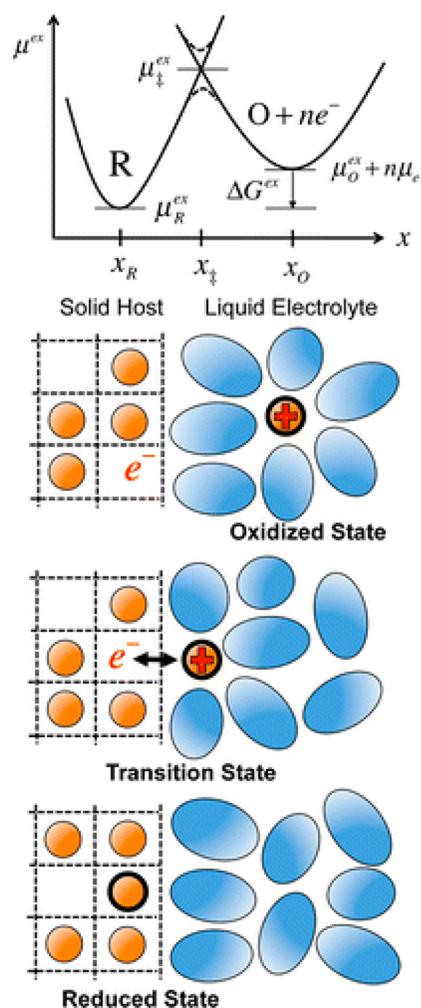

Figure 14. (top) Faradaic reaction $O + ne^- \rightarrow R$ in concentrated solutions. Each state explores a landscape of excess chemical potential μ^{ex}. Charge transfer occurs where the curves overlap, or just below, by quantum tunneling (dashed curves). (bottom) Example of ion intercalation into a solid electrode from a liquid electrolyte. Reproduced from ref 132. Copyright 2013 American Chemical Society.

microscopy.[134] In particular, the authors found that spatial variations in rate and in composition controlled the lithiation pathways. The previously established skewed relationship between exchange current density and composition is found to amplify the reaction heterogeneities upon delithiation but suppresses them upon lithiation.[131,132] These findings underline the key role of the surface reaction rate in lithiation, paving the way toward potential new electrode designs and battery operation strategies.

Other MSM approaches supported on the phase-field methodology have recently been extended to other types of materials. For example, in order to explain the unique properties of Ti-doped $LiNi_{0.5}Mn_{1.5}O_4$ (LNMO), Lim et al. combined the phase-field modeling with first-principles calculations and finite element method.[135]

From first-principles calculations, Ouyang et al.[136] estimated the migration energy barrier along the 1D diffusion pathway for Li ions and Cr ions in $LiFePO_4$ to be about 0.6 and 2.1 eV, respectively. Such results thus outlined the ability for lithium to move easily along the diffusion pathway, whereas heavy Cr ions are characterized instead by difficulty in diffusing away from their initial positions, these latter having thus a tendency to

block the one-dimensional diffusion pathway of the material. MC simulations then indicated that the capacity loss due to the Cr ion doping is very sensitive to the amount of the dopant and to the particle size. This computational investigation also mentioned that both larger amount of dopant and larger particle size are disadvantageous factors to the reversible capacity. Another class of polyanion-based materials that has been extensively studied corresponds to the tavorite family (see, for example, refs 137 and 138) for which DFT+U calculations complemented by QTAIMAC approaches[138] were able in particular to account for the various charge transfers occurring upon delithiation as a function of the transition metal element. Due to its quantitative character, such kind of analysis can be considered as more beneficiary than, for instance, scrutinizing electron density difference maps upon charge or discharge and furthermore gives the opportunity to evaluate the various Coulombic interactions involved in each of the two phases (either lithiated or delithiated one). The AIMD simulations undertaken by Ramzan et al.[139] to study the diffusion of lithium in sulfate tavorite LiFeSO$_4$F predicted that although not isotropic it is of the three-dimensional type.

2.4. Negative Electrodes

At present, graphite-based materials are widely used as anode materials in commercial LIBs due to their low voltage with respect to lithium, long cycle life, low cost, and abundance, despite their low gravimetric and volumetric specific capacity. The Li intercalation process in graphite involves multiple stages. In such studies, the stage number n accounts for n empty layers between each Li-filled graphite layer. Persson et al.[140] used DFT, cluster expansion, and MC methods to investigate Li-graphite structures with regard to their thermodynamic and kinetic properties. The computational results highlighted the necessity to treat the system by including van der Waals (vdW) interactions, which are not captured with standard DFT methods. The staging of phases observed in the Li-graphite system was found to directly arise from the competition between Li−Li repulsive interactions and C−C attractive vdW interactions. While homogeneous Li concentration in all planes is beneficial from the viewpoint of the Li−Li interactions, by minimizing the Li−Li distances, it is preferable for the vdW interactions to keep some planes free of Li. The study focused on Li$_x$C$_6$ having a stage I and stage II structure predicted a Li$_x$C$_6$ phase diagram that was in good agreement with the experiment for high Li concentrations ($x > 0.5$) (Figure 15).

An investigation on Li diffusion in graphite was also performed by Persson et al.[141] by using NEB to study the in-plane Li vacancy hopping at different Li concentrations and lithiation stages, as well as cluster expansion and KMC methods over a wide range of Li concentrations from $x = 0.2$ to 1.0 (stages I and II). The high incidence of the different stages along with the c axis spacing of the graphite layers on the Li diffusion was evidenced. In the direction parallel to the graphene plane, a high lithium-ion diffusivity was observed (ca. $10^{-7}-10^{-6}$ cm^2 s^{-1}), which contrasted with the sluggish lithium-ion transport along grain boundaries (ca. 10^{-11} cm^2 s^{-1}). Additionally, a focus on the best methodology to treat this system was achieved by Ganesh et al.[142] They used highly accurate quantum MC computations to study the adsorption and lithium diffusion in AA-stacked graphite and proved that the lithium−carbon system requires a simultaneous highly accurate description of both charge transfer and vdW interactions. Recently, Raju et al.[143] developed an MSM approach (involving ReaxFF to describe Li interactions),
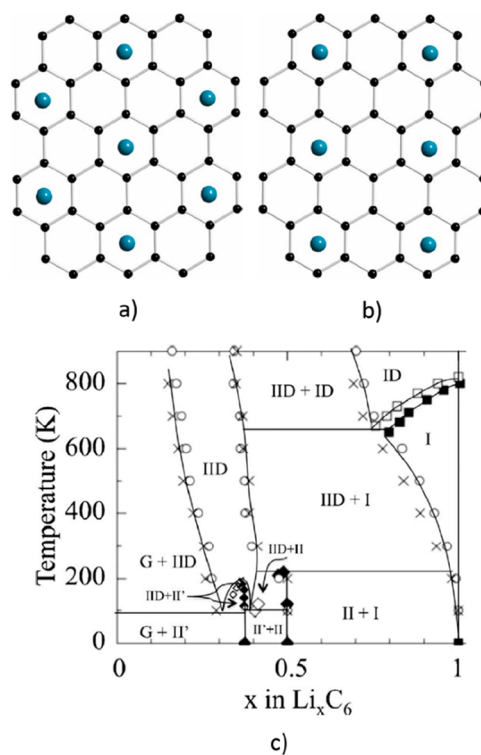

Figure 15. Li-graphite system. (a) In-plane Li ordering in fully lithiated stage I and stage II (left) and (b) 2 × 2 Li ordering [found in stage II′ (right) seen from above on the carbon honeycomb lattice]. (c) First-principles phase diagram obtained from MC simulations based on stage I and stage II separate cluster expansions. The phase regions are denoted in the following way: G graphite, II (stage II), IID (disordered stage II), I (stage I), ID (disordered stage I), and II′ (stage II with 2 × 2 Li ordering). Different symbols refer to cooling and heating runs, respectively. Reproduced with permission from ref 140. Copyright 2010 American Physical Society.

which was applied to the study of Li/C interactions in carbon-based materials with and without defects. ReaxFF employed a bond order/bond energy relationship, characterizing bond formation and bond dissociation during MD simulations. They first searched for force field parameters able to account for Li−C systems using DFT modeling that included a vdW correction. With the use of this force field, grand canonical MC simulations of Li intercalation in perfect graphite were undertaken, allowing one to capture the in-plane Li ordering and the interlayer separations for stage I and II systems. In the presence of vacancy defects, they noticed a raise in the Li/C ratio along with an upward shift in the voltage profile both proportional to the number of these point defects. Both phenomena were related to larger adsorption energy of Li in the defects. The interior of onionlike carbon (OLC) was found to be inaccessible for energy applications which may lead to lower Li storage capacities, although the outer surface of OLC offers on the other hand sites for fast Li adsorption/desorption, thus proving their suitability for applications as electrode materials (Figure 16, panels a and b). While zero-dimensional (0D) defective OLC favors fast charging/discharging rates through surface Li adsorption, this study proved that a one-dimensional (1D) defect-free carbon nanorod requires a critical density of Li for intercalation to occur at the edges.

The lithiation behavior of the a-SiO$_{1/3}$ suboxide was examined using AIMD calculations by Chou et al.[144] By focusing on the structural evolution, bonding mechanism, bulk modulus
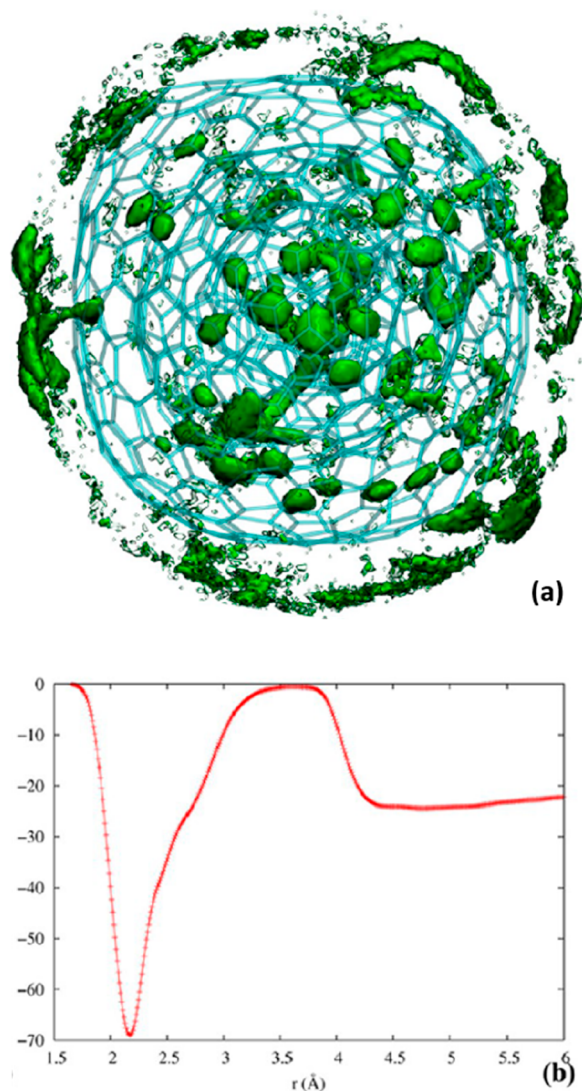
Figure 16. (a) Density plot of Li (green) atoms in the simulation box during an NVT simulation at 1000 K obtained as an average over a time period of 250 ps in an OLC. The green color represents all grids (regions) that registered a Li count during the simulation. (b) Free energy landscape for Li diffusing out from the OLC through a 12-membered ring. Reproduced from ref 143. Copyright 2015 American Chemical Society.

variation, and lithiation energetics, they evidenced that on top of the lithiation voltage lying between 0.2 and 0.8 V (within the desirable range for LIB anode applications), Li incorporation in this matrix is predicted to be highly favorable, with a capacity comparable to that of fully lithiated Si (Li:Si ratio ≈ 4). The crucial need to control the Si:O ratio as well as O spatial distribution in view of tailoring the desired lithiation properties was also outlined.

2.5. Organic Electrodes

Organic batteries can represent a new generation of energy-storage technology and thus offer more alternatives in the design of metal-free stationary and redox flow rechargeable batteries (see, for example, refs 145−149). Therefore, increasing attention is geared toward organic-based electroactive materials, offering excellent opportunities for constructing greener devices due to their unique features, including sustainability, low cost, ease of scalability, and structural diversity of organic molecules

allowing for highly tailorable redox properties. Despite critical issues, such as poor electronic conductivity, easy dissolution into liquid electrolytes, (this latter aspect being sometimes circumvented by the introduction of ionic functional groups such as COO^-), and low volumetric energy density that need to be generally addressed in order to promote their widespread usage and their commercialization, another important advantage of organic electrodes certainly lies in the higher number of possible fabrication routes, due to softer mechanical properties of these compounds compared with those of inorganic materials, therefore allowing flexible or stretchable battery electrodes.

For the time being, computational materials scientists have mainly focused their attention on first-principles modeling of this new kind of electrodes at the molecular state, which have been very helpful for predicting molecular redox potentials, migration pathways, etc. and which have furthermore provided insights on structure−property relationships.

Increasing the degree of understanding regarding structure-redox activity may indeed pave the way toward advertised selection prior to experimental characterization. An attempt in this area was performed for the identification of electrophilicity (ω) as a simple model to account for the reduction potential ranking of a few quinone compounds.[150] To really reach this goal, however, one of the main difficulties lies in the fact that various contributions of the diverse constituents of a molecule cannot be disentangled when dealing solely with global molecular indicators. Premises for going beyond this encompass the scrutinization of spin density values (see e.g. examples for singly reduced quinones.[151−153]) Further tools can be used to rationalize redox potential trends such as nuclear independent chemical shift,[154] harmonic oscillator model of aromaticity,[155] electron delocalization, δ,[156] and aromatic fluctuation FLU[157] indices, etc. by giving the opportunity to appreciate electron delocalization on various rings/bond paths. The partitioning of the global energy of the molecule (e.g. using the code described in supplementery information of ref 158) may also constitute a strategy to shed light on the relative role played by the various pieces of molecule. Specifically, it allows for identifying the ones having the main incidence on the stabilization/destabilization upon reduction. For illustration, a deep insight was recently reached into the mechanisms underlying the division of quinoneazine [i.e., quinonoid-like structures separated by an azo (N═N) group] and corresponding derivatives into low-/high-voltage systems (Figure 17) according to the indirect incidence of the bridge chemical bonding nature.[159] Similar approaches were exploited in order to account for the incidence on redox potential of isomerism/N substitution in pentalene-dione derivatives[160] and for deciphering the ranking of naphtho-, biphenyl-, and biphenylenequinone isomers.[161] Research area on redox-active compounds bearing azo groups seems indeed to be promising thanks to recent investigations having demonstrated that quinoneazine can accommodate 1.2 electrons at its carbonyl ends when grafted to Cu(110),[162] whereas azobenzene-4,4-dicarboxylic acid lithium salt (ADALS) can correspond to a highly reversible electrode material for alkali-ion batteries,[163] with charge/discharge plateaus at 1.50 and 1.55 V vs Li^+/Li, respectively. Additional insight on the structure−property relationship may also be gained through the consideration of plots of electrostatic potential on the molecular surface.[164−166] Besides investigations performed at the molecular stage, the study of crystalline materials whenever they are known from the experiment in either the lithiated or the delithiated phase has also been attempted.[167−170]
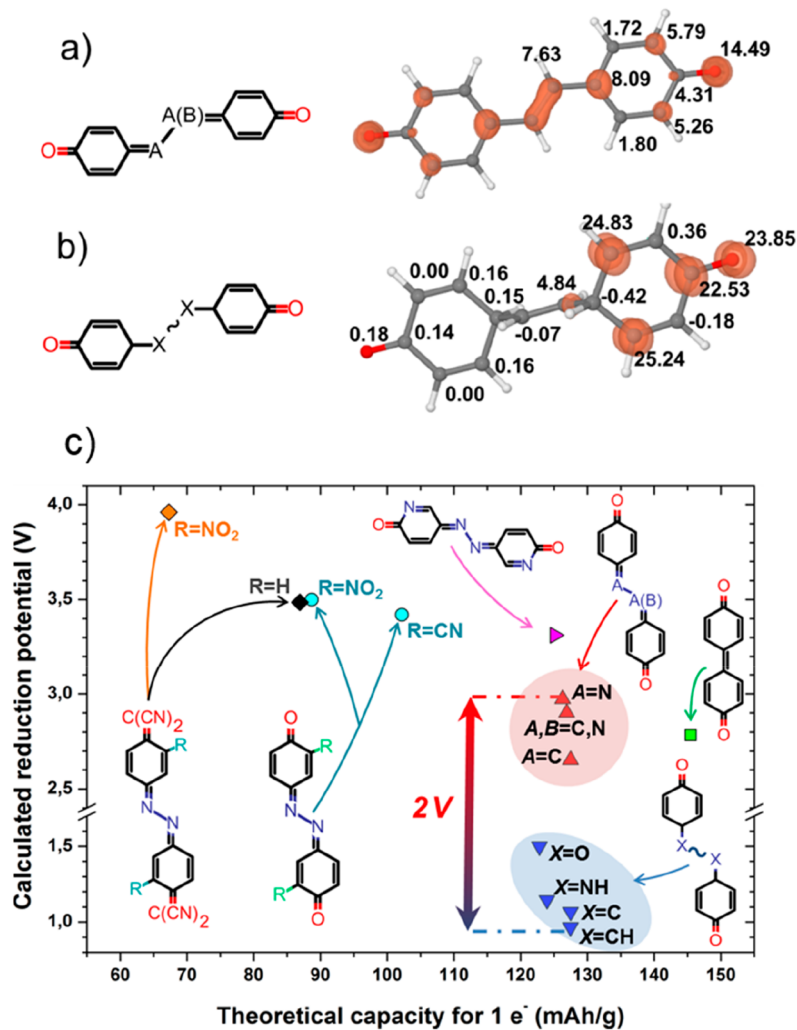
Figure 17. C=A−A=C, C=A−B=C and CH−X ∼ X−CH systems: (a) High- and (b) low-potential molecular systems (with A/B equal to N or CH and X equal to NH/O (X−X bond), CH (X=X bond) or C (X≡X bond)). The spin density distribution and Bader's atomic spin density populations (in hundredths of electrons) of two representative systems are shown to highlight their difference (a) A=CH and (b) X=CH. (c) Calculated reduction potential (in V vs Li$^+$/Li) as a function of the capacity for a one-electron process. Reproduced with permission from ref 159. Copyright 2015 Royal Society of Chemistry.

However, the quest for crystal structure of either reduced or oxidized forms of electroactive materials can become crucial in this area whenever they are difficult to obtain from the experiment, and this is where MSM can play a relevant role. Seo et al.[171] predicted the crystal structure of the unknown $Li_{2+x}C_6O_6$ ($x = 2$) rhodizonate phase, the key amphoteric species among $Li_2C_6O_6$ and $Li_6C_6O_6$, through a combination of DFT and force-fields (FF) derived from the DFT, AIMD, and grand canonical MC calculations. This multiparadigm computational methodology allowed one to probe the energetics and changes in packing of $Li_4C_6O_6$, one of the first envisaged organic electrode.[172] A good agreement between the experimental pattern and the XRD one generated from the structure with the lowest DFT energy was evidenced. In order to understand the charge/discharge mechanisms, crystal structure predictions of $Na_xC_6O_6$ (with $x = 2.5$, 3, 3.5, and 4)[173] have then been carried out by combining first-principles calculations with an evolutionary algorithm (USPEX).[174] Thanks to this approach, a favored new stacking of C_6O_6 molecules (i.e., the γ-stacking, which is different from the well-known α-stacking of $Na_2C_6O_6$, with space group *Fddd*) was evidenced. In the α-stacking, which

is found to be favorable only at $x = 2$, the C_6O_6 molecules stack so as not to completely overlap with neighboring molecules, whereas in the sodiated structures ($2.5 \leq x \leq 4$), the C_6O_6 molecules stack by sharing the 6-fold rotation axis (i.e., the γ-stacking). The calculated voltages involving this new phase were found to be consistent with the experimental result within approximately ± 0.2 V accuracy. Recently, the sodium insertion mechanism in the tetrasubstituted quinone $C_6Cl_4O_2$ was also studied[175] within the framework of DFT combined with the evolutionary algorithm, USPEX. The crystal structures of the compound $Na_xC_6Cl_4O_2$ ($x = 0.5$, 1.0, 1.5, and 2) were thus elucidated, and the results have highlighted great structural changes upon sodium insertion reaction with a volume change going to about 14% when x varies from 0 to 2 (in the PBE+D2 approach). Otherwise, Chen et al.[176] have performed simulations of voltage−capacity curves of polymeric positive electrode materials. In order to take into account the large required numbers of atoms and structures, the authors combined MD and density functional tight binding (DFTB) methods. For investigating the oxidation of the amorphous polyaniline (PANI) solid, ClO_4^- anions were incorporated into

amorphous structures through 18 different configurations corresponding to different numbers of ClO_4^- anions within the PANI solid and representing different degrees of oxidation. For each configuration, ten random structures were generated and optimized (both atoms and lattices) using MD. The lowest energy structure of each configuration was selected for further analysis with DFTB. They further demonstrated that functionalization of PANI with cyano groups on the nitrogen would lead to a significant increase of the voltage, by about 0.7−1.1 V depending on the degree of oxidation (Figure 18).
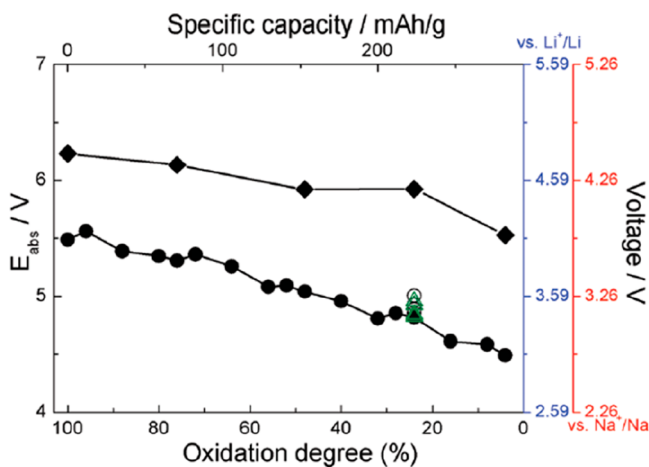

Figure 18. Absolute oxidation potentials (left axis) and estimated voltages (right axes, blue for Li and red for Na) for (●) PANI and (◆) CN-functionalized PANI at different degrees of oxidation. ○ indicate the potentials obtained from pristine PANI at 24% oxidation with different spatial positions of ClO_4^- anions. Green △ indicate the potential obtained from PANI at 24% oxidation using a larger unit cell.[176]

3. ELECTROLYTES

The electrolyte is at the heart of the battery cell. It balances the electron conduction by its function to provide ion transport between the electrodes, and selecting the electrolyte plays a crucial role for battery cell design. There are several practical electrolyte requirements that can be translated into physical properties of primary material choices which will impact the decision process, including solubility, thermal, and electrochemical stability, mechanical strength, etc. Here we will solely focus on MSM of bulk electrolyte properties, leaving the electrode−electrolyte related issues, properties, and processes to section 4.

For disordered materials such as liquid electrolytes, it is challenging to outline any straight relationships between macroscopic observables such as sustained current without depletion/decomposition and microscopic properties such as ion transport and molecular interactions. MSM can here offer a connection between these two-three "worlds". Indeed, a proper description of bulk properties such as lithium ion transport requires addressing different length- and time-scales; diffusion of charge carriers ultimately depends on ion aggregation and changes in solvation structure, which in turn depend on interaction best described using quantum mechanics. Hence, among different MSM techniques, MSMSL is the most frequently used. Within these, models based on atomistic molecular dynamics (i.e., first principle MD, reactive MD, classical MD) employ results from quantum molecular

calculations, whereas coarse grained MD- and MC-based models need dynamic parameters generated by atomistic dynamic simulations.

Altogether, these MSM techniques make use of FPMD, classical MD, and coarse-grained MD simulations, as well as MC-based methods to evolve systems dynamically to explore bulk transport properties. For most battery electrolytes, no main chemical reactions in terms of oxidation/reduction occur, and reaction-predictive methods such as reactive MD are therefore of limited use. The wide range of side-reactions that do occur at the electrode interfaces are here treated in section 4.

3.1. First-Principles Molecular Dynamics

FPMD (or AIMD) has been used for MSM of dynamic changes for almost all types of electrolytes: organic liquid, ionic liquid, solid polymeric, and solid inorganic, but the size of the system possible to treat is still highly limited by the computational cost. Nonetheless, these studies usually concern small-sized bulk electrolytes, trapped in the box, except a few examples (indicated below), where FPMD is used to extend DFT calculations by adding temperature to the system.

Starting with MSM of organic electrolytes, most studies have comprised salt and solvents normally used commercially and/or experimentally. One of the primary targets has been to explain experimental observations, a typical example being simulations to explore the structure and composition of the Li^+ coordination shell, which is crucial to address in order to properly understand the ion transport mechanism. This can aid interpretation of experimental data from a range of spectroscopic techniques. For example, Tachikawa simulated $LiBF_4$ in EC applying static and dynamic *ab initio* calculations of small clusters[177] and found EC to very strongly solvate Li^+ by creating a $[(EC)_3(Li^+BF_4^-)]$ complex. The calculations also showed that the complex easily dissociates by substitution of the BF_4^- anion by another EC molecule. Application of both, static and dynamic, techniques gives a wider insight into these processes and explain the observed results by calculated potential energy surface and dynamic trajectories.

The observed Li^+ coordination number of 4 is commonly seen in most simulations of liquid electrolytes,[178−183] with the preferred solvation structure strongly dependent on both the salt and solvent. For example, linear carbonates such as DMC and DEC provide too weak interactions with Li^+ to completely dissociate solvent-salt complexes, resulting in a very short distance between cations and anions during the simulations.[181,184] Ion-pairs ultimately decrease the number of free charge carriers present in the electrolyte and hence, in a direct way, impacts the lithium ion conductivity in a negative manner. Adding better solvents such as acetonitrile[184] or cyclic carbonates[181] to the electrolyte resolves this problem, where simulations have been used to clearly show strong solvation of cations while at the same time maintain weak anion−solvent interactions. While anions are usually free and undergo Brownian-like motion, cations are often more strongly trapped in their solvation structure.[179]

Detailed analysis of FPMD MSM results have allowed one to better distinguish between the two commonly discussed modes of Li^+ diffusion: carrier-based/vehicular diffusion with the lithium ion trapped within its solvation shell and jump diffusion involving hopping/jumping of the lithium ion from one solvent configuration to another.[182] Bhatia et al. found evidence for the latter process when using a bond topological analysis of $LiPF_6$ in EC and found the presence of short-lived transient solvation

structures with 3 or 5 EC surrounding Li$^+$ to be crucial.[183] This kind of connection between the solvation shell composition and diffusion type is highly important for the understanding of the ionic transport properties but can really only be obtained using MSM at this level. For an EC:EMC-based electrolyte, a strong caging effect of Li$^+$ has been seen present and therefore only vehicular motion were observed, which clearly reduced the ion diffusion/transport (Figure 19). This is surprising, since long ion
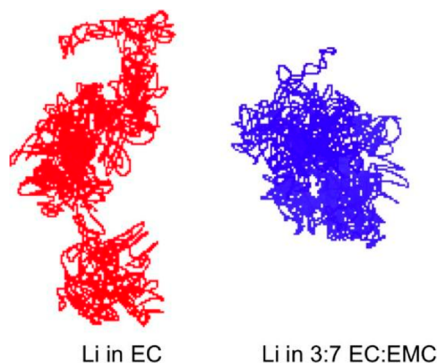

Figure 19. Comparison of the Li$^+$ trajectory in pure EC and the 3:7 EC:EMC mixture showing stronger caging effects in the mixture. Reproduced from ref 179. Copyright 2017 American Chemical Society.

jumps between neighboring cages were observed in models of both EC- and EC:DMC-based electrolytes.[179,182] A similar jump-behavior as for EC-based electrolytes was found also for PC-based electrolytes, although EC solvates lithium ions more efficiently.[180]

So far, FPMD simulations have been much more scarce for electrolytes for next generation batteries such as Li-S and Li-O$_2$. In these, the solvents typically used are different than in Li-ion batteries, and several of the fundamental issues regarding structure-dynamic properties remains to be addressed/resolved. In this context, Chen et al. used FPMD simulations to investigate the impact of the anion on the equilibrium between polysulfides in a 1,3-dioxolane (DOL)/1,2-dimethoxyethane (DME) system,[185] which is a typical electrolyte in Li-S batteries. They found that the disproportionation reactions, which cannot easily be targeted using standard MD, leads to the formation Li$_2$S$_3$, Li$_2$S$_4$, and Li$_2$S$_5$ species and that the exact balance of these should be able to be tailored by the salt selection, where especially LiTDI effectively decreased the polysulfide solubility. More detailed studies of Li$_2$S$_4$, supported by DFT, indicated large clusters forming and hence stabilization.[186] This is important, since shuttle effect and loss of active material, both caused by presence of polysulfides in the electrolytes, are the biggest issues to overcome developing new Li-S electrolytes. For Li-O$_2$ cells, Scheers et al. applied FPMD to study the influence of both electrolyte solvent and the lithium cation for the stabilization of O$_2$*$^-$ and found a strong tendency to form LiO$_2$* contact ion pairs, especially in low permittivity media such as DME.[187] On the basis of this insight, high donor number solvents, as DMSO, can be suggested for better stabilization of O$_2$*.

In ionic liquid based electrolytes, which display very extensive electrostatic interactions, lower ionic mobilities are generally observed than in organic solvent based electrolytes, partly due to their high viscosity. Therefore, any simulation performed requires longer simulation times to properly describe the dynamics. As a result, FPMD studies are usually coupled with

classical MD, with the former determining the structural properties and validating the FF used in the classical MD, which is then used to study the dynamics of the system.[188−190] Overall, the FPMD simulations of these systems have confirmed previous spectroscopic analysis,[191,192] showing that addition of lithium salt to the IL cause the lithium cations to be trapped in cages of 2−3 TFSI anions, which limits the mobility and decreases the overall ion conductivity.[193]

This shows that to facilitate lithium transport, weaker coordinating anions have to be used.

Even more restricted ion mobilities are observed for solid polymer electrolytes, while applying FPMD puts further limitations to the possible size of the model system that can be applied. Xue et al. studied LiTf-PEO$_3$ and compared the lithium ion diffusion and structure for crystalline and amorphous phases.[194] To get an idea of the system sizes possible to investigate, the crystalline system was created using PBC and a repeat unit of the primitive cell comprising 4 lithium cations, while for the amorphous phase a repeat unit of two crystalline cells was used (8 lithium cations) after a "melt-and-quench" scheme up to 900 K to introduce some structural disorder. Such limited-sized supercells may be a less useful representation of any real system and can well display restricted dynamics and a small amount of available configurations. However, the study still revealed some basic underlying phenomena for the observed differences in the lithium ion transport between the phases; the variance in Li-O distances in the amorphous phase causes a lower force of repulsion during lithium ion migration and thus lower diffusion barriers than in the crystalline phase.

FPMD approaches have also been used for crystalline inorganic electrolytes. As the inorganic particles generally are small and the system is almost fully crystalline, the reduction to one supercell with PBCs should generally be reasonable. Simulated systems include Li$_7$P$_2$S$_8$I and Li$_{10}$GeP$_2$S$_{12}$, where a focus has been on Li-ion conductivity and different diffusion mechanisms.[195,196] These FPMD simulations were able to predict that isovalent cation substitution can cause only minor changes in conductivity and also provide an assessment of the impact of lattice parameter changes on transport properties, corroborating the experimental studies which could correlate Li$^+$ conductivity with lattice parameters. Decrease of the lattice parameters resulted in an increase in the activation energy which slows down lithium diffusion, as the size of transport channels in the crystal lattice became small.

Computational techniques have been extensively used to better understand ionic transport also in ceramic and glassy electrolytes, both for Li-ion and Na-ion battery systems, and have recently been reviewed elsewhere.[197−199] These studies span LISICON and NASICON materials, perovskites, LiPON, amorphous, and crystalline phosphosulfides (LiP$_x$S$_y$ and NaP$_x$S$_y$), perovskites and antiperovskites, garnet oxides, Li$_3$N, etc. For MSM approaches, primarily AIMD and DFT-MD have been applied for different forms and phases of doped and undoped phosphosulfides, where cation transport inside solid-state electrolytes has been examined by MSD analyses. For example, the well-studied "superconducting" phase of Li$_{10}$GeP$_2$S$_{12}$ was simulated using AIMD by Oh et al., showing that defects in the material generally facilitate Li$^+$ diffusion by enhancing the charge carrier concentration and flattening the site energy landscape.[200] Somewhat similarly, Li$_3$PS$_4$ was studied using a combined DFT and MD approach by de Klerk et al.,[201] showing how the activation energies of different ionic jumps and their attempt frequency could be obtained from a single MD

simulation. Moreover, Chu et al. studied diffusion mechanism in $Li_7P_3S_{11}$ and found collective Li^+ motion together with flexible P_2S_7 ditetrahedrals, both responsible for superionic properties.[202] Modification of this material in terms of its sodium analogue showed much lower conductivity for the oxide $(Na_7P_3O_{11})$ and only a little higher for the selenide $(Na_7P_3Se_{11})$, related to higher and lower activation energies for the cationic transport, respectively.[203] As for the Na-conducting analogue, studies of glass-ceramic Na_3PS_4 indicated defects formation as a key factor for enhancing sodium conductivity.[204−206] Doping the structure with Si, Ge, or Sn induces disorder by the introduction of excess Na^+ and an increased Na−Na Coulombic repulsion which causes a slight displacement of their positions and thus lower activation barriers.[205] Similarly, halogen-doping introduces Na^+ vacancies and enhances the chance of cation movement toward a neighboring site, observed as an order of magnitude higher conductivity upon introduction of 2% vacancies.[206] For Li^+-conducting perovskites, Dawson et al. used a MSM approach to study both the bulk transport with AIMD[207] and the impact of grain boundaries with classical MD on the conductivity in Li_3OCl.[208] The materials possess a high grain boundary concentration, and the simulations predicted a slower diffusion through boundaries which could be explained by a higher migration activation energy.

Much less abundant for MSM of electrolytes are semi-empirical methods, where we bring forth the coupling of PM7 and dynamics by Chaban.[209−211] Here, the forces for the MD part are generated by a PM7 semiempirical Hamiltonian, with some integrals predetermined based on experimental data, to save computational cost, but preserving the QM nature of the method. The method was applied to the composition of lithium-ion solvation shells for clusters-in-vacuum models and basically pair correlation functions, with satisfactory agreement with AIMD studies.[210] In detail, a PC:DME (1:1) system with a single lithium cation resulted in a first solvation shell of 5 PC and 1 DME molecule to be the most common. A similar analysis of the BF_4^- or PF_6^- anions replacing Li^+ resulted in much weaker interactions and no clearly distinguishable first solvation shells, but the dominance of PC remained. Studies of $NaBF_4$ and $NaNO_3$ dissolved in different ionic liquids, hence very different systems altogether, were studied with the purpose of revealing the effect of various cation−anion interactions on the sodium-ion solvation.[211] Here the formation of hydrogen bonds to the IL cations were found to be beneficial for the Na^+ dynamics by weakening its solvation.

3.2. Reactive Force-Field MD

As mentioned, the chemical reactions of the electrolytes are usually restricted to the area interacting with the electrodes (section 4.2) and are hence seldom included in models describing bulk properties of electrolytes. In one recent example,[212,213] however, reactive FF MD simulations were applied to study the evolution of mechanical properties of structural battery electrolytes. The electrolyte was composed of $LiPF_6$ in cross-linked poly(propylene glycol) diacrylate, rendering comparatively mechanical robust properties. The impact of the salt concentration on the material stiffness in the presence of EC as a plasticizer was studied. Simulations were also performed of inelastic deformation, which considered bond dissociation during mechanical stress. The results displayed a reduced material strength and failure strain at increased salt

concentrations, due to formation of $Li(PF_6)_n$ clusters that cause local viscoelastic properties anisotropy in the material.

3.3. Classical MD

Classical MD is a tool for fast atomistic simulation of transport properties of electrolytes, as interactions are simply calculated based on a FF, which most often is developed based on quantum chemistry data for single molecules, clusters, and small systems. Hence, this methodology can be considered belonging to the MSMSL paradigm. The higher speed as compared to the computationally expensive simulations using quantum mechanical based interactions/equations allows for studies of properties of much extended spatial- and timescales. Typical examples of problems addressed for electrolytes are the structure-dynamic of the solvation shell of Li^+ and the mobility of different forms of clusters.

The FFs used can basically be divided into two classes: unpolarized, with charges fixed at atomic centra,[214−216] and polarized, where the charges are allowed to positionally deviate from the atomic centra (i.e., to mimic polarization induced by other electrolyte components) (mainly Li^+).[217−220] The choice of FF is usually motivated by the computational aim and the type of system; classical MD simulations are one of the most universal dynamic modeling tools, allowing one to simulate almost all types of battery electrolytes, from organic solvent based liquid electrolytes, containing carbonates,[221−226] glymes,[227−237] and acetonitrile[238,239] via ionic liquid based electrolytes[189,193,240−247] to solid and gel polymer electrolytes.[248−260]

Starting with the liquid electrolytes, the primary target of the simulations has been to explore the Li^+ coordination by solvent and anions and how these influence the ion transport. Similarly to the FPMD simulations (see above), most simulations predict Li^+ to have a coordination number of four and to primarily be coordinated by the carbonyl oxygen atoms of the carbonate solvents.[222,226] Naturally, this coordination number decreases with increasing salt concentration due to aggregate formation as exemplified for $LiPF_6$ in EC. The major achievements of these MD simulations of conventional electrolytes, typically organic carbonates, have been achieved using polarizable FFs,[218,219] whereby the ion diffusion and conductivity have both been predicted with a maximum error of 37%, also including temperature dependence. Using nonpolarizable FFs leads to predicted ion diffusion deviating by factors 2−10 (lower). Furthermore, also more local structural properties such as free ions and fraction of solvent-separated ion pairs (SSIPs) has been targeted, where the DMC:EC/LiTFSI electrolytes have a fraction of free ions increasing linearly with the concentration of EC, while a higher temperature decreases this fraction. Using MD allows uniquely addressing both the dynamic degree and static degree of ion dissociation. Since the former is always being found higher, this indicates that ionic clusters contribute significantly to the ionic conductivity.

Moving to glyme-based electrolytes, these provide an option for explaining the unique properties of solvate ILs (SILs).[231,233,237] Here, the simulations work has displayed a pivotal role of the lithium salt anion: the lower Lewis basicity of the TFSI anion allows for a complete coordination of the lithium ion by the glyme solvent, unlike when $LiNO_3$ is used as a salt.[232] Also the flexibility of TFSI has been shown to play a key role for the formation of SIL, as the rigid anion TDI, but yet weakly coordination anion TDI forms a wide range of different ionic clusters under the same conditions.[228] MD simulations were also employed to study next generation battery electrolytes; Park et

al., for example, constructed a system to reproduce experimental data for state-of-the-art electrolytes for Li/S batteries: LiTFSI and LiNO$_3$ in DME and DOL. A study of the first lithium solvation shell gave structural insights and helped with the understanding of the fundamentals of lithium diffusion and electrolyte conductivity.[227] DME was shown to be much more preferred in the Li$^+$ solvation shell than DOL and also more effectively separates the TFSI anion from cation. That results in a decreased conducitivty with increased fraction of DOL as a solvent. The diffusion coefficients for a 1 M LiTFSI electrolyte obtained by Park et al. match the experimental values within 20%.[227] Much larger errors toward experiments were reported by Rajput et al., with the diffusion reported to be >10 times slower for 1 M LiTFSI and 100 times slower for 3 M LiTFSI.[261] Nonetheless, the observed trends in self-diffusion coefficient changes as a function of increased salt concentration was reproduced and connected with increased viscosities. Kuritz et al. used MD to study the O$_2$ diffusion in a solvent mixture of triglyme and perfluorinated carbons, simulated as a model system for potential electrolytes for lithium oxygen batteries (LOBs).[235] The simulations revealed faster O$_2$ diffusion in perfluorinated solvents and problems with miscibility of these two types of solvent. This is important for future electrolyte design, since improvement of O$_2$ transport in the electrolyte is essential for development of LOBs as it affects the availability of O$_2$ molecules at the electrode surface. For multivalent cation (Mg^{2+}, Ca^{2+}, Zn^{2+}) electrolytes, several structures were studied by MD to evaluate impact of aggregation on cation transport properties.[230,236,262] It was suggested that the large degree of ionic clustering, observed in these electrolytes, is the main challenge when solving the problem with the low diffusion coefficient of multivalent cations.

For IL-based or -containing electrolytes, the target has often been to obtain reasonable and transferable MD simulations. Therefore, FF development has been and will be crucial for the advancement of the field. There exists an interplay of strong electrostatic interactions affecting polarizable molecules, but which is less evident for how to properly treat computationally. With respect to this, Borodin et al. have developed many-body polarizable force-field models (APPLE&P) which have generated good comparisons with experimental data of structural and thermal dynamical properties (e.g., self-diffusivity, ionic conductivity, viscosity, etc.) for a wide range of pure ILs as well as electrolytes based on LiTFSI in ILs and generated Li$^+$ transport data, often lower, but not strikingly different from experimental data.[263] Nevertheless, it is still debatable whether the use of polarizable FFs is necessary considering the high computational cost and time devoted to the FF development. In the meantime, some strategies have been developed to exclusively treat the effect of bulk polarization using classical FFs; Maginn et al., for example, have suggested for one to solve polarization implicitly by reducing the net charge in an all-atom FF model.[264] This was demonstrated for the BMIm-PF$_6$ IL using a combination of *ab initio* calculations and CHARMM parameters to construct the FF. Chaban et al. in turn showed how uniform scaling of electrostatic charges can generate adequate approximations for imidazolium-based ILs, exemplified by BMIm-PF$_6$ and MMIm-TFSI, through estimations of scaling factors via DFT calculations.[265] Another parametrization method employed by Köddermann et al. has confirmed the possibility to achieve good refinements of an all-atom FF through adjustment of Lennard-Jones parameters. These researchers further optimized the methodology in an integrated

united-atom model for faster simulations of [CnMIm]-TFSI ILs.[266] These examples show that polarizable FFs might not be necessary to adequately model the ion transport in ILs, but the implementation of the approximations might be system-specific and time-consuming, and there is no guarantee that either of them works for IL-based electrolytes; they are developed for "pure" ILs. Generally, the Li coordination number to TFSI and FSI has been ca. 4, regardless of pyrrolidinium- or imidazolium-based ILs as matrices, comprising both monodentate and bidentate configurations. MD simulations have shown a preference for the monodentate coordination,[245] in contrast to several spectroscopic analyses and DFT calculations.[240,267] For the mechanism, while the Li$^+$ transport in liquid electrolytes primarily is vehicular, a few MD simulations of IL-based electrolytes have proposed Li ion jumping between different anions to be the main mechanism. In other words, Li$^+$ ions do not seem to possess any stable first coordination shell in these systems.[245]

MD simulations of SPEs are, as for experiments, totally dominated by studies of poly(ethylene oxide) (PEO)-based electrolytes,[268−273] with only a very limited amount of MD simulations of other SPEs published.[274,275] For PEO, several specific FFs have been developed, where the torsional parameters have been obtained by fitting analytical expressions to QC calculated data and validated against crystallographic or spectroscopic data. The main effort was taken by Borodin and Smith, who developed a polarizable FF for both pure PEO and LiX-PEO electrolytes validated against both structure factors, dielectric loss, and vs ^{13}C NMR spin−lattice relaxation times.[217,218,276] With the use of these FFs, amorphous linear and branched PEO of different molecular weights systems have been simulated, at different temperatures, and concentrations of 7 different salts, LiCl, LiI, LiPF$_6$, LiBF$_4$, LiCF$_3$SO$_3$, LiClO$_4$, and LiTFSI.[248,272,276−281] This has provided a picture of several fundamental structure−property relationships in PEO-based SPEs (e.g., PEO usually coordinates lithium cation creating loop) that disturbs the normal structure of the polymer and slows down polymer chain motions. Borodin and Smith, however, examined earlier achievements when they showed that Li$^+$ motion is subdiffusive in amorphous PEO up to 30−40 ns at ambient temperatures.[259] This implicates necessary-to-perform MD simulations with long times in order to precisely determine diffusion coefficients in these systems. In contrast, crystalline PEO-based electrolytes,[269] polyelectrolytes with tethered anions,[282] and electrolytes containing ceramic nanoparticles[283] have been much less simulated using MD. These simulations usually have been made to address structure and dynamics inside solid electrolyte and showed that Li$^+$ is coordinated by subsequent mers forming a loop around the Li$^+$. Thus, presence of cations is perturbing PEO helix formation and reduces the polymer chain motions by physical cross-links. MD studies have shown that the mechanism of Li$^+$ transport is rather related to diffusion along the chains than between the chains. Additionally, anions were found to be responsible for the transfer of cations from one polymer chain to another. Formation of ion pairs, suggested in literature to inhibit ionic transport, can to some extent support Li$^+$ diffusion, and neutral ion pairs and clusters were seen traveling together. These ionic clusters exhibit a lot of dynamics, related to continuous binding and releasing cations. However, although the segmental motion of the polymer, which is directly linked to the conduction mechanism in solid polymer electrolytes, occurs at timescales

which are clearly accessible in MD simulations, the transport is still slow in these materials and difficult to directly assess.

3.4. Coarse-Grained Molecular Dynamics

To study the correlations between ionic association and structural order in SPEs, where dynamics are slow, techniques applicable to greater timescales are naturally preferred. Coarse-grained molecular dynamics (CGMD) is one such MSM technique which relies on reducing of the physical degrees of freedom by using basic units (bead) defining a set of atoms (Figure 20) to speed up the simulations by several orders of
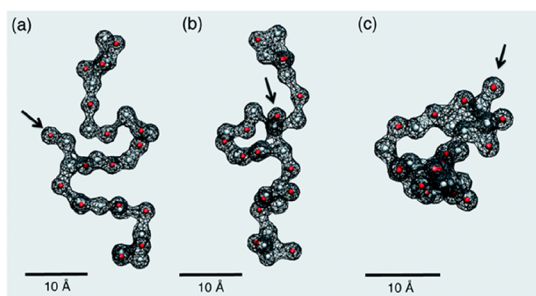

Figure 20. Representation of polymer chains using a coarse-grained model in 3 different perspectives. Reproduced with permission from ref 284. Copyright 2014 The Royal Society of Chemistry.

magnitude.[284] This allows for significant increase in system size and sampling statistics. The interactions between the bonded beads are represented by springs, whereas nonbonded interactions are treated by Coulombic potentials. All interaction parameters are generally extracted from DFT and/or MD calculations using force-matching methods like the Yvon–Born–Green procedure,[285] making this a MSMSL approach. CGMD simulations have been successfully used to simulate dynamics in electrolytes for hundreds of nanoseconds.

Hall et al. applied CGMD simulations to study ionic aggregation in low dielectric constant ionomers like poly-(ethylene-*co*-acrylic acid), using beads to approximately map three CH_2 groups for various polymer architectures: charged beads were employed either in the polymer backbone (ionenes) or pendant side-chains and for various spacing between the charged beads (Figure 21).[286−288] These simulations predicted the formation of two types of aggregates: discrete units and a
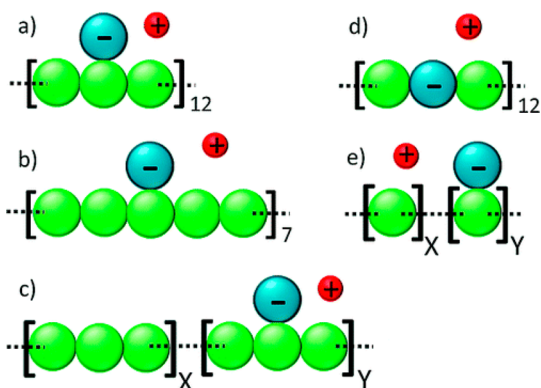

Figure 21. Schematics of simulated polymers with uncharged polymer beads in green, charged polymer beads in blue, and counterions in red: (a) and (b) periodic pendants, (c) random block pendants, (d) periodic ionenes, and (e) fully random pendants. Reproduced from ref 287. Copyright 2012 American Chemical Society.

percolation network throughout the simulation box, where the latter was found to be the preferred aggregate for ionenes and for pendant side-chains with low spacing. Interestingly, these structures were unstable in higher dielectric constant media. The formation of a percolating network structure is important, as it was found to lead to faster dynamics and higher ion conductivities. No ion hopping mechanism was observed in any of these materials, using this MSM technique, instead ions travel through continuous reformation of the cluster network.

The influence of percolation on ion transport was also studied by Lu et al. for PEO-based ionomers where the beads consisted of 13 PEO monomers with negatively charged sulfo-iso-phthalate groups and where the ionic aggregates serve as conduction paths.[284,289] The mechanism is schematically shown in Figure 22 and describes how local excess cations can
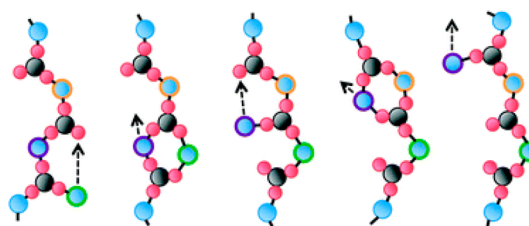

Figure 22. Schematic of charge conduction through ionic aggregates. Blue-filled circles are cations and red/black circles are sulfonate groups. Selected cations involved in the movement are highlighted with green, purple, and orange circles. Reproduced with permission from ref 289. Copyright 2016 The Royal Society of Chemistry.

coordinate to the ionic chains, moving from one center to another along the chains. Additionally, the charge transport can also involve collective cation movement, which may allow for even faster diffusion than any individual ion moving along the chain. The simulation methodology applied relies on a separation of timescales of the ion motion and the polymer segmental motion, that allow for "ion-only" simulations (Figure 23).[289]

Ting et al. performed CGMD simulations of ionomer melts in the presence of a static external electric field,[290] showing that even low fields strengths (<0.76 V/nm) render the ions to move in a synchronized manner for percolated aggregates, while higher fields are required for isolated ionic aggregates. This is due to the fact that local ionic motion of ions is affected already at low fields, while higher fields are required to break isolated aggregates. For the percolation networks, the structure did not need to change significantly to promote conductivity. A similar effect on how electric field can trigger collective motion in highly structured SPEs was also explored for crystalline $LiPF_6PEO_6$ using classical MD based on a DFT-derived FF.[291]

Another example of a CGMD simulation of SPEs is a study of the ordering transition using a system of diblock PEO-PS copolymers doped with generic lithium salt.[292] Here, both polymer blocks were modeled as neutral beads connected by springs and the salt cations and anions as beads of opposite charge (Figure 24). The electrostatic interactions were treated explicitly, to allow for the investigation of order−disorder transitions, to distinguish the influence of two competing effects: ion association and solvent dilution. The results show that dilution with neutral solvents reduces the repulsive interactions between polymer blocks, causing a higher repulsive strength required for phase separation and thereby effectively lowering the transition temperature. The influence of salt concentration
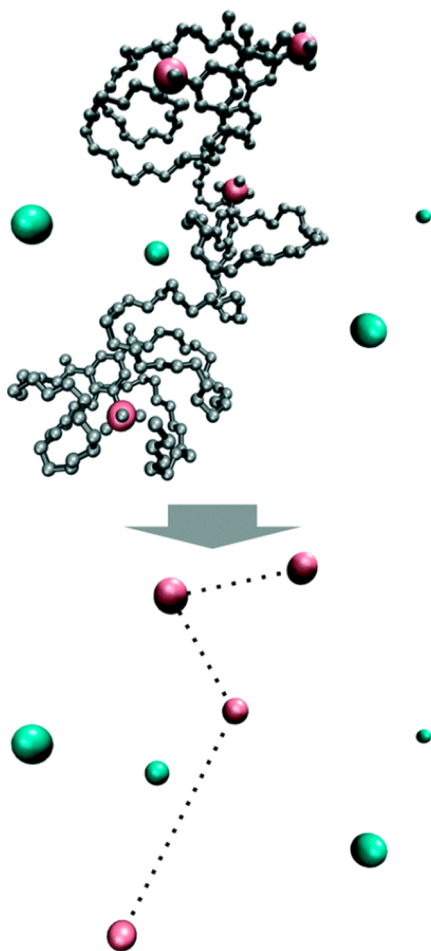
Figure 23. Backbone polymer (gray) in the atomistic chain is completely removed through coarse-graining, leaving only anions (pink) bonded together with weak harmonic springs, neutralized by sodium cations (cyan). Reproduced with permission from ref 289. Copyright 2016 The Royal Society of Chemistry.
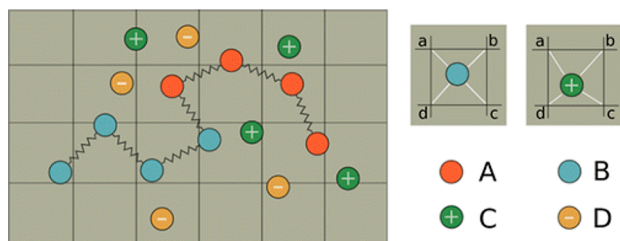

Figure 24. Schematic illustration of coarse-grained model for salt-doped diblock copolymers. The density fields as required by the Hamiltonian are constructed by mapping bead positions onto an underlying grid. The mass and charge of beads are mapped onto the eight nearest-neighbor grid sites (a, b, c, d, etc.) and the contributions of different sites to the free energy are determined by the relative distance of each bead to a nearby grid site. Reproduced from ref 292. Copyright 2016 American Chemical Society.

was shown to be rather complex; for intermediate salt concentrations, ca. $x_{salt} = 0.1$, the addition of salt increases the transition temperature due to stabilization of separated phase by placing ions inside PEO-rich domains. However, with further salt addition, the PEO domains cannot retain all of the ions, and some of them end up in PS domains causing a reduced separation between the two blocks making up the copolymer,

leading to more mixed system. Similar MSM simulations could in principle be used as a design tool for the construction of block copolymeric systems which combine mechanical robustness (through formation of stable blocks) and high ionic conduction (through formation of percolating ionic clusters in the conductive domain.

3.5. Monte Carlo (MC) Methods

To even further extend the simulation scale of SPEs, different models based on MC approaches have been used to obtain microscopic descriptions of motion inside the electrolyte. The dynamic bond percolation (DBP) theory provides a simplistic yet useful approach to describe generic aspects of ion diffusion in these systems.[293] The transport is then analyzed in terms of random walk processes in a disordered lattice of the host and by hopping between neighboring sites in this fluctuating lattice. The model is characterized by two specific time constants related to "hopping" time and "renewal" time, where the latter is attributed to local structural relaxation processes governed by the polymer dynamics. Despite the simplicity of the model, it has been successfully used to study the cation conductivity in polyelectrolytes and polymer-salt systems at different temperatures.[294] The results showed, similar to several atomistic scale models described above, the importance of local anion motion for promotion of lithium transport. Another approach to understand cation diffusion, the microscopic transport model, has more recently been developed by Borodin et al.[259] Here, each lithium cation occupies 4 coordination sites in the one-dimensional lattice, which corresponds to a polymer chain. The cations are allowed to either move along chains, move together with chain segments, or hop between chains (Figure 25). The
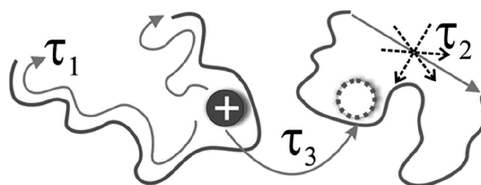

Figure 25. Timescales of different events: τ_1 is the time for intrachain ionic motion, τ_2 is the relaxation time of the polymer chain, and τ_3 is the waiting time of an ion between two interchain jumps. Reproduced with permission from ref 295. Copyright 2007 American Physical Society.

parameters for these events are determined by a Monte Carlo scheme involving short MD simulations performed prior to the long-run simulation. The model allows dividing cation dynamic in the polymer electrolyte into these three transport mechanisms and results in the contributions from diffusion of Li$^+$ along PEO and together with PEO are approximately equal, while intersegmental hopping is responsible only for about 10% of the total cation conductivity (Figure 26). Additionally, the results showed that an increase of salt concentration primarily impedes the diffusion along the polymer chains.[259]

A comparative study using a microscopic transport model of the analogous binary (EO_{12}/LiTFSI) and ionomeric ($EO_{12}TFSI^-$/Li$^+$) systems showed larger contributions from local motions of the cation along the chain for the latter, but a decrease in temperature reduces this contribution and lithium transport is limited by interchain hopping.[296]

Maitra et al. tried to merge dynamic bond percolation and miscroscopic transport models, by description of the interchain hopping as "renewal events" according to the DBP theory.[295] The model was employed to study the influence of polymer
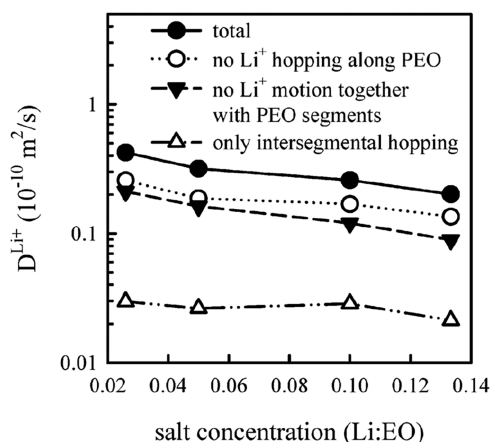
Figure 26. Macroscopic Li$^+$ diffusion coefficients originating from various contributions to the Li$^+$ transport and the total for EO:Li = 20 concentration. Reproduced from ref 259. Copyright 2006 American Chemical Society.

Figure 27. Alternative strategies for obtaining ion transport properties in polymers. The dashed arrow indicates the conventional brute-force approach, in which transport properties are obtained by running long and computationally expensive MD trajectories. The black arrows indicate the approach of the CS-DBP model, in which short MD trajectories are used to obtain parameters for kMC simulations that predict transport properties at a reduced computational cost. Reproduced from ref 299. Copyright 2015 American Chemical Society.

chain length on cation diffusion. With an increase in chain size, the contributions from vehicular motion of Li$^+$ associated with the chain decreases, and the renewal processes, described by DBP theory, will start to play a more important role for the cation conductivity.

To overcome computational limitations with classical MD, trajectory-extending kMC (TEKMC) was used by Hanson et al. to study the effect of adding nanoparticle fillers in polymer electrolytes.[297] This technique exploits the fact that the long-term dynamics consists of diffusive jumps from one state of the system to another, which can be described individually based on short MD simulations. Atomistic simulations are therefore used to construct a lattice framework and thereby generate a probability matrix that can be used to extend the simulation time-scale significantly. Such larger timescales allow modeling the influence of nanoparticles on polymer conformation by analysis of lithium diffusion and polymer segmental relaxation time. The longer relaxation time of the polymer chains which result from the addition of the nanoparticles directly affects lithium cation diffusion by slower dynamics of polymer segments. Additionally, Li$^+$ are preferentially attracted by nanoparticles to strongly bind oxygen atoms, which significantly slows down lithium-ion mobilities in nanocomposite polymer electrolytes.[298]

An even more advanced model was proposed by Webb et al.[299] A chemically specific dynamical bond percolation (CS-DBP) model was established as a framework for ion transport that is both computationally tractable and flexible enough to be applied to a wide diversity of polyethers (Figure 27). This allows studying promising candidates of polymer hosts for electrolytes. Like TEKMC, CS-DBP is based on short MD simulations, which are used to indicate solvation sites in the polymer and to estimate hopping rates between them. In this way, the hopping rates are a function of the solvation sites distribution and connectivity. The obtained data are used in kMC simulations to study long-term diffusion of Li$^+$, where two types of moves are permitted at each time: hopping to another solvation site or a restructuring of the solvation site network. Such a model allows for extension of the few nanoseconds associated with MD simulations, to the milliseconds scale. The results from different polymer matrices explain the slower lithium dynamics associated with lithium-ion hopping in poly(ethylene oxide-*alt*-methylene
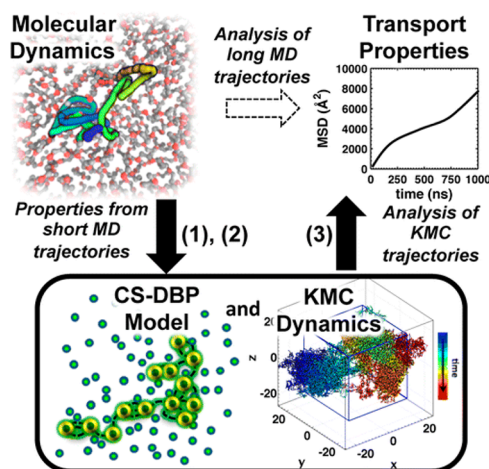
oxide) and poly(methylene oxide) through high reorganization energy or the low density of solvation sites in poly(propylene oxide) and poly(trimethylene oxide). The model also showed that the most efficient lithium transport occurs through short hopping that involves exchange of only one or two oxygens in the solvation shell.

3.6. Modeling of Macroscopic Properties

The last level of the MSM paradigm for electrolytes is the modeling of macroscopic properties, for example melting/boiling/flash points, glass transition temperatures, solubilities, viscosities, etc. The developed procedures are generally fast and allow for screening of a large number of compounds to discover some tendency between easily obtained data from high-level calculations and observed electrolyte parameters. The approach is proven to be an effective and reliable screening tool for pharmaceutical drugs and separation thermodynamics. Moreover, it can be seen as a computational version of chemical intuition and will moreover constitute a cornerstone when machine learning techniques will be more widely employed. It is important to note that screening is often only interested in the correct ranking, not a correct value with respect to experimental data.

The electrolyte parameter that most easily can be directly connected with data from DFT calculations is the electrochemical stability. Borodin et al. calculated the absolute oxidation and reduction potentials to assess electrolyte stability for a wide range of carbonate and phosphate molecules.[14] However, Husch et al.,[300] Brox et al.,[301] and Korth[302] showed that much cheaper computationally parameters like the ionization potential (IP) and electron affinity (EA), or even HOMO and LUMO energy levels, can be successfully used as for estimating electrochemical stability. Additionally, Husch and Brox introduced data from a COSMOtherm analysis of DFT calculations to the procedure, thereby predicting viscosity melting, boiling, and flash points, all important parameters for electrolyte solvents for LIBs[300,301] and LOBs.[303]

Another important parameter for new generation battery electrolytes, e.g., for Li-air and Li-S batteries, is the solubility of the cathode active material: oxygen and sulfur.[303,304] In this context, Jeschke et al. showed on a thermodynamic approach to estimate the elemental sulfur solubility in Li-S electrolytes based on COSMOtherm simulations. The calculated chemical potential of sulfur in different solvents were used to quantitatively describe solubility, whereas the shielding charge density distribution gave more qualitative information about the roles of specific solvent interactions.

4. ELECTROLYTE INTERFACES AND INTERPHASES

The borders between the electrolyte and the electrodes are essential for the funtionality of any battery; it is here the ions are transferred to or from the active materials to realize the operational redox reactions. For LIBs, the contact interface also usually leads to a certain degree of electrolyte decomposition, especially at the negative electrode due to the inherent electrochemical meta-stability under the potentials applied and thereby the formation of an "interphase at the interface", the solid electrolyte interphase (SEI) of the decomposition reaction products. Ideally, the SEI will transport lithium cations rapidly, while insulating with respect to electron transfer and hereby block any further electrolyte decomposition, and hence passivate the electrode surface. The SEI itself is a function of both all the materials used, salts, solvents, and additives in the electrolyte, and the composition of the electrode (in terms of chemistry and formulation), as well as the cell operating conditions (e.g., potential, cycling rate, temperature, etc.). All of this can, at least in priniciple, be described by MSM, from the very ion transfer and reduction/oxidation reactions creating the initial SEI to the growth of the interphase as a function of cycling, with various targets for the different types of MSM approaches (Table 1). Modeling of interfaces between battery

Table 1. Types of MSM Applied to Electrolyte Interfaces and Interphases

	MSM approach	SEI property/scientific problem
first principle MD	MSMSL	composition and decomposition reactions
reactive MD	MSMSL	decomposition reactions
classical MD	MSMSL	transport and mechanical properties
hybrid MC MD	MSMIC	formation process
kMC	MSMSL	formation process
macroscopic models	MSMTC	cell capacity fade

electrodes and electrolytes generally employs subsequential (MSMSL) or iterative (MDMIC) linking between different levels of models. Studies of simple formation and transport processes rely on data that are obtained thanks to quantum-mechanical models. More advanced modeling of battery properties needs much longer timescales that are achieved by coupling dynamic simulations with a statistical approach either using MSMSL (kMC) or MSMIC (hybrid MD/MC). Finally, to describe the impact of the interfacial layer formation on macroscopic battery performance requires models to describe reactions, diffusion, etc., simultaneously (MSMTC).

4.1. First-Principles Molecular Dynamics

First-principles MD simulations have been successfully used to model the very initial steps of the various processes at the electrolyte–electrode surfaces in detail, including the electrolyte degradation and SEI formation, as this technique is restricted to very short timescales, max. ca. 20 ps. As for the scientific field at large, most studies have focused on the decomposition of the organic carbonate electrolyte solvents at different common negative electrode surfaces: graphite,[305,306] lithium metal,[307−309] silicon,[310] and tin.[311] Starting with graphite and the processes that occur during (over)charging and the risk of lithium plating and/or electrolyte degradation was modeled using fully lithiated LiC_6 layers in contact with the electrolyte in order to specifically study the effect of surface functionalization of different graphite edges.[305,306] Thereby, no lithiation process of the electrode can be simulated but rather the relevant electrolyte decomposition mechanisms. Both studies by Leung et al.[305] and Ganesh et al.[306] showed fast EC solvent decomposition initiation at graphite edges rich in oxidized sites such as terminal C=O, where electron density transfer to EC results in the formation of CO_3^{2-}/C_2H_4 and $O(C_2H_4)O^{2-}/CO$ pairs. Similar results were found for C-OH terminated edges, followed by a transfer of H^+ toward ethylene glycol formation. For C−H terminated edges, however, no EC decomposition was observed, that is consistent with generally observed electrochemical activities.[312] Leung et al. explained the positive effect of the presence of oxygen atoms at the graphite edges on reduction initiation with facilitation of charge transfer.[306] These oxygen atoms can coordinate lithium cations and provide a way to directly transport electrons from LiC_6 to EC. A similar explanation was presented by Ganesh et al. studying the Li-ion diffusion from the electrode into the solvent, showing a correlated movement of EC and electrode edges to be crucial for the diffusion of Li^+. O/OH groups of both electrode and solvent interact with the cations and thus facilitate diffusion through the interphase, while for C−H terminated edges, the lithium remains inside the graphite electrode.[305]

Yu et al. simplified the system to study EC decomposition, making use of experimental data, suggesting that the decomposition mechanisms at both graphite and lithium metal electrode surfaces are analogous but faster for the latter surface,[313] which is why it can be successfully employed as a model electrode to study the mechanism.[309] With the use of this approach, simulations resulted in breaking of the bond between $C_{carbonyl}$ and O_{ring}. Furthermore, Yu et al. showed that complement prediction can be obtained with one- and two-electron excess in the liquid phase of the electrolyte in the absence of any electrodes.[309] Such simulations rendered the excess electron to be delocalized onto two EC molecules, albeit primarily on EC molecules not coordinated to Li^+. Furthermore, the predicted barrier of bond cleavage for EC with an excess electron (EC^-) is lower than for the EC^--Li^+ complex, resulting in decomposition of the former, while the presence of Li^+ thus considerably stabilizes EC. The second injected electron usually attacks EC^-, causing breakdown via a classic two-electron mechanism. The decomposition mechanism has been the subject of many FPMD studies targeting the competition between distinct types of bond cleavage in EC.[306,308,309] Leung et al. performed simulations of 32 EC molecules between two Li metal slabs of 6 atom thickness to mimic a cell of Li|EC|Li, resulting in 11 out of 12 of the decomposed molecules breaking down via $C_{carbonyl}$−O_{ring} bond cleavage versus only 1 via C_{ring}−O_{ring} bond cleavage. This is remarkable as both reactions have extremely low-energy barriers and the product of the latter, CO_3^{2-}, is thermodynamically very stable.[308] The reason for this behavior is speculated to be the presence of bend geometry of

EC close to the lithium electrode, which easily decomposes. Brennan et al. used FPMD simulations to determine the preferred adsorption sites and orientations of both EC and PC at a lithium metal electrode using a model system of 7 bulk Li crystal layers.[307] Three types of orientations: A, EC connected to two lithium atoms by two oxygen atoms; B, EC connected to two lithium atoms by one carbonyl oxygen; and C, EC connected to one lithium atom by one carbonyl oxygen, were found to occur for both EC and PC (Figure 28). (A) was found
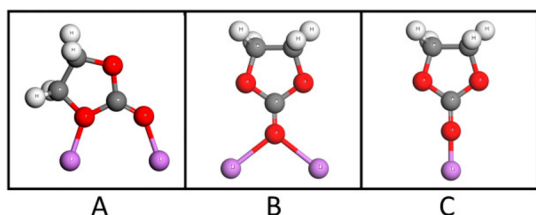

Figure 28. Classification of the types of adsorption orientations for EC/PC. Reproduced with permission from ref 307. Copyright 2017 Elsevier Ltd.

to be the most stable orientation and thus the one studied in more detail. In (A), EC decomposed by first accepting an electron from the electrode and subsequently breaking the $C_{carbonyl}-O_{ring}$ bond, followed by transfer of another electron from the Li surface and breaking the second $C_{carbonyl}-O_{ring}$ bond. The decomposition of PC was found to be very similar, albeit much slower; EC was found to decompose within 7 ps, whereas PC needed more than 20 ps, which was ascribed to a higher barrier of bond dissociation induced by the presence of the methyl group, a fact not commented upon further or explained.

FPMD simulations have also been applied to study EC reduction at Si electrodes.[310] Here various degrees of lithiation resulted in significant impact on the reduction mechanism, in terms of EC decomposition, and furthermore different compositions and physical properties of the SEI. EC reduction was found possible even at the very early stages of Si electrode lithiation ($LiSi_4$, $LiSi_2$), initiated by the formation of C—Si bonds during adsorption and followed by simultaneous two-electron reduction of EC (Figure 29). The more reactive surfaces of various Li_xSi_y alloys reduced EC according to two two-electron mechanisms: simultaneous reduction by two electrons of the solvent molecule adsorbed at the electrode and sequential reduction by one and another electron of molecules in the electrolyte close to the interphase. The surface of the heavily lithiated phase, $Li_{13}Si_4$, is very reactive and reduces EC via a four-

electron mechanism. Overall, the reactivity of Si electrodes was found to be dependent on bulk geometric factors such as crystallographic planes and atom—atom distances,[310] in stark contrast to the main activity being at the edge groups for graphite electrodes. The simulations show that the ability of EC to interact with the lithium atoms at the surface plays a most important role: too short distances between atoms at the electrode surface can hinder Li-EC interaction and even obstruct the reduction process.

Another electrode surface was studied by Moradabadi et al., comparing the reduction of EC on different Sn- and Li-based electrodes: unlithiated Sn, Li-covered Sn, lithiated Sn ($Li_{17}Sn_4$), and Li metal.[311] Decomposition of EC was found for all surfaces except for the unlithiated Sn. Additionally, a lower degree of electron transfer was required to reduce EC via a two-electron mechanism toward CO_3^{2-} on the Li-covered and lithiated Sn electrodes (−1.90 e and −1.84 e, respectively), as compared to the Li metal electrode (−2.4 e).

FPMD simulations have also been used to study interphases created by using another distinct family of electrolytes (e.g., based on DME/DOL), a solvent combination generally applied to Li−S batteries.[314,315] Here, two types of Li metal electrode representations were used: a lithium slab composed of 6 layers and a lithium cluster of 35 atoms. A higher reactivity, resulting in decomposition of both DOL and DME was obtained for the latter model, while only DOL decomposed on the former.[314]

This was inferred to be due to the higher activity of lithium atoms exposed to the solvent molecules in a cluster, and hence, the latter model was to be preferred.

As also the anion decomposition is important for the SEI formation and stability, Ganesh et al. studied $LiPF_6$ salt decomposition and formation of LiF near the anode surface,[305] while even more pronounced anion decomposition has been observed for LiTFSI[315−319] and LiFSI.[316,318,320] The presence of a TFSI anion in the electrolyte seems to prevent reductive decomposition of solvents like DME, DOL, and AN by the anion being reduced prior to the solvents,[316,317] corroborated also for TFSI-based ILs, using a Li metal electrode surface model, leading to anion decomposition but no decomposition for the Pyr14 cation.[319] A rapid decomposition of the TFSI anion is initiated by C−S and/or S−N bond cleavage due to charge transfer from the Li electrode.[319] A comparison of the TFSI and FSI anions showed that their decomposition paths differ significantly;[316,318] TFSI undergoes a less complete reduction, larger fragments were found as SEI components, and facilitates charge transfer from the anode, whereas FSI
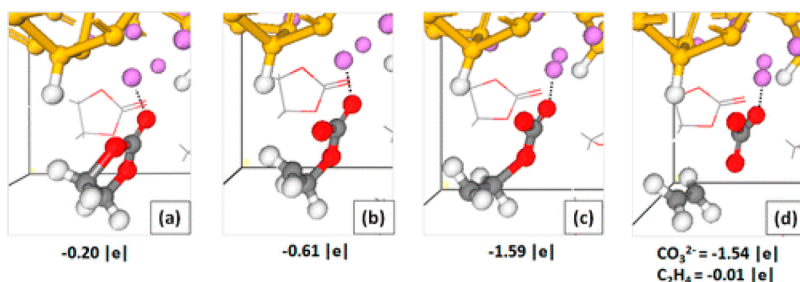

Figure 29. Decomposition of EC. Initially one electron is transferred from the surface to (a) Li-EC, causing a (b) $C_{carbonyl}O_{ring}$ bond to break. Subsequently, a second electron is transferred to (c) the EC− radical anion, triggering the breaking of a second $C_{carbonyl}-O_{ring}$ bond and (d) generating the $C_2H_4 + CO_3^{2-}$ pair. The net charges of the EC molecule and the CO_3^{2-}/C_2H_4 products are shown. Reproduced from ref 310. Copyright 2013 American Chemical Society.

shows a more complete decomposition and easily releases F⁻, resulting in LiF formation (Figure 30).
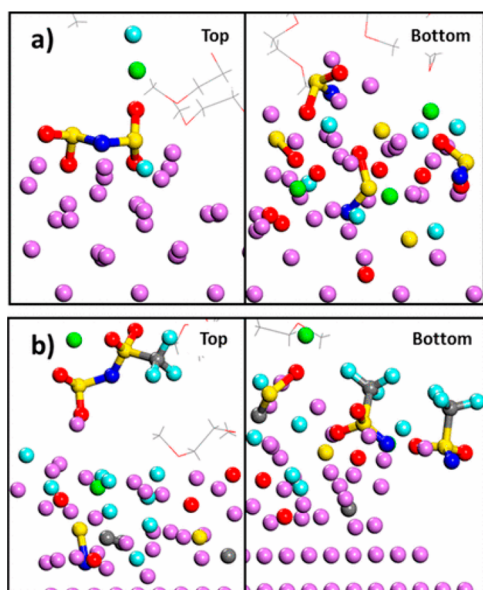

Figure 30. SEI after 16 ps of simulation using 4 M (a) LiFSI or (b) LiTFSI in DME electrolytes vs a lithium surface. Reproduced from ref 316. Copyright 2017 American Chemical Society.

4.2. Reactive Molecular Dynamics

While the FPMD MSM approach can target the very details of the fundamental reactions, the entire process of SEI formation calls for other MSM approaches. At the next level of MSM, this can be studied using reactive MD simulations, so far employed mostly for electrolytes based on organic carbonates[321−325] but also for some less common solvents like tetraglyme.[326] Here the parametrization and validation of the reactive FF vs QC calculations is usually made before the MD simulations. As an example, Bedrov et al. focused on the development of the FF to correctly reproduce the ring-opening reaction of Li⁺-EC⁻ (Figure 31), as this transition is considered to be essential, see above, for the entire EC decomposition process and therefore must be accurately predicted.[321] Reactions of EC⁻ in both gas and liquid phase have been targeted in order to explore possible reaction pathways between EC-based radicals.[321] The gas phase calculations revealed a probability of lithium butylene dicarbonate (LiBDC) formation, which was also obtained for low concentrations of radicals in the liquid phase. The influence of the bulk EC environment on the free energy barrier on the EC-ring opening reaction was thus found to be minor.

A more detailed analysis of the SEI-formation process, however, requires an introduction of an electrode to the system. Kim et al. considered two different electrode models together with EC and DMC solvents: a slab of Li metal and lithium atoms randomly placed at 1 nm from the surface (Figure 32).[325] The latter approach was used to assess the role of the Li atom density for the SEI formation process and more generally mimic a chargeable electrode. This showed that (i) lithium ethylene dicarbonate (LiEDC) is formed at the very early stages of the SEI formation, as an effect of recombination of two radicals with release of C_2H_4, unlike the study of Bedrov,[321] focusing on simple recombinations leading to LiBDC, and (ii) a high Li atom concentration leads to further decomposition to Li_2CO_3 and Li_2O. The primary and secondary decomposition reactions
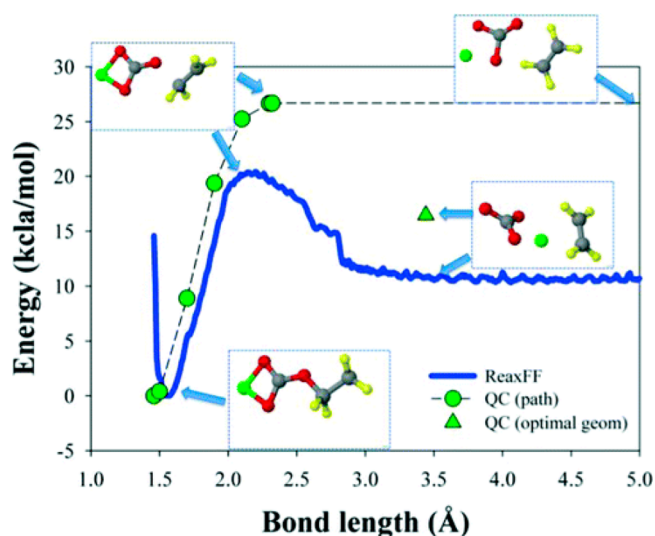

Figure 31. Energy profile for breaking C_2H_4 from o-EC⁻/Li⁺, as obtained from QC calculations and gas phase simulations using ReaxFF at 10 K. Reproduced from ref 321. Copyright 2012 American Chemical Society.
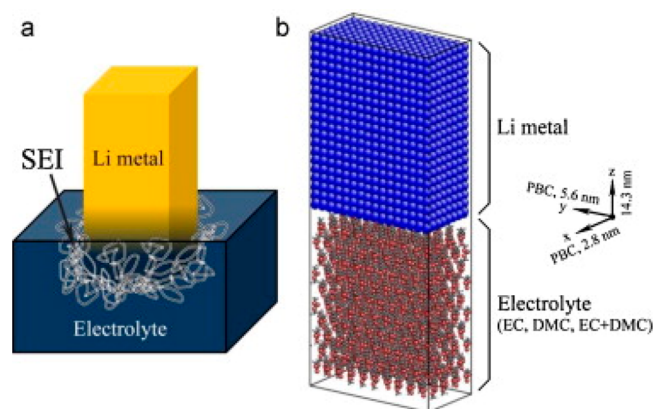

Figure 32. (a) Schematic of a Li metal electrode dipped in an electrolyte. (b) Initial configuration of the cell. Reproduced with permission from ref 325. Copyright 2011 Elsevier Ltd.

showed on the formation of two SEI-layers for the lithium metal slab electrode model: one inner layer closer to the electrode containing inorganic salts and one outer layer of organic salts. This is in agreement with the experimental literature showing higher concentration of compounds like Li_2CO_3 and LiF in the layer closer to the electrode.[327−330] DMC-based electrolytes showed less reactivity and generated the formation of $LiOCH_3$ together with a smaller amount of $LiOCO_2CH_3$ in the outer layer rather than LiEDC, while the inner layer is still dominated by Li_2CO_3.[325] An application of an equimolar mixture of EC and DMC gives, as expected, the mixture of all types of compounds with decomposition products of EC more expected (Figure 33).

The SEI formation on Si electrodes showed dangling Si atoms to act as catalysts for the dissociation of EC, resulting in evolution of C_2H_4 and CO gases, even in the absence of any lithium (i.e., at a fully discharged state of the electrode).[323] Comparing the electrolyte decomposition on pristine and oxidized (SiO_2) Si electrodes showed an inhibiting effect of oxygen atoms, due to the reduction of the dangling Si atoms and thereby a better passivation of the surface.
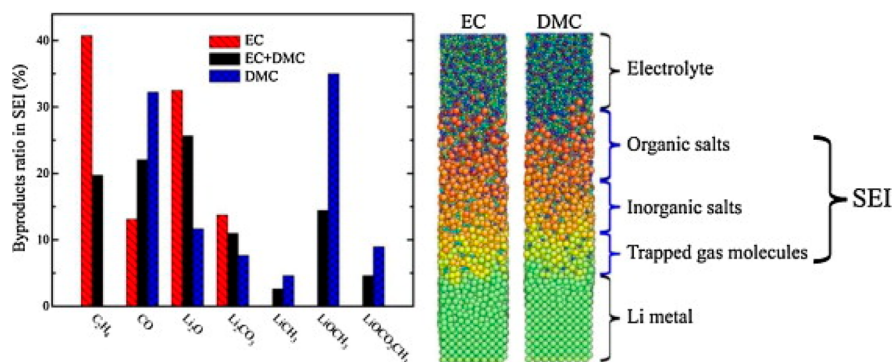
Figure 33. Distribution of the SEI components for different electrolytes (left). Atomic configurations from MD simulations; the components of the SEI are identified (right). Reproduced with permission from ref 325. Copyright 2011 Elsevier Ltd.
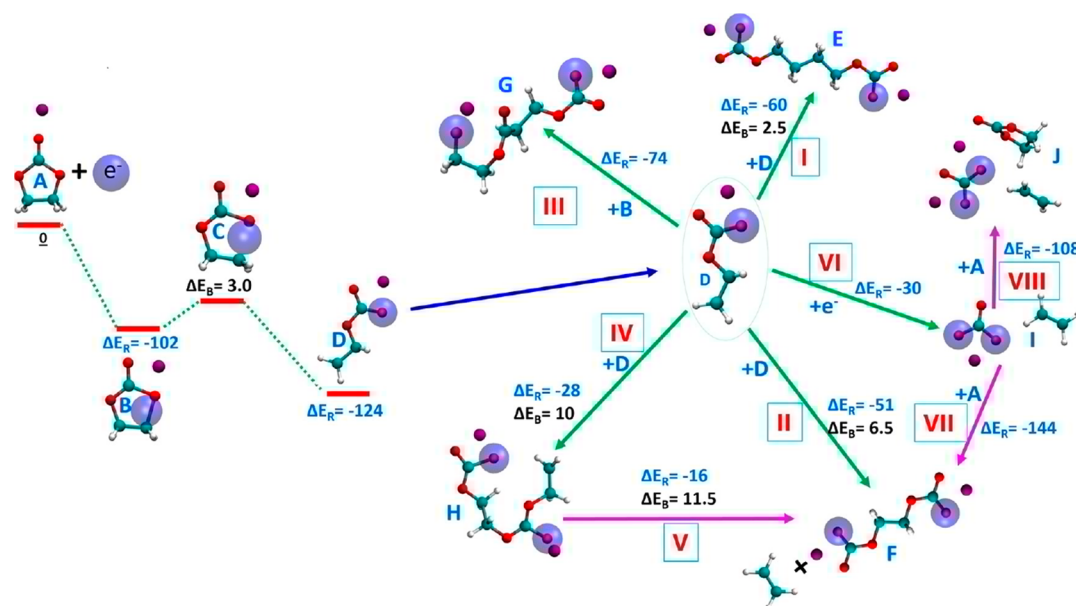

Figure 34. Potential energy profile for the reduction of EC/Li$^+$ and the radical termination reactions according to various pathways. ΔE_R and ΔE_B denote the reaction energy and reaction barrier, respectively. Color scheme: cyan, carbon; white, hydrogen; red, oxygen; purple, Li$^+$; large blue sphere, electron. Reproduced from ref 322. Copyright 2016 American Chemical Society.

Reactive MD simulations were also used to study the efficiency of preventing solvent decomposition by employing SEI-forming additives[323] or PEO-graphite artificial SEI-layers.[324] The electrode was modeled as a four-layered AB-stacking graphite, and both approaches were found to suppress solvent decomposition, the latter to prevent solvent cointercalation. Using the PEO-style of protection, the thermal stability of the SEI-layer has also been targeted, showing a much better stability at 353 K for PEO chemically bonded to the electrode than PEO coated at the H-edged graphite plane.[324] Kim et al. rather focused on the mechanical properties of the SEI, showing components formed by DMC decomposition to lower the Young's modulus as compared to SEIs formed solely by EC decomposition.[325]

The ReaxFF method is supported on a quite sophisticated scheme to treat electrons in its energy functional, but its implicit description of electrons makes it impossible to separate out any long-range charge transfer, even between molecular fragments that are well-separated.[331] The consequence is, for example, inaccurate values of EAs and IPs, which is why ReaxFF has a somewhat limited ability and applicability to describe redox reactions. Extensions to ReaxFF have, however, been developed specifically to enable studies of electron transfer reactions; eReaxFF[332] was recently applied by Islam et al., wherein an electron is included as a particle. It enables one to track the role of excess negative charge during the entire decomposition path (Figure 34). For an EC-Li$^+$ complex, the excess charge was predominantly found to be located between the C$_{ring}$ atoms and the O$_{ring}$ atoms, causing these bonds to eventually break. Subsequently, the termination reactions of the radicals produced was found to be highly dependent on the radical concentration; a low concentration reduces the probability of reaction between two radicals, while spontaneous production of Li$_2$BDC and Li$_2$EDC + C$_2$H$_4$ occurs at higher concentrations. These simulations were not able to predict any formation of Li$_2$CO$_3$, even if it is generally observed in the experimental studies.[327,329] The difference between the prediction and experiment is due to relatively low concentrations of lithium and excess electron concentration in the simulation set.[326]

Cheng et al. performed extensive (500 ps) QM-based reactive MD simulations of a Li/Li$_6$PS$_5$Cl interface and could thereby target several decomposition products, Li$_2$S, Li$_3$P, LiCl, and LiP, which were detected through simulated XRD patterns and compared with experimentally determined diffractograms.[333] It

was concluded that the weak bonding between P and S poses an intrinsic stability problem at lower potentials. This led also to a deterioration of the transport properties in the simulated small-scale battery cell and thereby to a degradation of the modeled battery performance.

4.3. Classical MD

Moving to larger systems, the MSM modeling using classical MD is often still restricted to investigating the SEI-layer structure and the Li$^+$ mobility within the SEI-layer. The requirement for this technique's force field is generally based on the quantum chemistry results, as also mentioned in section 3.3. To study properties of the passivation layer, Borodin used an APPLE&P force field and performed a fitting of the FF parameters based on the *ab initio* data for LiCO$_2$OCH$_3$ and Li$_2$EDC prior to simulations.[334] Developed FF was shown to predict binding energies between lithium cation and both solvent and anionic components of SEI with very good agreement versus values from the DFT level.[335] Such prepared and validated polarizable FF was used to investigate SEI layers made up of Li$_2$EDC and Li$_2$BDC.[334−336] The temperature dependence of the Li$^+$ transport in an SEI layer composed of Li$_2$EDC was found to be minor, but dependent on the structure; the diffusion in an ordered SEI-layer was found to be 2−3 times faster than in a disordered/amorphous layer.[334] The activation energy for Li$^+$ solvation-desolvation was found to be lower than the activation energy for Li$^+$ transport in bulk Li$_2$BDC,[335] which indicates that Li$^+$ transport, not desolvation, is the limiting process. The former layer showed similar behavior, although observed activation energy of solvation-desolvation was slightly larger.[335] When investigating other SEI layer components, the activation energy of Li$^+$ transport in Li$_2$EDC and Li$_2$BDC was shown to be only slightly lower than for Li$_2$CO$_3$, and practical improvements can be achieved by allowing formation of highly ordered SEI layers by employing very slow C-rates (Figures 35
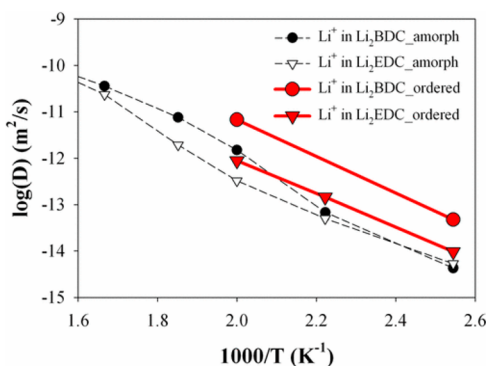

Figure 35. Li$^+$ cation diffusion coefficients for ordered and amorphous SEI models consisting of Li$_2$BDC and Li$_2$EDC. Reproduced from ref 336. Copyright 2017 American Chemical Society.

and 36).[336] For Li$_2$EDC versus Li$_2$BDC, the increase in the length of the alkyl chain spacer between the carbonate groups results in the formation of ordered layers of Li$^+$, which increase the mobility. At the same time, however, this makes the SEI softer and thereby reduces its ability to resist dendrite growth.[336] A study of the PC decomposition product, Li$_2$PDC, suggests the formation of a lower density SEI more soluble in the electrolyte as compared to the corresponding EC path product.[337] This was ascribed to the additional methyl group, weakening the adhesion to the graphite surface by interaction between the methyl group and graphite. Despite the fact that there are a number of studies
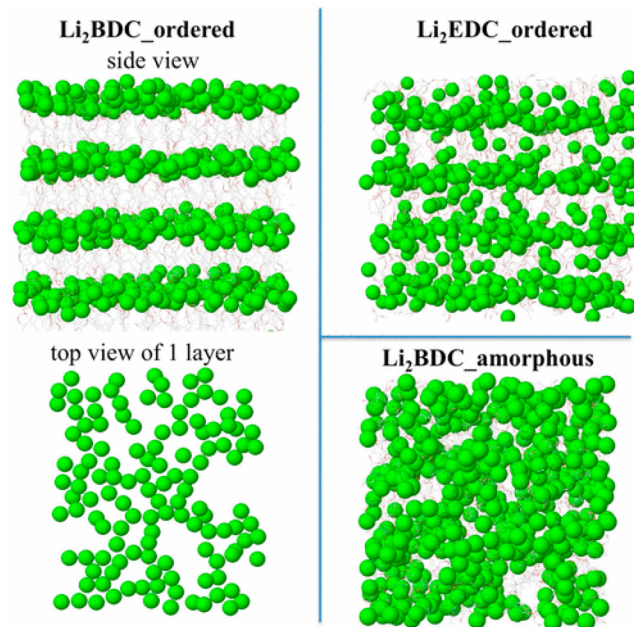

Figure 36. Snapshots highlighting the Li$^+$ distribution in ordered Li$_2$BDC and Li$_2$EDC, and amorphous Li$_2$BDC, all at 393 K. Reproduced from ref 336. Copyright 2017 American Chemical Society.

suggesting PC cointeracalation and exfoliation of the graphite,[338−340] the simulations were not able to predict this happening, as already reduced products of PC decomposition, predicted by DFT calculations, were used for the simulations.

Jorn et al. simulated SEI layers of a graphite electrode with an external potential of 3 V across the cell applied,[341] an approach providing a molecular level insight into the distribution of solvent and ionic species in the SEI layer under more "realistic" conditions which in turn revealed local ion adsorption to be crucial for their correct description (Figure 37). The amorphous SEI formed significantly affected the electrolyte by screening the electric field and thus reducing the restructuration of the solvent.

MD simulations have also been used to study the behavior of electrolytes close to a polarized electrode, especially for ones that are stable toward a low potential of graphite and do not cause fast formation of passivation layer like ILs and solvate ionic liquids (SILs).[234,244,246] For the latter, the electric field changes the structure of the Li-tetraglyme(G4) complex in the Li(G4)TFSI electrolyte toward coordination of lithium ions by more than one glyme molecule,[234] while Haskins and Vatamanu showed for more regular IL base electrolytes, like [Pyr14][TFSI], [Pyr13][FSI], and [EMIm][BF$_4$], that the orientation of the ions strongly depend on the electrode potential and that the presence of lithium cations induces disorder in the electric double layer by their strong anion coordination (Figure 38).[244,246]

4.4. Monte Carlo (MC)

Different MC-based MSM approaches have been used to model SEI-layers, primarily hybrid MC/MD and kinetic MC with the aim of investigating the formation of the SEI, targeting longer "timescales". Hybrid MC/MD simulations were employed for a graphite electrode, modeled as a pile of 10 graphene sheets, and in contact with 1.1 M of LiPF$_6$ or NaPF$_6$ in EC- and PC-based electrolytes.[342,343] To mimic SEI formation by charging the cell, an initial electrode potential of ca. 2 V was introduced by employing a single point charge at the center of each carbon
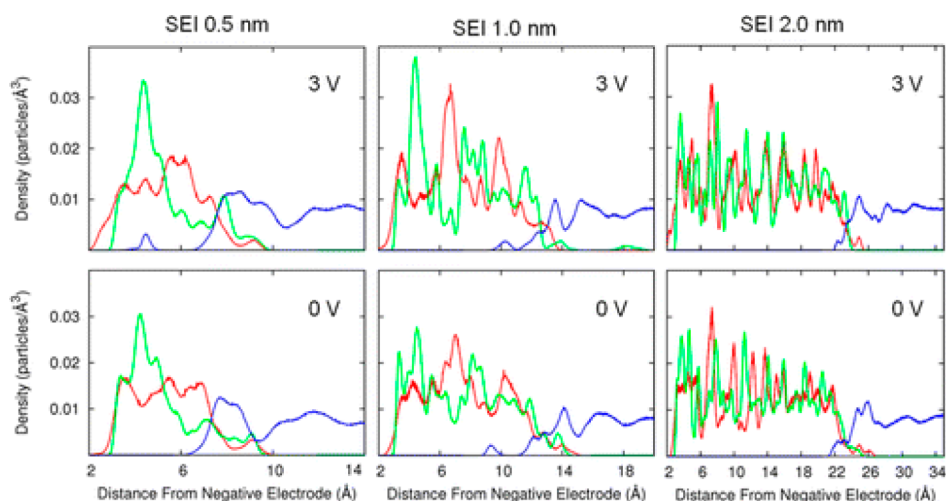
Figure 37. Density distributions for an electrochemical cell composed of an SEI-layer consisting of Li_2EDC with varying thickness. The thickness and voltages are indicated in each panel, with the density of Li (red lines) and carbonate groups (by center of mass, green lines) in the SEI and the EC (by center of mass, blue lines). Reproduced from ref 341. Copyright 2013 American Chemical Society.
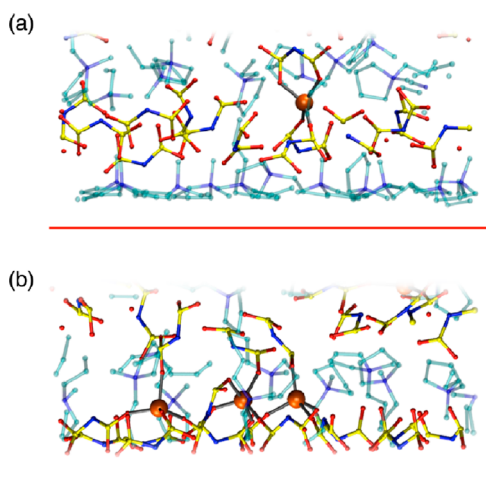

Figure 38. Representative Li^+-anion coordination in the double layer at (a) negative electrode potentials and (b) positive electrode potentials. Red and blue bars indicate the (x,y) plane of the anode and cathode surfaces, respectively. Reproduced from ref 244. Copyright 2016 American Chemical Society.

Figure 39. Model system and reaction scheme (cyan, carbon; red, oxygen; white, hydrogen; orange, phosphorus; green, fluorine; blue, lithium). Reproduced from ref 342. Copyright 2014 American Chemical Society.

atom of the graphite electrode and the intercalation of Li^+ was restricted, all in order to focus on the differences resulting from specific SEI-formation processes, introduced based on experimental and DFT-derived data (Figure 39). The introduction of specific reaction steps to the MC/MD simulations consisted of creating a list of pairs of reactive atoms followed by a random selection of a pair from the list of possible reactions. Subsequently, the atomic potential parameters and potential functions were applied to the new molecules resulting from the formation reactions and this latter system subject to a short MD simulation. From this, the change in energy during the overall reaction was computed, and based on a Metropolis algorithm, the reaction was either accepted or rejected.[342] These MC/MD MSM simulations can treat SEI-layer formation for systems several hundred times larger and for several tens of thousands times longer than FPMD simulations but, on the other hand, only for a limited number of preselected reaction paths. While this methodology has been successfully applied to compare the SEI-layer formation processes in EC- and PC-based electro-
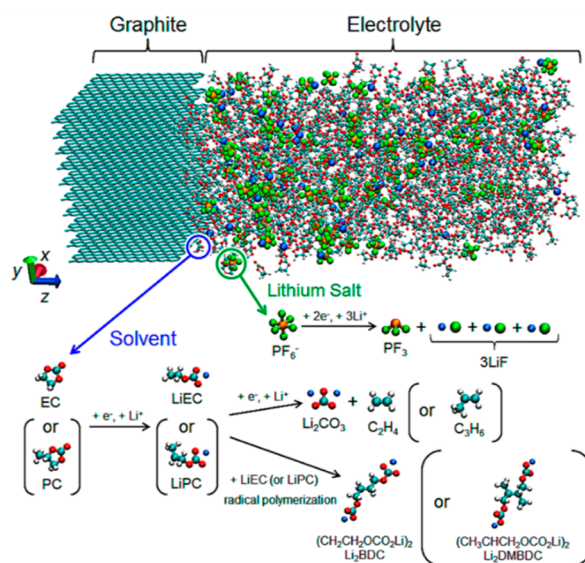
lytes,[342] it has also been used for the altered mechanism of SEI-layer formation when having FEC as an additive in a PC-based SIB electrolyte.[343] The observed decrease in irreversible capacity and SEI film thickness using FEC was shown to be due not only to the FEC decomposition reactions but also to the presence of the strong electronegative fluorine atom, causing a suppression of solvation of organic salts into the bulk electrolyte by enhancing the network formation between SEI species.[343]

kMC has been applied to study the SEI formation on a graphite surface,[344] using a 25 × 25 molecular mesh where 4 types of events can occur: adsorption, desorption, surface diffusion, and formation of passive (inactive) material (Figure 40). The rate of each reaction was determined based on the electrode state of charge (SOC), and once a given event was (randomly) selected, the transition to the new configuration was executed. Additionally, all lithium metal formed was assumed to intercalate immediately (i.e., no lithium metal plating is
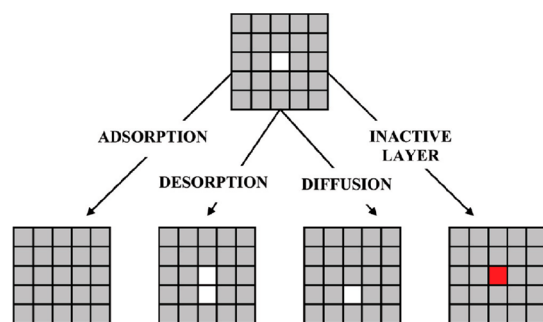
Figure 40. Schematic representation of the 4 types of events selected to occur in the kMC simulations. Reproduced with permission from ref 344. Copyright 2011 The Electrochemical Society.

possible). This makes it possible to explicitly address properties such as surface heterogeneity and mimic an experimental setup of an electrode being charged under a constant potential. Running the cell for over 100 cycles showed that the active surface coverage, a phenomenon connected with the formation of the SEI, decreases slowly in the very initial stages of the cell operation and then more rapidly. Thus, despite the rate of SEI formation being higher in the initial cycles, this does not significantly affect the capacity, as the surface is not fully covered.

An even more advanced kMC MSM was developed by Hao et al. in order to investigate the growth of the SEI at a graphite electrode during charging,[345] wherein the process was described in 3 steps: adsorption of Li^+ and solvent on the SEI surface, diffusion through the SEI, and electron transport followed by Li^+ intercalation or SEI formation. The simulation describes the SEI fully in 3D and allows for an analysis of the SEI thickness, with a linear relationship between the thickness and the square root of charging time obtained for extensive cycling. As expected, the lithium intercalation rate and charging time were both found to be governed by the lithium reduction rate and the lithium transport through the SEI. At lower temperatures, a high Li reduction rate was found but also a higher resistance of the SEI, diffusion likely being the limiting process. At higher temperatures, on the other hand, a low Li reduction rate causes increased total charging time and a minimum of the required time (Figure 41). Three stages of SEI growth during the very first charging cycles were found: (i) sluggish SEI formation
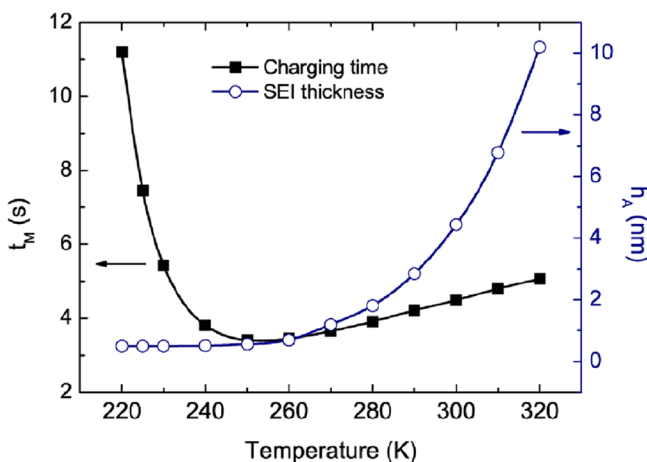

Figure 41. Temperature effect on the total charging time and SEI thickness during a full charging process. Reproduced from ref 345. Copyright 2017 American Chemical Society.

above 0.8 V, (ii) rapid SEI growth, using the abundancy of solvent adsorbed on the electrode surface, and (iii) reduced SEI growth rate due to the complete consumption of the adsorbed solvents and subsequently limited by the transport of solvent through the SEI. Thus, the diffusion within the SEI significantly affects its growth rate; faster lithium cation transport and/or slower transport of solvent molecules result in a decrease in the reduction of solvent and SEI growth (Figure 42).
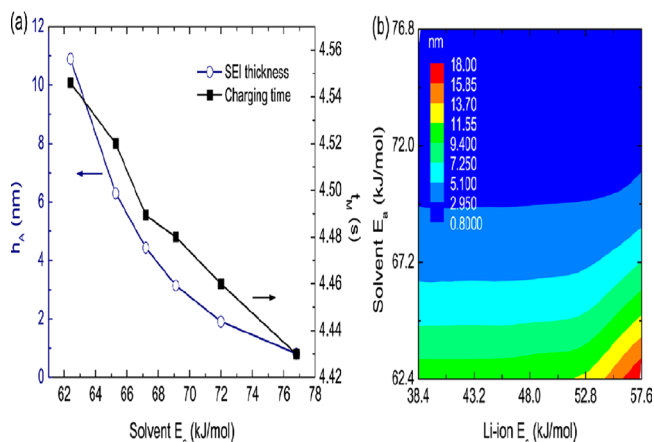

Figure 42. Effect of SEI solvent activation energy on the total charging time and SEI thickness during a full charging process. Reproduced from ref 345. Copyright 2017 American Chemical Society.

More recently, Roder et al. implemented a kMC model with a few reaction mechanisms to study the formation of Li_2CO_3 and LEDC as products of EC reduction on graphite (Figure 43),
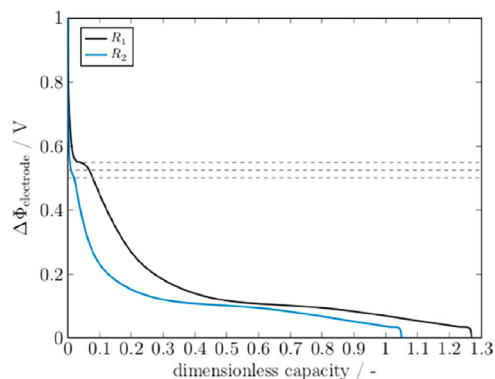
Figure 43. Calculated electrode potential during the first charge of the formation process for electrodes with particle radius $R1 = 3 \times 10^{-6}$ m and $R2 = 10 \times 10^{-6}$ m. Dashed gray lines correspond to the potentials 0.55, 0.525, and 0.5 V from top to bottom. Reproduced with permission from ref 346. Copyright 2017 The Electrochemical Society

resulting in the two-layer structured SEI previously mentioned, the inner being inorganic and the outer organic,[346] that was also observed experimentally.[327−330] In addition, an investigation of the particle size dependency showed impact on the growth rate rather than the final thickness of the SEI: smaller particles lead to larger surface areas and more SEI is formed, resulting in a more distinct plateau at the beginning of the charge event and a higher capacity.[346]

Shinagawa et al. extended this kMC model even further,[347] introducing a cathode to simulate the SEI growth in a LIB full cell, with both electrodes described using a single particle model

(Figure 44). Simulations of hundreds of charge and discharge cycles were conducted prior to analysis, including surface defect

Figure 44. Schematic of the single-particle model used to simulate SEI film growth by kMC. Reproduced with permission from ref 347. Copyright 2017 The Electrochemical Society.
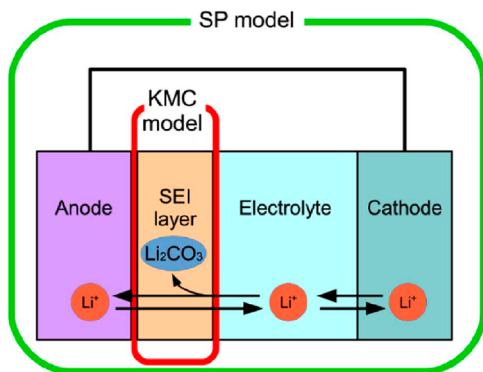
effects on the SEI growth, showing that presence of defects causes higher rate of SEI growth and ruggedness of the surface. All of that together can cause faster fade of the battery capacity.

4.5. Modeling of Macroscopic Properties

The largest spatial scale of MSM used for interfaces is from continuum-scale mathematical models, primarily describing the SEI growth and its lithium ion transport.[348−350] These simulations are based on macroscopic well-developed relationships describing mass and electron transport, using physical parameters obtained either by experiments or computations at more accurate levels. In this context, Christensen and Newman[349] presented a mathematical SEI model used to estimate the growth rate, its resistance, and the irreversible capacity related to the SEI formation. The growth rate was found to depend on the electron mobility in the film, low electric conductivity as well as the layer thickness both limit formation due to hindrance of transport of electrons to the solvent to be reduced.[349] Colclasure et al. chose another strategy and developed a model incorporating the kinetics of several reversible chemical reactions leading to charging the graphite layer and/or formation of the SEI.[348] The growth of the SEI was studied both under open circuit voltage (OCV) at different SOC and charge/discharge conditions (Figure 45), with an increase in electron and Li$^+$ concentrations in the SEI with increasing
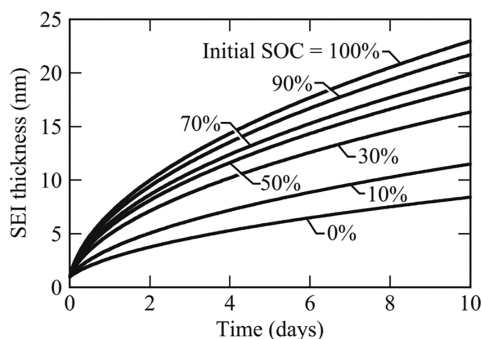

Figure 45. SEI film thickness under OCV as a function of time for various initial SOC. The simulations assumed an initial SEI thickness of 1 nm. Reproduced with permision from ref 348. Copyright 2011 Elsevier Ltd.

intercalation. Higher concentration of both cations and electrons promoted SEI growth, which was mainly limited by slow electron diffusion.

To primarily explain the role of SEI properties and thickness for capacity, fade MSMTC approaches have been employed to include diffusion, decomposition reactions, and electrode charging.[351−356] As a first example, a capacity fade model was built based on active material (lithium) loss due to the solvent reduction,[357] resulting in a dimensionless loss of lithium and a surface film resistance increase both as a function of overpotential and the rate of side-reactions occurring. The studies of Pinson and Safari both used single-particle models to predict battery aging,[351,358] assuming a uniformity of the SEI, neglecting any expansion and contraction of active particles during cycling, applying constant reaction rates, and assuming linear solvent diffusion. A more complicated porous electrode model accounting also for concentration gradients created in the direction of lithium ion propagation did not show any significant spatial variations for the SEI formation,[351] while a one-dimensional model employed to simulate the EIS response during cycling (Figure 46)[351] allowed for estimating the impact
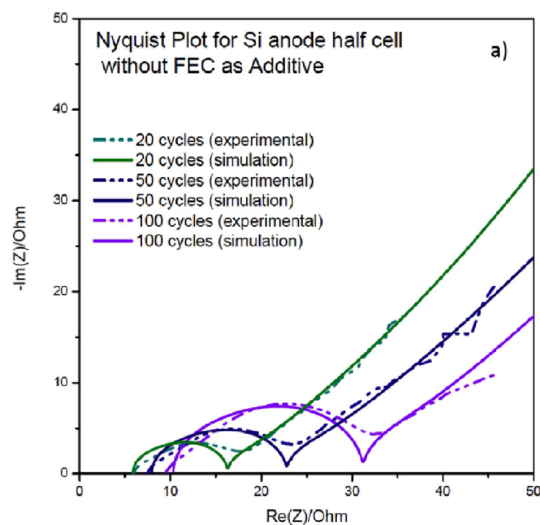
Figure 46. Experimental and simulated Nyquist plots for Si-anode-based half cells. Reproduced with permission from ref 351. Copyright 2017 Elsevier Ltd.

of the evolution of the morphology. A somewhat different model, based on porous electrodes and concentrated solution theory, was used to study the fade caused by SEI growth as a function of different charging protocols,[353] showing fast-charging to create undesired stress and decrease the charge stored but also limit the SEI growth. This unexpected relationship of increasing SEI growth together with a decrease in charging rate can be due to a longer charging time, which means also longer time for side reactions to occur, or it can be related to induction by a high rate mechanical stress that provides a fresh electrode surface.[353] A comparison of constant current and constant current-constant voltage charging protocols for different rates from C/8 to 2C resulted in higher capacity for a single cycle for the latter but faster decrease over the entire life of the battery cell. The constant voltage stage provides a very slow charging, increasing the stored energy but significantly contributing to SEI growth causing capacity fade.

Figure 47. Different structural models for LIB electrode proposed in literature. (a) Assumed main geometrical features. Reproduced from ref 360. Copyright 2010 The Electrochemical Society. (b) Reconstructed by tomography (in blue). Reproduced with permission from ref 362. Copyright 2014 Elsevier Ltd.

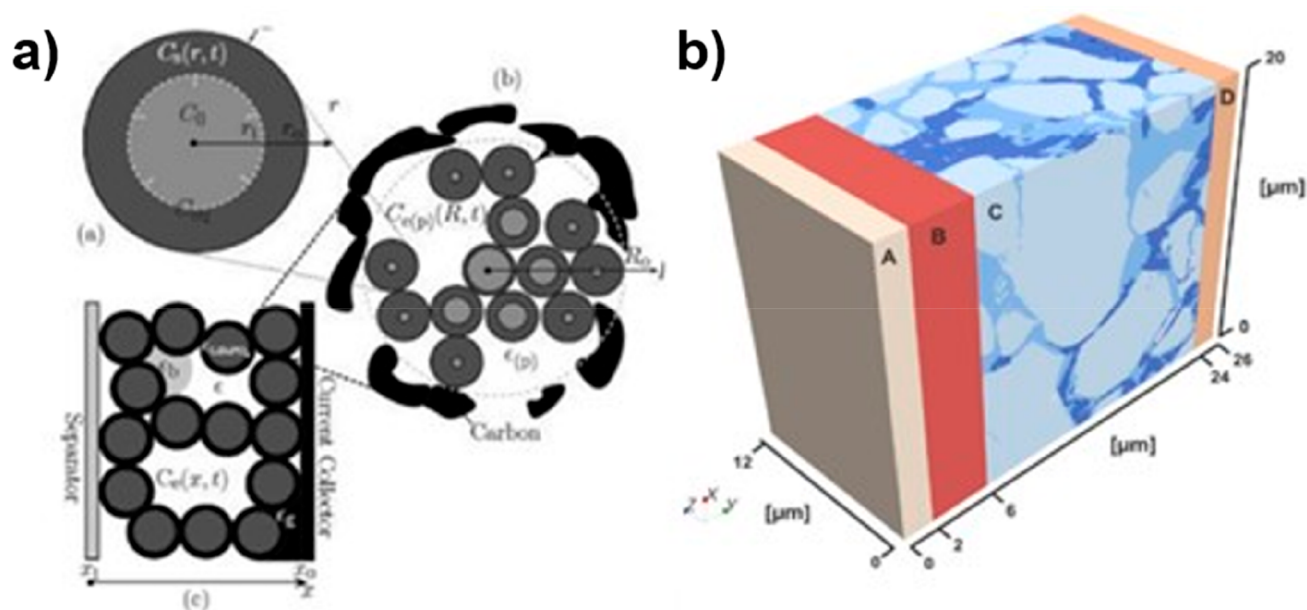To summarize, any accurate computational description of the interfaces and interphases between electrodes and electrolytes must include processes at different time- and length-scales. The basic reactions that create the SEI can only be correctly described by QC simulations. Deployment of this data explicitly or implicitly (e.g., via a FF) under dynamic conditions has been shown to provide a proper relationship between the chemical structure of electrolyte/electrode and the composition of the SEI. From a practical battery properties point of view, the rate of the SEI-layer growth is crucial and this can indeed be described by a combination of parameters that describe single formation processes and statistical approaches. MSM thus seems to be a necessary tool for any correct prediction of the full impact of changes made at the atomistic level on the properties on the macroscopic and finally battery cell level. Unfortunately, most of the approaches of MSM to study interphases is based on MSMSL, which does not fully cover interactions between different scales. Progress is within reach by employing MSMIC to enable better descriptions of the processes.

5. COMPOSITE ELECTRODES

The state-of-the-art MSM efforts at the composite electrode level widely target deepening the understanding of the operation principles of already fabricated composite electrodes, involving carbon, binder, and active material. Indeed, at fixed chemical composition, an approach to ensure high battery energy density and lifetime to meet EVs requirements is to optimize the electrode mesostructural properties.[359] A very ignificant amount of performance MSM has been developed in an attempt to capture the impact of the composite electrode mesostructure on the transport processes and the resulting cell electrochemical response. These models have been applied mainly to LIBs with standard active materials such as $LiFePO_4$, $LiCoO_2$, and graphite, and they fall within the MSMSL and MSMIC categories.

Within this scope, a majority of MSM approaches have been supported on abstract representations of the electrode structure aiming at capturing the main features of real electrodes, such as their porosity, tortuosity, and constituting particles shapes.[360,361] Other MSM models have been built from reconstructed electrode images obtained by using X-ray tomography and 3D focused-ion beam/scanning electron microscopy-FIB/SEM-characterizations of the real composite electrode mesostructure (Figure 47).[362]

5.1. Volume Averaging Method

The volume averaging method (VAM) is among the most used modeling approach for the modeling of batteries. The basic idea of VAM is to circumvent the description of complex microstructural features found in a typical composite electrode. This is done by averaging the relevant properties over a region of the composite electrode small enough with respect to the overall dimensions but large enough compared to the pore detailed morphology (Figure 48).[363,364] Therefore, the subjacent
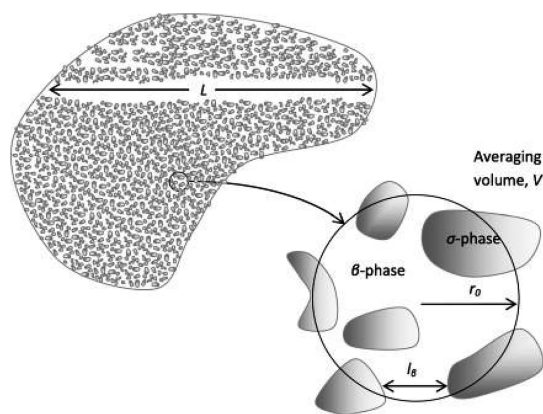

Figure 48. Representation of the volume averaging method applied to a porous medium made of a solid phase, σ, filled with a liquidphase, β. The scale of the entire domain is L, while the pore-scale characteristic length is l_β. Reproduced with permission from ref 364. Copyright 2013 Elsevier Ltd.
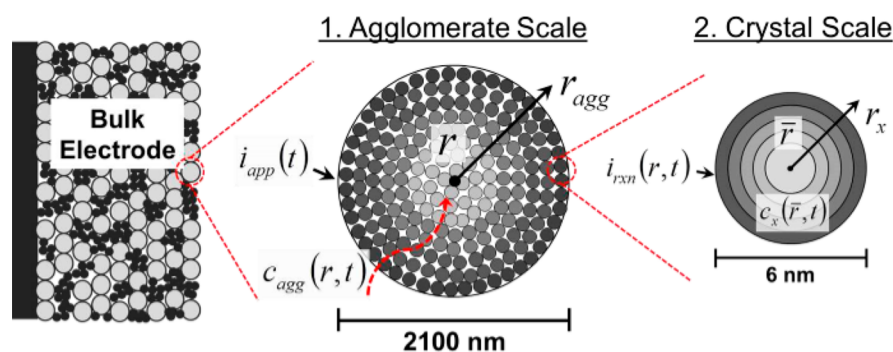
Figure 49. Schematic representation of the agglomerate scale (a scale between the crystal and electrode size). Reproduced with permission from ref 367. Copyright 2015 The Electrochemical Society.

approach can been seen as a MSMSL, as the resulting averaged volumes, capturing the microstructural properties of the composite electrode, are subsequently injected into macroscopic performance models resolving conservation equations through them. More specifically, the electrode is treated as a continuous medium that allows movement of ions and electrons along two superposed continua: an electrolytic solution (ionic transport) and a solid matrix (electrons transport). The porous nature of the electrode is appropriately taken into account. The interfaces between the electrolyte and the solid crystals are treated as sinks/sources of charge via introducing an appropriate electrochemical reaction. This reaction (most commonly quantified by using the Butler–Volmer equation) thus links the transport on the electrode scale ($\sim 10-100$ μm) and the transport inside the solid active crystals ($\sim 10-1000$ nm).

Since its introduction,[128] VAM has evolved significantly in order to take into account different electrode chemistries and different specific structural or morphological phenomena discovered experimentally. Also, improvements in terms of thermodynamic consistency of this approach have been proposed. For example, Lai and Ciucci performed volume averaging of generalized Poisson–Nernst–Planck equations on a de Levie straight pore model to derive an electrochemical model for porous electrodes.[365] Unlike the Newman's model, the proposed approach considers the innate correlation between the thermodynamic and kinetic material properties. There are several important differences as regards the model outcome: for example, the diffusivity in either liquid or solid is related to the conductivity and thermodynamic property (chemical capacitance, thermodynamic factor, or activity coefficient) in the same material.

Despite the successful development and application of the phase field models for certain cases of interest, as discussed in section 2, it should be reiterated that in practical treatments the VAM has been successful due to its robust electrode level framework, rather than due to specific treatment of transport on the particle or subparticle level. This is because, under conditions of practical interest, the transport in batteries is mainly governed by electronic and ionic transport across the whole electrode, whereas the local transport inside the storage crystallites is of secondary importance. The predominance of electrode level transport in realistic batteries is frequently associated with difficulties in electrode engineering where a huge number of active particles (up to 10^{14} per 1 cm^2 of electrode surface) needs to be optimally dispersed and electronically and ionically wired in order to mimic the theoretical conditions found in VAM.

Due to these evident difficulties, many authors have tried to upgrade the original "homogeneous" VAM by introducing complications that mimic the realistic structures. This way a third scale, usually referred to as the agglomerate scale extending over several micrometers, has been introduced and successfully used to explain the effect of nonhomogeneities on the overall transport.[360,366] Later on, the high impact of agglomerate formation on the overall transport properties was also demonstrated in the case of magnetite (Fe$_3$O$_4$)-based electrodes (Figure 49).[367]

In search for the optimal particle distribution inside the electrodes, Chadha et al. have explored the properties of one-dimensional (columnar) structures on the overall transport in TiO$_2$ based electrodes.[368] The Newman's approach is used whereby the transport in solid cylinder is modeled in axial and radial directions, but no phase transformation was included. The authors identified, thanks to their model, optimal column lengths and column spacing as a function of the discharge rate.

Gully et al. showed that the prediction power of state-of-the-art mathematical homogenization techniques can be significantly increased if modeling is combined with suitable imaging and computational tools.[369] In contrast to earlier works,[370,371] they considered three constituent phases of an electrode material, namely the electrolyte, active particles, and carbon-doped binder. The work demonstrates that the effective transport coefficients of a given material with a complex microstructure can be determined based on the properties of the individual phases.

Although VAM has appeared very successful, it has several shortcomings. The assumption of a homogeneous medium within the electrodes is often an oversimplification. Similarly, the electrochemical reaction rate at the solid–liquid interface may depend significantly on the local microstructure.[370] More recently, the effectiveness of the variational multiscale enrichment method was demonstrated.[372] Unlike MSM based on the homogenization method, this method can decompose the scales without assuming scale separation. The approach was directly compared to the predictions of the so-called pseudo-2D model. The latter essentially combines a one-dimensional macroscale model which describes the concentration evolution of active species and electric potential in the electrolyte across the anode/separator/cathode sandwich on one side and a microscale model for the electrode(s) on the other. The variational multiscale enrichment method showed clearly an improved prediction capability in terms of the effects of tortuosity, conductivity, diffusivity, and specific surface area.

Emerging battery technologies such as lithium sulfur batteries (LSBs) and LOBs pose interesting new challenges in under-

standing the electrode mesostructure/performance relationships and open new perspectives for MSM.

Thangavel et al.[373] adopted a MSMIC to study the influence of the cathode mesostructural properties on the Li−S battery cell performance. Such properties include the interparticular porosity between the carbon particles, the mesoporosity within the carbon particles (by assuming mesoporous carbon as electrode constituent), the particle and the mesopore size distributions, and sulfur loading. For this approach, the authors assumed the sulfur impregnated into the interparticular pores and mesopores within the carbon particles (Figure 50).
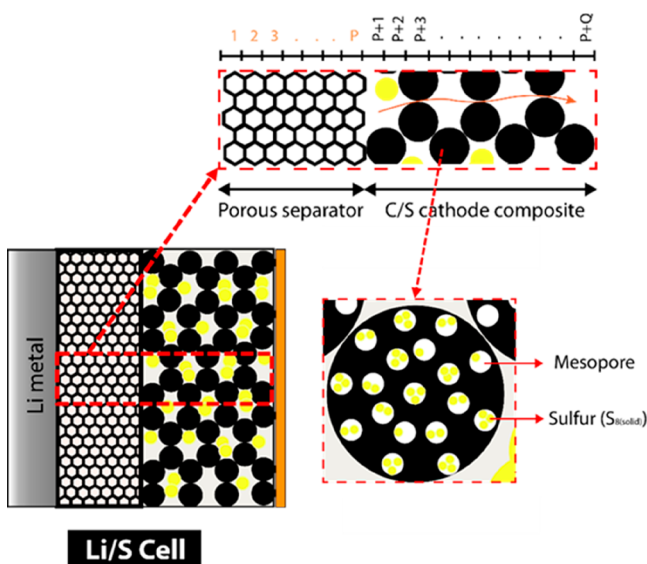

Figure 50. Scheme of the MSM of a Li-S cell proposed by Thangavel et al. Reproduced with permission from ref 373. Copyright 2016 The Electrochemical Society.

Dissolved sulfur, polysulfides, and lithium ions in the electrolyte, produced during the discharge, were assumed to be allowed to exchange between the two scales of pores. This model allows predicting the $Li_2S_{(solid)}$ precipitation process depending on the electrode design and the applied current density by considering its impacts on transport and reduction reaction kinetics, providing a versatile platform to study the roles of the electrode manufacturing and cell operation parameters.

Several continuum mathematical models have been reported to simulate the discharge behavior of LOBs:[374−381] all these models solve transport equations for O_2 (getting inspiration from polymer electrolyte membrane fuel cell models) and some of them for Li^+, coupled with Butler−Volmer or Tafel electrode kinetics. However, characterizing the impact of the detailed electrode mesostructure onto the cell performance has been recognized as a fundamental challenge in LOBs. The cathode mesostructure controls the transport of O_2 and Li^+ species and consequently the location of Li_2O_2 formed upon discharge. Conversely, the formed Li_2O_2 reduces the porosity and affect these transport processes.

Within a continuum paradigm, a MSMIC of a LOB accounting for the cathode pore size distribution and its influence on electrochemical and transport processes has been proposed by Xue et al.[382] In this model, the morphology of the discharge product, Li_2O_2, is assumed to be a thin film covering the pores surface. During discharge the active surface area decreases due to (i) the decrease of the effective pores radius resulting from the Li_2O_2 coverage increase, (ii) the choking of small pores (with a diameter of two times the electronic tunneling distance through Li_2O_2, estimated to be 10 nm), and (iii) the blocking of electronic tuinneling along thick enough Li_2O_2 films.

Simulations were performed with Super P and Ketjen Black carbon-based cathode electrodes. The Ketjen Black cell is observed to offer a larger discharge capacity because of the high

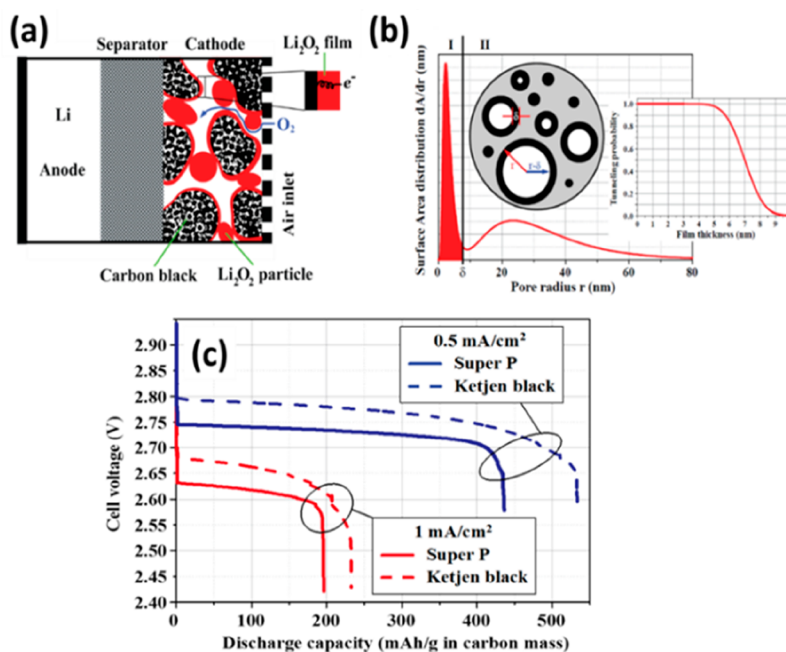

Figure 51. (a) Schematics of the LOB cell model. (b) One of the surface area distributions (related to a pore size distribution) and electronic tunneling function adopted in the model. (c) Simulation results for Super P and Ketjen Black carbon-based positive electrodes for two discharge current densities. Reproduced with permission from ref 382. Copyright 2014 The Electrochemical Society.

Ketjen Black specific surface area, leading to a slower Li_2O_2 thickness growth rate. This is known at the experimental level, but the authors' model was the first one in literature to be able to reproduce this fact. The model highlighted the importance of designing electrodes having an appropriate compromise between high surface area (small pore size) and large pore radius (slow degradation rate of active surface) (Figure 51). The model results and conclusions were later on reproduced by other authors.[383,384] The authors proposed an extension of the model accounting for both the formation of Li_2O_2 as a thin film (surface limited reaction mechanism) and the formation of Li_2O_2 in the solution phase (solution phase reaction mechanism).[385] The relative impact of the two mechanisms on the overall discharge performance was captured through an escape function, quantifying the extent to which the reaction takes place in the solution phase. Such an escape function quantifies the O_2^- radicals going far away from the carbon electrode surface to reach the largest open space of the cathode where they may disproportionate to form Li_2O_2 particles. Simulations were fitted to experimental data arising from two cells with TEGDME and DMSO as solvents, respectively: from this, it was confirmed that the escape rate was higher in the high donor number solvent DMSO.

For several years, the VAM introduced a very useful tool for the description, quantification, and optimization of complex phenomena operating within the LIBs, obtaining very good results in agreement with the main features of the experimental ones. Although modification and new approaches have been added to the classical VAM models, heterogeneities and anisotropy of the real electrode structures are not captured in the description.

5.2. Meso-Structurally Resolved Models

The shortcomings of conventional homogenized approaches can be overcome through detailed simulations conducted on 3D-resolved mesostructures. The resulting simulation data can then be incorporated into existing cell models, such as the P2D model, by coupling the necessary state variables to produce a MSM. However, such an approach can increase dramatically the computational costs. One way to overcome the computational issues is to use the so-called surrogate modeling approach for coupling the macroscopic (electrode) and microscopic (particle) length scales (Figure 52).[386] The special aspect of this
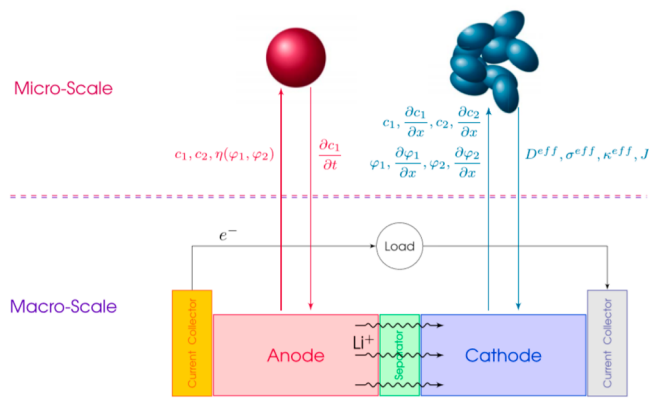

Figure 52. Macroscopic and microscopic scale models with multiscale coupling variables shown. Reproduced with permission from ref 386. Copyright 2014 The Electrochemical Society.

method is that the state variables of the length scales are not coupled explicitly but rather implicitly via surrogate functions constructed from precomputed simulation data. As the functions are defined analytically, the computational cost of evaluating a surrogate function is negligible compared to standard techniques. Still this model approach remains in the scope of MSMSL.

A different approach to two-scale modeling at the continuum level was proposed by Salvadori et al.[387] At the macroscale, the electrode is considered as a porous continuum, whereas at the micro level it is heterogeneous and multiphase. The authors justify their continuum approach by the fact that the microscopic length scale is still much larger than the molecular dimensions. The key pillar of the approach is the formulation of the microstructural boundaries and the application of averaging techniques to couple the micro and macroscales. The macroscopic output variables are recovered from a microstructural representative volume element solution (micro-to-macro transitions) (i.e., in the sense of the MSMSL approach). In an upgrade,[388] the authors also considered the electro-magnetics via the electro-quasi-static formulation. Capacitive effects were also included.

With regard to the continuum approach, the main challenge in the development of a feasible 3D cell performance model is the inclusion of all the phases constituting the electrode (active material, carbon additive, binder, and pores). Because the characteristic length scales of the materials composing the electrode can be orders of magnitude apart, an enormous computational effort is needed to simulate cell operation and, on the other hand, consider all scales needed if one wants to take into account the interplays between the phases.[389]

3D-resolved performance models fall generally by construction within the MSMIC category as they resolve through iterative coupling Li^+ transport in the electrolyte, lithium and electrons in the solid, as well as the interfacial (lithium insertion/deinsertion) electrochemistry on the actual (or close to actual) electrode mesostructure (without the use of effective parameters, such as in the case of the VAM). Some of the existing 3D models are discussed below.

Wiedemann et al.[390] developed a MSMIC to evaluate the influence of the cathode mesostructure on the LIB performance. The mesostructural geometry was reconstructed from FIB-SEM experimental data and processed into finite-volume discretizations. The model describes transport and electrochemical processes within the solid phase of the electrode mesostructure using a 3D extension of Newman's model and considering different porosities for $LiCoO_2$ commercial cathodes. In simulations of the discharge process, all the solid part was considered as active material and the authors did not evaluate the potential in the electrolyte and cathode, assuming that both remained constant. This model demonstrates how the measured electrode mesostructures, together with their 3D structural heterogeneities, can be incorporated into a MSM approach.

Thiele et al.[362] reported a 3D-resolved finite volume LIB cell model. The positive electrode is represented as a spatially resolved three-phase domain based on FIB/SEM and nanoscale computer tomography reconstructions (Figure 53). The reconstructed geometry considers three phases: active material, carbon binder domain, and the electrolyte-filled pores. Several authors do not report the number of time steps and minimal mesh size needed for a realistic representation of the electrodes. Thiele et al. $LiCoO_2$ electrode model was built from 200 images, composed of 572×518 square pixels each, with an edge length
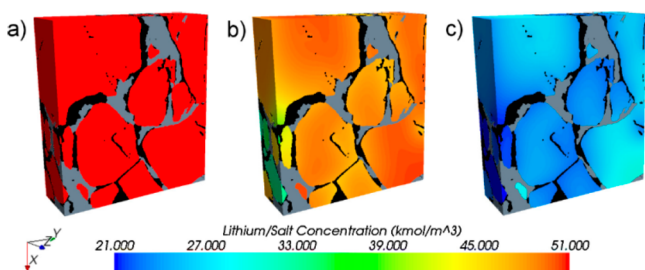
Figure 53. Simulated lithium concentration within the cathode at various states of charge (electrolyte-black, carbon-binder domain-dark gray). (a) SOC 0 (initial state). (b) SOC 0.1. (c) SOC 1 (fully charged). Reproduced with permission from ref 362. Copyright 2014 Elsevier Ltd.

of 35 nm. The reconstructed volume is 20.02 × 18.13 × 12.4 μm^3. This probably provides a very realistic and quite accurate representation of the actual cathode. The cell was meshed to form a 3D domain with about 21 million hexahedral cells. The separator was modeled as an effective electrolyte-filled region between the electrodes. It is important to underline that despite their explicit consideration of phases in the reconstruction, in the actual cell simulation, the authors consider the carbon and binder to be transparent toward the lithium transport. Their simulation was performed using the commercial software platform STAR-CCM+. The simulation time was 27 days using 8 CPUs.

The authors found that the binder partial coverage of the active material surface ensures excellent transport of electrons to and away. However, it reduces the specific active area needed for the ions insertion. The authors identify the optimization of the binder coverage on the active material as a critical aspect to be considered composite in electrode engineering. Additionally, they found that significant gradients of lithium concentration in the active material appeared while charging the cell.

Wieser et al.[389] developed a mesostructure-resolved simulation tool of a LIB half-cell with a graphite-based negative electrode and correlated the electrical performance with the material morphology obtained from image analysis. Imaging of the active material and the binder was carried out by using different techniques because of the scale difference of the two components. An important finding is that the simultaneous computational treatment of both the active material and the binder is not reasonably feasible and requires alternative approaches. The proposed solution was to bridge the scales considering the active material from segmented image data, and the additive was added in the pore space of the electrode structure wetting the active material preserving the transport properties obtained from nanotomography. As in most other reports in literature, the model was based on the Newman approach. Transport equations in the additive region were solved using the same approach as that in the electrolyte domain but considering effective transport parameters. Preliminary simulations show a negligible impact due to the additive at low
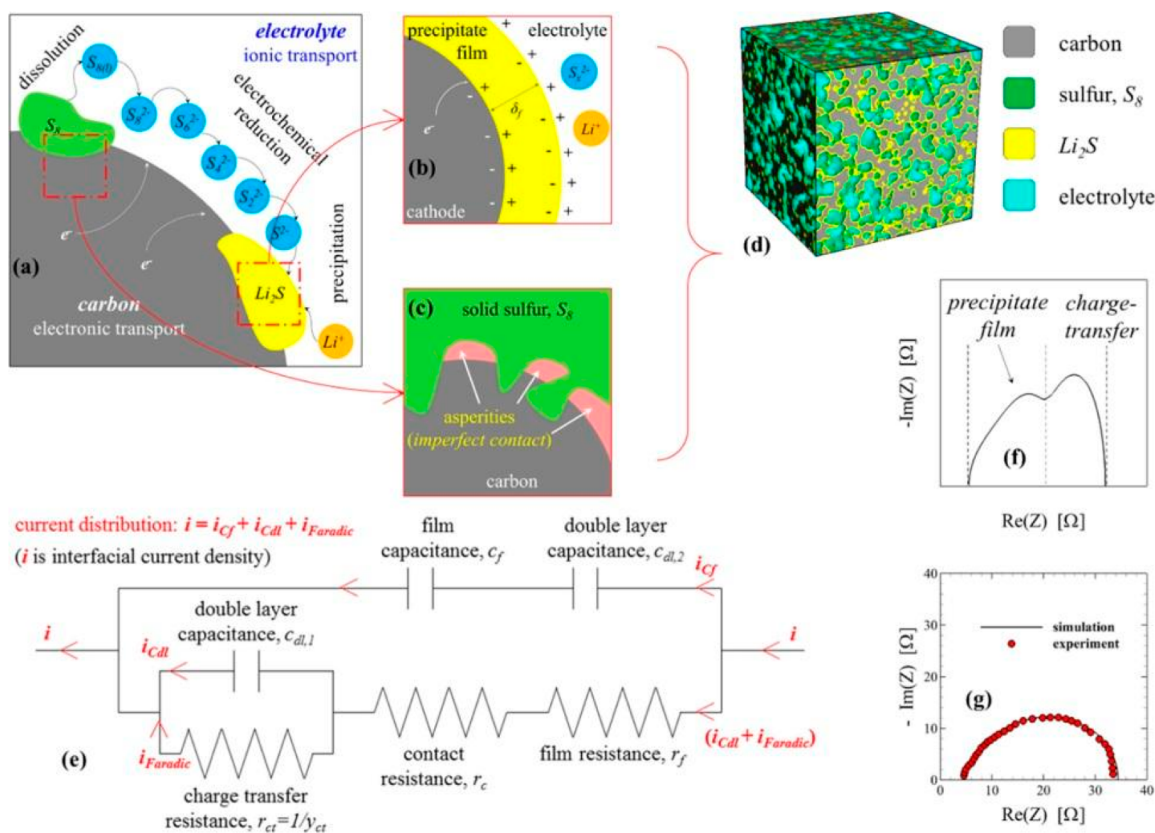
Figure 54. Scheme of different physicochemical processes taking place in a Li−S positive electrode which may affect the cell electrochemical impedance spectra: (a) reactions at the pore-scale, (b) precipitate film and electrochemical double layer, (c) imperfect contact between the precipitate film and the carbon substrate, and (d) electrode microstructure. (e) Interfacial impedance contributions are represented in terms of an equivalent electrical circuit. (f) Schematic illustration of a simulated electrochemical impedance spectrum, (g) and example of its validation against the experimental one. Reproduced from ref 395. Copyright 2017 American Chemical Society.

electric load, while for elevated electric load there is a visible impact.

Danner et al.[391] developed a 3D mesostructure resolved model to investigate limiting factors in graphite/NMC LIB cells performance. In particular, the model is used to study the effect of materials heterogeneities in thick electrodes on the cell charge and discharge performance. 3D structures were collected from tomography data for NMC cathodes, whereas graphite electrodes were generated using GeoDict software.[392] The authors used their in house BEST software (Battery and Electrochemistry Simulation Tool) to carry out the simulations.[33] In the 3D model three phases were taken into account (active material, binder, and carbon additive), and as in the models mentioned before, the authors made simplifications both in the electrode reconstruction and the mathematical formulation. In this study, the binder was described by a no-flux condition of lithium to neighboring phases, whereas the carbon black was modeled as a surface layer active material with a high electric conductivity.

Dysart et al.[393] reported a MSMSL to describe the operation principles of LSBs. The authors used graphene models to mimic carbon in contact with nanosulfur, as a representation of the actual cathode composite material as graphene flakes with sulfur. Polysulfide species adsorption energies were calculated using a DFT approach, while motion of ions was modeled using *ab initio* MD. The effects of sulfur loading and Li_2S precipitation were simulated using virtual 3D cathode mesostructures (representing a network of interconnected pores) reconstructed from SEM micrographs by using GeoDict software. For the macroscale performance model, the authors used a simplified mathematical model, where the electrochemical kinetics was described by the Butler−Volmer equation, while for the chemical reactions the usual forward−backward reaction kinetics was assumed. The microstructure impact was captured through effective properties such as porosity, tortuosity, and electrolyte ionic conductivity. By using mass conservation equations, the authors were able to quantify the evolution in species concentrations and in volume fractions of solid sulfur.

Barai et al. extended this model, still within the MSMSL approach, by including the influence of the volume changes in the cell performance during charge/discharge processes in Li−S batteries.[394] The authors attributed the total volume change of the electrolyte in the pores to the (a) solid sulfur dissolution and Li_2S precipitation and to the (b) shrinking/swelling of the cathode microstructure to accommodate the pore volume changes arising from the electrolyte-induced hydrostatic pressure. The impact of mechanical volume change on the overall cell performance was analyzed as well as the impact of different pore sizes and the mechanical stability of different cathode microstructures under the influence of nonuniform precipitation or pore-confinement effect. Additionally, a computational methodology was introduced in order to analyze the mechanical deformation and stress response at the pore scale in a porous electrode microstructure. In this work, authors showed that at the beginning of the discharge curve, which is governed by the dissolution of solid sulfur, the mechanical volume change has a minor impact on the overall cell voltage. However, in the last part, when the precipitation of lithium sulfide occurs, the cell voltage decreases in the beginning due to contraction and increases at the end because of expansion of the carbon microstructure.

Chen et al.[395] reported a porous-electrode model, based on a MSMSL approach, that captures as the Li−S cathode mesostructure evolution and reaction kinetics within. The

authors analyzed the impedance response of the cathode as a function of the interfacial area of contact between electrolyte and carbon substrate, Li_2S film thickness, interfacial charge-transfer resistance, and the electrolyte ionic conductivity (Figure 54). Impedance calculations were carried out at different depths of discharge. In particular, the impact of mean pore size on the spectra was investigated. The authors analyzed several cathodes with the same porosity and sulfur loading but different pore-size distributions, concluding that smaller pores resulted in smaller impedance values with a more efficient charge transfer. This work illustrated the complex dependence of the electrochemical impedance spectra on the cathode microstructure as a function of the depth of discharge of the cathode.

Three-dimensional-resolved modeling has recently been attracting a growing interest in the field of LOBs. A three-dimensional MSMSL[396] was proposed by reusing the mathematical formulations of the physics previously reported by Xue et al.[382] The model permits simulating a Li-O₂ battery discharge performance by capturing nanoscale and mesoscale details of a reconstructed cathode via a particle-packing method, reconstruction compared to SEM experimental data. The model was used to calculate the rate-dependent morphology of Li_2O_2 growth on the surfaces of the interconnected pores in three dimensions (Figure 55). Following a simulation multiscale
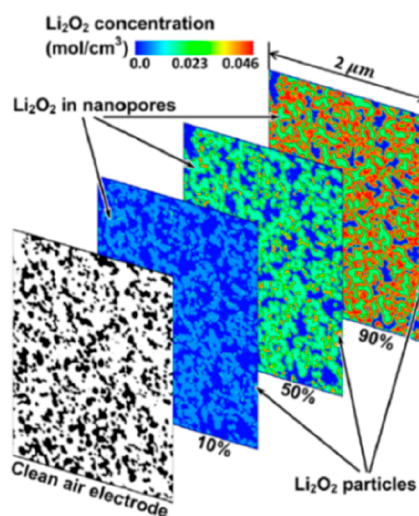
Figure 55. Three-dimensional calculation of Li_2O_2 formation in a reconstructed carbon-based Li-O₂ battery. Reproduced with permission from ref 396. Copyright 2015 American Chemical Society.

strategy random deposition, this permitted them to derive active-surface-to-volume ratio relationships incorporated in a macroscale model designed to predict discharge curves. Although this model is still very simple with regard to the description of the electrochemical reaction (the solution phase mechanism is not considered), this kind of simulation approach may open tremendous opportunities toward the optimization of the electrode architectures in Li-O₂ but also in other battery technologies.

Large experimental variations in the electrochemical performance of LOBs have been reported in the literature. Such variations are often assumed to result from differences in cell design, electrode structure, handling, and cell preparation at different times. In order to investigate possible reasons of these variations, Torayev et al.[397] developed a pore network model to simulate the discharge response of 3D-resolved lithium−oxygen
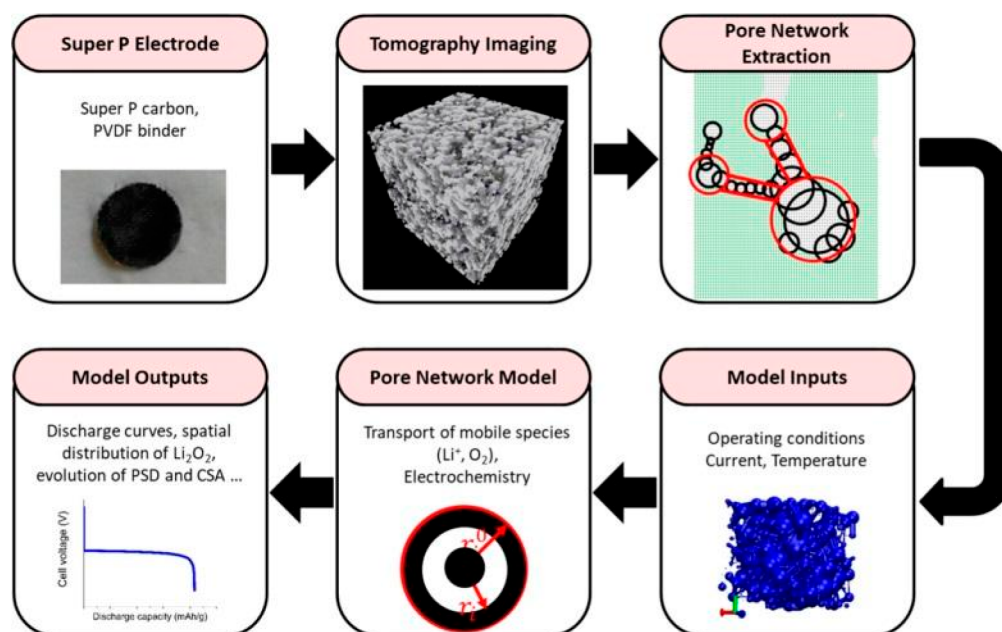
Figure 56. Workflow of the pore network approach. Reproduced from ref 397. Copyright 2018 American Chemical Society.
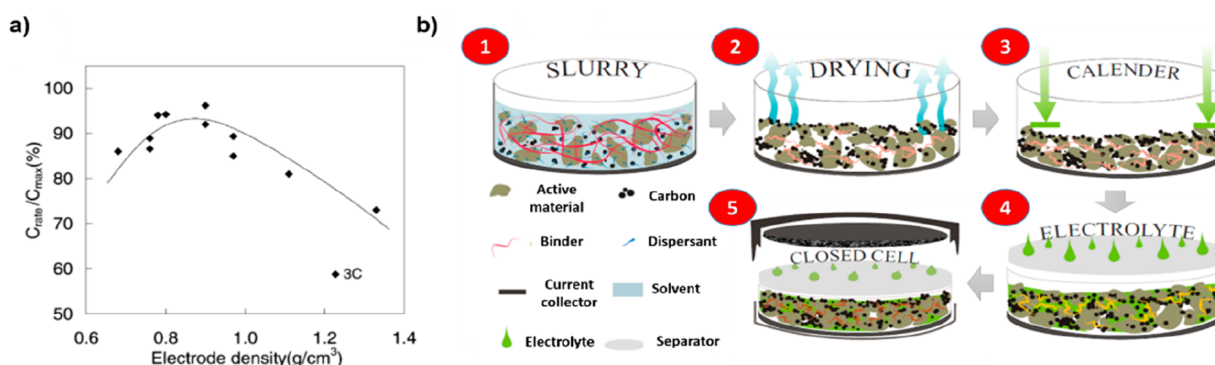
Figure 57. (a) Electrode density effect on its capacity. Reproduced with permission from ref 399. Copyright 2003 Elsevier Ltd. (b) Schematic representation of the typical LIB electrode fabrication steps at the industrial level.

cathode mesostructures, made of Super P carbon, obtained from TXM tomography. The overall workflow constitutes a MSMSL (Figure 56). The calculation of model discharge curves was made in several steps: (a) preparation of a porous carbon electrode made of Super P carbon, (b) image reconstruction, (c) segmentation of images, and (d) binarization of the final structure.

Then, by using the maximal approach, the porous space in the tomography data was mapped to a three-dimensional network of spherical and cylindrical pores.[398] Finally, the authors performed the simulation of a Li-O_2 battery using the pore network approach. Discharge curves were calculated, using identical conditions for different zones in the electrode and their reversed configurations. They concluded that the stochastic nature of the microscopic arrangement of pores and their interconnectivity can explain, at least partially, the variations in that observed experimentally in terms of cell discharge performance.

5.3. Discrete Modeling of the Composite Electrode Fabrication

The electrode mesostructure is strongly affected by the adopted fabrication process.[399] At the industrial level, the electrode fabrication process of commercial LIBs mainly consists of five

successive steps (Figure 57): (1) the preparation of slurries from the active material/carbon particles/binder mixture by using an organic solvent and a dispersant, (2) the casting of the slurry on the current collector and the subsequent drying to evaporate the solvent, (3) the mechanical compression of the resulting coating (called "calendering"), (4) the filling of the arising porous electrodes with the electrolyte needed for the battery operation, and (5) the battery assembly. In view of the lack of a general theory allowing one to predict the electrode mesostructure from the adopted fabrication parameters such as the temperature used to evaporate the solvent, and the pressure used for the calendering, optimizing this fabrication process is a difficult task.

The improvement of LIBs can be also attained by incorporating a new generation of active materials in both LIB negative and positive electrodes. The incorporation of such "new chemistries" in the conventional industrial fabrication processing raises questions which are yet to be answered, regarding whether their manufacturing scalability (and the associated costs) and the desired battery volume density (and the associated electrochemical performance) are achievable. Therefore, processing conditions need to be carefully reconsidered for optimal battery performance. Indeed, the rheology and self-organization phenomena of slurries is dependent on the
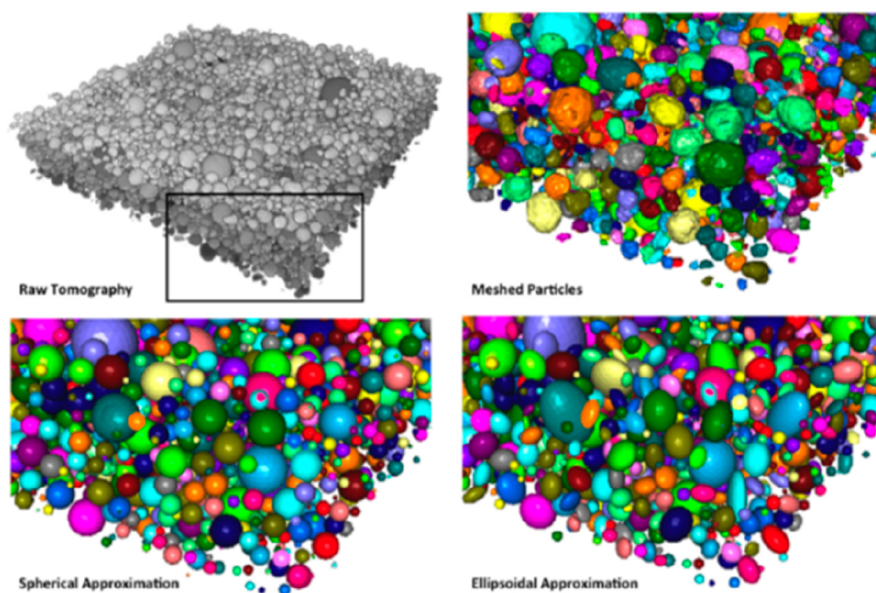
Figure 58. DEM model of a LIB cathode calendaring for different hypothesis of particles morphologies. Reproduced with permission from ref 406. Copyright 2015 Elsevier Ltd.

chemistry of their constituents which governs the interplay between the forces among the active material, carbon and binder in the slurry, such as the van der Waals, electrostatic and Brownian forces, and the steric and hydrodynamic interactions. Multiple spatiotemporal scales are involved in the fabrication process; therefore, it constitutes a multiscale problem which cannot be addressed in an efficient way only based on trial-error. As a consequence, there is an urgent need for a general theory serving as a guide to electrode fabrication for the optimization of their mesostructural properties. Indeed, enabling precise control of material arrangement and distribution in the electrodes is of paramount importance for designing the next generation of battery electrodes. Such a theory should provide deep insights on the fundamentals of conventional fabrication processes, from the slurry to the electrode formation, and on the influence of the electrodes' mesostructural properties on the cell performance for EV applications.

In the literature, one can find only very few and recent theoretical modeling efforts addressing electrodes fabrication for batteries. Brownian Dynamics (BD) simulations have been applied to suspensions of active material particles by Zhu et al.[400] and by Cerbelaud et al.[401,402] analyzing the effect of parameters such as temperature and mass ratio between carbon and active materials on the resulting number of contacts between the conductive additive and the active material. The dynamics equations are functions of fitted interaction parameters which may been refined by employing molecular-level simulations, and in that sense, these modeling frameworks can be seen as a MSMSL. Cerbelaud et al.[403] applied this simulation technique to a system composed of carbon black aggregates and silicon nanoparticles. The authors show that at fixed carbon concentration, the suspension structure changes with the size of the active nanoparticles relating the particle size and carbon concentration with the connection between active material and carbon domain and the formation of the percolating network. The authors conclude that their simulation results can assist in choosing the type of interactions between the different components in the suspension to be modified experimentally in order to improve the structure of electrode

slurries. The authors do not, however, describe the influence of the solvent evaporation on the resulting composite electrode micro/mesostructure, probably because of the inherent limitation of the BD technique to treat larger spatial scale systems and longer timescales.

In a similar way as for anodes, understanding slurries with cathode active materials upon the LIB electrode fabrication process is of crucial importance toward the development of highly efficient cells. Several stochastic models based on energy-based structural optimization have been developed in the recent years, ready to become MSMSL but not yet having this characteristic.[404] This approach allows for the prediction of equilibrium particle positions and orientations at given electrode densities. The assessment of the efficiency of the predicted microstructures to enhance Li$^+$ transport can be then quantified.

As an example, we here highlight the recently reported MC-like models devoted to the optimization of multiparticles energy-based spatial arrangements proposed to mimic the first stages of conventional LiFePO$_4$-based electrodes fabrication and to estimate structural properties.[405] These models are developed in one plane neglecting the presence of dispersant and considering the binder as nanoparticles. But despite these assumptions, they are able to predict interesting features, such as the influence of the solvent evaporation rate on the resulting electrode porosity. In these approaches, the total energy of the system is a function of the number of interactions between the particles of type i and j (solvent, active particle, binder, and carbon) and of the corresponding binary interaction energies. Due to the empirical character of these energies, it is not possible to use these models to predict the influence of the solvent and materials chemistry on the resulting electrode morphogenesis and mesostructural properties. Important aspects like the influence of the type of solvent, which is experimentally known to significantly influence the slurry homogeneity, remain unexplored with these models.

Stershic et al.[406] have proposed a DEM model to describe the effect of calendaring on a cathode electrode microstructure. Their model permits analyzing the particulate assemblies in terms of interparticle connectivity, a property expected to
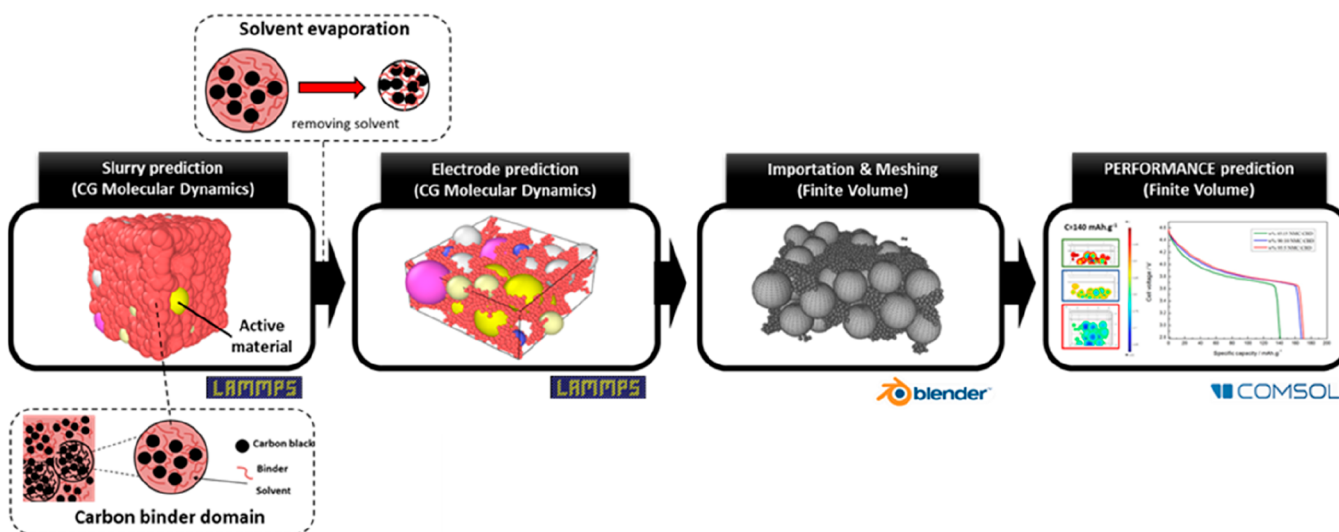
Figure 59. Scheme of the computational workflow proposed in ref 409 to simulate the LIB electrode fabrication and its impact on the cell performance. Coarse grained molecular dynamics is used to simulate slurries, the coating, and the effect of solvent evaporation, whereas the resulting predicted electrode mesostructure is used in a 3D-resolved continuum model to simulate the cell operation. Adapted from ref 409. Copyright 2017 American Chemical Society.

determine the overall Li and electronic transport properties in the solids within the composite electrode. The model received as inputs X-ray tomography data sets for positive electrode made of lithium nickel manganese cobalt oxide, for several compositions and calendering pressures (Figure 58). The authors showed that their model captured the evolution of interparticle contact distribution within the electrode. However, they also demonstrated that the use of electrode microstructures represented like spherical particles did not entirely follow the experimental trends. Furthermore, they stressed that their model might also offer a formulation to represent the deformation and deterioration (aging) of the active material particles in operating electrodes at the macroscale.

On the other hand, Forouzan et al.[407] developed a model for simulating a NMC electrode fabrication process using a mesoscale-level MD. NMC and carbon binder domain (CBD) particle interactions were simulated with shifted-force Lennard-Jones and granular Hertzian functions using the open source code LAMMPS.[46] The model is parametrized for a single electrode mass composition, from slurry viscosity, elasticity of the dried film, shrinkage ratio during drying, volume fraction of materials, slurry and dried film densities, and microstructure cross sections.

Nelson et al.[408] studied the intercalation of Li$^+$ in NMC active material particles by combining X-ray imaging, microstructural characterization, and modeling. The paper presents a deep analysis of the NMC particle size distribution and shapes before and after the cathode fabrication and an image analysis prior to the embedding of electrode into a performance model. The performance evaluation was based on a 3D extension of Newman's model with several simplifications.

Ngandjong et al.[409] reported an innovative MSM platform linking the simulation of fabrication process with the cell performance prediction (Figure 59). Indeed, the platform falls in the MSMSL category. The fabrication was simulated with the use of CGMD, first to predict the equilibrated slurry configuration (spatial distribution of NMC active material and effective particles representing aggregates of carbon, PVDF binder, and NMP solvent (Carbon Binder Domains, or CBD).

Then CGMD is used to predict the impact of the solvent evaporation on the resulting electrode mesostructure: such an evaporation effect is simulated by reducing the size of the CBD particles to mimic the solvent evaporation. Here, CGMD used shifted-force Lennard-Jones and Granular Hertzian potentials describing the solid and solvent behavior, respectively, similar to the work of Farouzan et al. referenced above. The predicted three-dimensional electrode mesostructures were imported in COMSOL Multiphysics software for the implementation of an discharge model (vs. Li) describing electrochemistry and the charge transport mechanisms. The CBD particles in the discharge model were considered implicitly, and the volume surrounding the NMC particles was divided by the authors into domains of ionic and electronic conductivity based on inputs from the CGMD model and considering an independent volume fraction for each of these components. The platform is able to predict the influence of the electrode mass composition (NMC vs carbon+binder) on the discharge profiles in good agreement with experimental trends. The explicit consideration of the CBD location in the mesostructure remains a challenge while importing it in the performance model, in order to evaluate the impact of such a location on the heterogeneity of Li$^+$ insertion in the NMC particles.

6. SEPARATORS

The effect of separator on electrochemical performance can be taken into account by upgrading the porous electrode model with typical separator features such as porosity and tortuosity. Mostly these quantities are treated using the conventional approach proposed by Bruggeman.[410] For some cases of interest, the properties of separator membranes have been found essential to obtain a good performance of LIBs.[411] Works report that the Bruggeman coefficient, which depends on the degree of porosity and tortuosity, has a strong influence on the values of the diffusion coefficient and ionic conductivity of lithium ions in the separator and, consequently, on the delivered LIB cell capacity.

Xiao et al. used a MSM approach for the stress analysis of polymeric separators in a LIB (Figure 60).[412] Instead of the
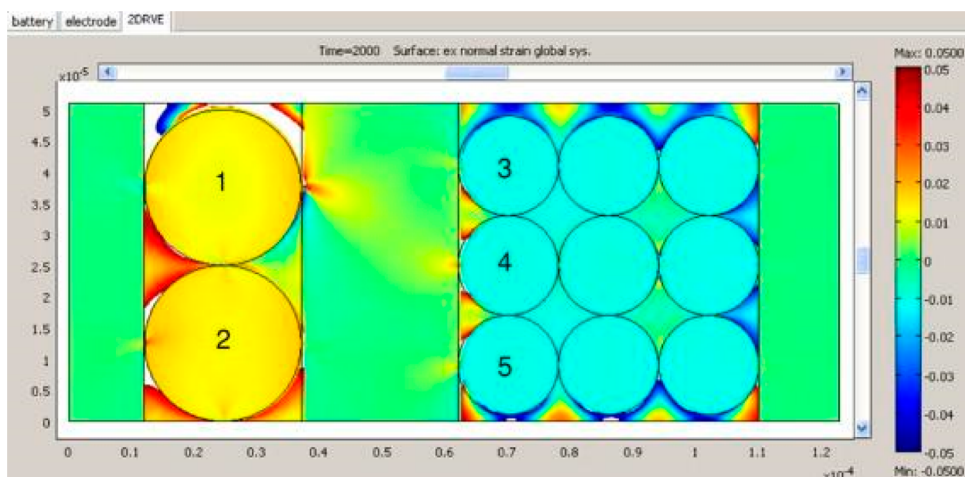
Figure 60. Predicted through thickness strain distribution at the end of discharge (2000 s) under a fixed-free (10 psi) boundary condition using a quarter-sized 2D RVE model. The areas with a voidlike appearance have a strain value beyond the range and hence are removed from the display. Particles 2 and 4 have a close-packed pattern, whereas particles 1, 3, and 5 have a loose-packed pattern. The maximum strain in the separator is found near a loose-packed particle of larger diameter. Reproduced with permission from ref 412. Copyright 2010 Elsevier Ltd.
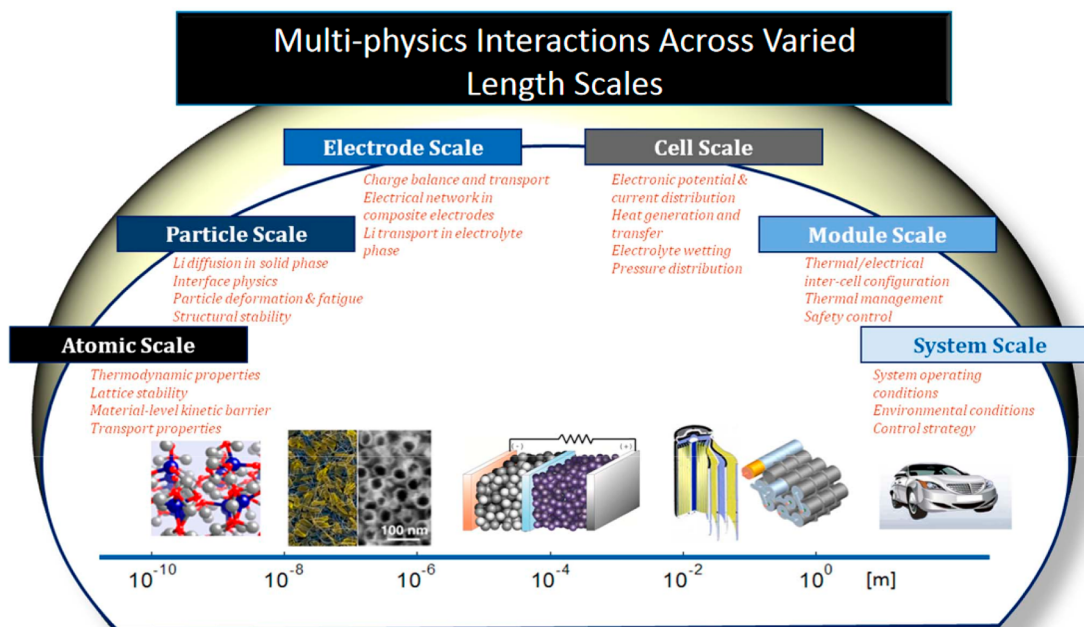
Figure 61. Length scale dependent physics impacting battery modeling. Reproduced with permission from ref 9. Copyright 2016 Elsevier Ltd.

Newman's model, the authors used a thermodynamically consistent 2D multiphysics microstructural resolved model with realistic electrode geometries. Species transport, electrochemistry, and the deformations and stresses of the components caused by Li^+ intercalation are all aspects considered in their model. For the specific case of a $LiC_6/LiPF_6/Li_yMn_2O_4$ cell, the authors found that the mechanical stress in the separator varied in phase with the cell cycles and that their magnitude depended on several parameters such as the separator Young's modulus, the active material particle size in the electrodes, and the pressure applied to the cell. In a follow-up work,[413] the same group investigated the influences of selected design related parameters, such as the friction between the separator and the electrode (defined as an effective friction), the active material particle size distribution and the thickness of the separator, on the stresses in the separator. The properties of separator,

however, become even more crucial when the whole battery at various conditions are considered and safety issues (thermal runaway, mechanical punctures etc.) are of primary importance. Examples of multiscale studies addressing these issues will be presented in the next section.

7. CELL

The electrochemical performance is only one important aspect of battery operation. Equally important for practical application are safety considerations which include the thermal behavior and aging (degradation) processes.[9] It thus seems natural to expand the electrochemical models in order to also capture those aspects. This naturally arises to models falling in the MSMTC category. It is reasonable to treat such phenomena on the cell level because this is usually the lowest enclosed, self-standing battery unit the properties of which can be measured
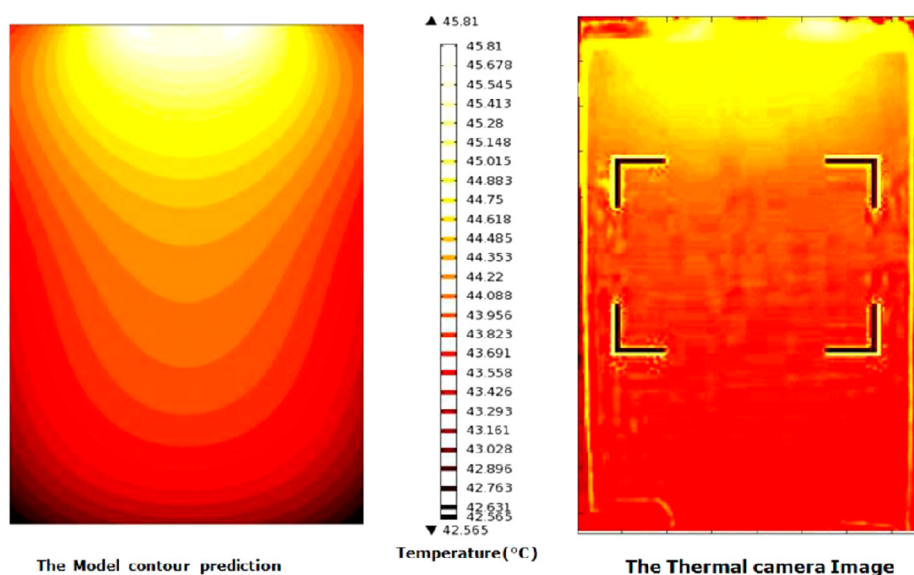
Figure 62. Comparison between temperature contour of the model result and the test. Reproduced with permission from ref 419. Copyright 2014 Elsevier Ltd.
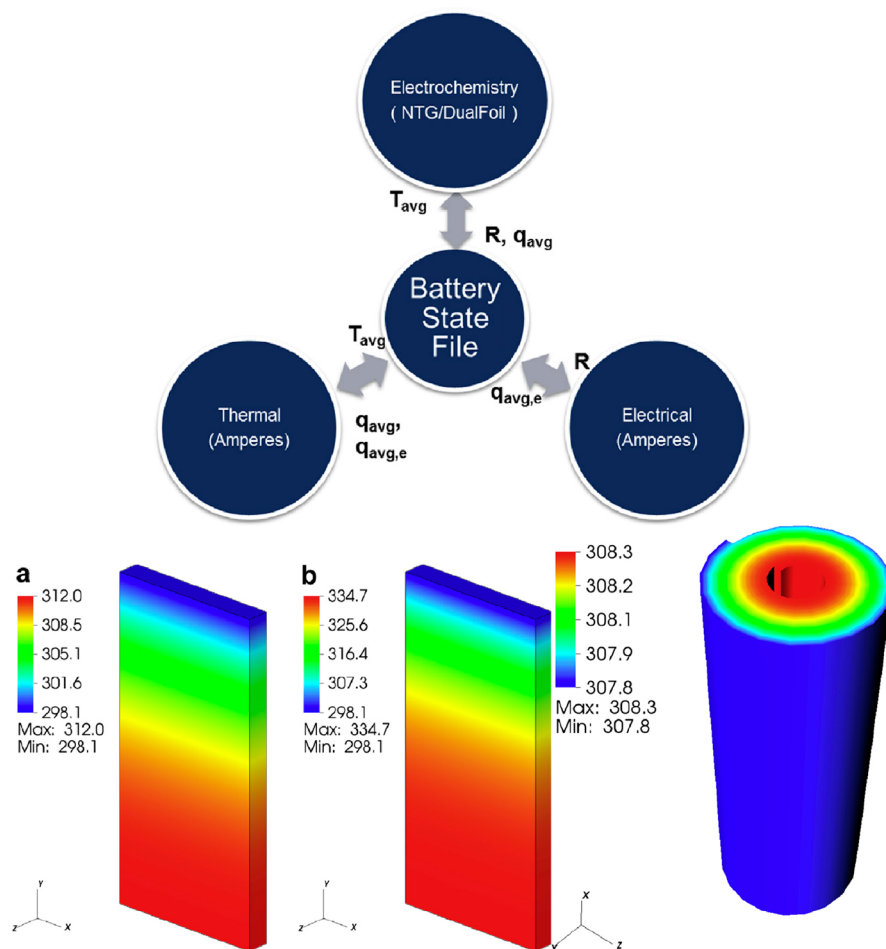
Figure 63. (a) MSM architecture and (b) temperature distribution in an unrolled (left) and a rolled cylindrical (right) cell subject to 2C discharge current. Reproduced with permission from ref 423. Copyright 2014 Elsevier Ltd.

quite reliably. A sandwich configuration with anode and cathode separated by an electrolyte field-porous separator is usually considered as a basic system, although other geometries are also used. Other components such as cell case and current collectors are also taken into account. Finally, the approach can extend beyond the cell level to consider a whole battery pack (Figure 61).

The first general and consistent thermal model considering all cell components was published more than 30 years ago.[414] Basically, already such one-dimensional models can capture the thermal behavior of smaller cells quite accurately. However, in order to treat larger cells and faster rates, one needs to resort to the 3D models which, as presented above, have become the state of the art approach during the past years. Typical outputs of thermal modeling are temperature fields generated at different charge−discharge rates, different electrode formulations, using different additives, different geometries, etc.

A literature survey shows that systematic attempts to include thermal and other safety issues into MSM have recently significantly intensified. Typical studies[415−418] are based on coupling of P2D or simplified 1D electrochemical models to 2D or 3D thermal models.

Usually two submodels, an electrochemical and a thermo-electric, are tight-coupled and are solved concurrently.[419] The electrochemical submodel predicts the voltage and heat generation rate of a cell during different load cycles. On the other hand, the thermo-electric model allows predicting the temperature and current distribution across the surface of the battery cell. The calculated temperature (heterogeneously distributed in space) enters into multiple parameters in the electrochemical submodel, therefore these models fall in the MSMTC category (Figure 62).

As underlined several times above, due to (much) increased complexity of mathematical treatment on the cell level, the underlying physical models need to be reduced in order to achieve appropriate computational efficiency. A nice overview of such efforts toward more efficient calculations is presented in the recent work by Kim et al.[420] The authors increased the computational efficiency of their MSM multidomain model by separating the timescales to decompose their model field variables. From this, a quasi-explicit linkage emerges between the multiple length-scale domains and thus reduces computational cost when solving model equations across multiple domains. In addition to the particle, composite electrode, and cell scales, the authors also treat the multicell module scale.

A reduced-order multi-dimensional MSM for the prediction of large-format LIB cell performance has been reported recently.[421] An analytical model order reduction approach based on a Galerkin projection method is adopted to save computational cost. The model performance is checked by analyzing appropriate experimental data at various current rates. Results confirm the significant decrease in computational complexity while retaining the accuracy of determination of distribution of the electrochemical properties and thermal features.

There are various possible practical applications of such a modeling. For example, Mortazavi et al.[422] used a coupling between the Newman's pseudo 2D electrochemical model and a three-dimensional heat transfer model based on average volumetric heat generation to explore the role of phase change materials like paraffin in thermal management of batteries.

Allu et al. integrated the individual physics models (i.e., electrochemical, thermal and electrical) and corresponding softwares into an open computational framework for battery simulations (Figure 63).[423] The work which focused on the importance of heat dissipation via metal current collectors was validated on several case studies (unrolled cell, pouch cell, and cylindrical cell). Later on, mechanical aspects were added into this open platform (termed VIBE, virtual integrated battery

environment) for analysis of crush scenarios such as vehicle crashes.[424]

A different approach to coupling the various scales, from atomistic to continuum levels, was proposed by Latz and Zausch.[425] The authors proposed a mathematical average formalism, using the framework of rational thermodynamics, which allows one to capture and couple the relevant physics on each scale, including the ionic and electronic transport and the heat. Among others, they showed that not all heat sources that exist on the microstructure scale are represented in the averaged theory due to cancellation effects of interface and bulk heat sources. Ohlberger et al.[426] showed how such numerically intensive models can be effectively reduced. Speedup factors of about 285 were obtained for the full strongly nonlinear battery model using the reduced basis method with empirical operator interpolation and around 253 for the linear parabolic heat conduction model using a parabolic extension of the localized reduced multiscale method.

In order to model selected extreme conditions such as the nail penetration test, special boundary conditions (i.e., shorting boundary conditions) need to be implemented in the coupled electrochemical-thermal model.[427] The results revealed a strong interplay between the cell thermal response and the electro-chemistry in such extreme situations. Beside the shorting resistance, the nail diameter and thermal conducitivy were found to be crucial parameters determining the overall cell behavior. The sequential linking (MSMSL) between the models was used.

The use of multiphysics tools have also made it more straightforward for researchers to apply the MSMTC approach, since different models can be implicitly connected in commercial software. For example, Priimägi et al. simultaneously used the thermal and battery modules in COMSOL to model the coupled thermal and electrochemical behavior of 3D-stuctured microbatteries employing different electrode architectures.[428] It was seen that the nonlinear current distribution through the electrolyte clearly affected the thermal evolution of the graphite/polymer electrolyte/$LiCoO_2$ cells, where especially interdigitated electrode plates gave rise to large temperature gradients during battery operation.

The thermal-electrochemical coupling also allows simultaneous study of aging effects. Aging mechanisms are generally complex. Furthermore, aging and thermal effects are strongly and nonlinearly coupled. Aging strongly depends on temperature and may lead to significant heat release. Aging occurs at the active material particle scale and at the composite electrode mesostructure, and the heat transport occurs at the cell scale, as shown by Kupper et al.[429] They used a MSM built from three 1D models, one for the active material particle, one for the composite electrode, and one for the cell. With this approach, the authors were able to capture all the relevant physics with moderate computational cost. The main and side reactions were described by using a multiphase approach. Finally, the thermal model provided a feedback between performance, aging, and temperature. In terms of the classification given in the introduction, the authors used the iterative coupling (MSMIC). Indeed, the cell scale provides to the electrode models the local temperature. Conversely, the electrodes models provide to the cell model their heat sources, where they are used locally.

Conceptually, the thermal effects can also be directly associated with mechanical strain, which in turn has an important influence on battery durability. Thus, coupling between the electrochemical and mechanical modeling can
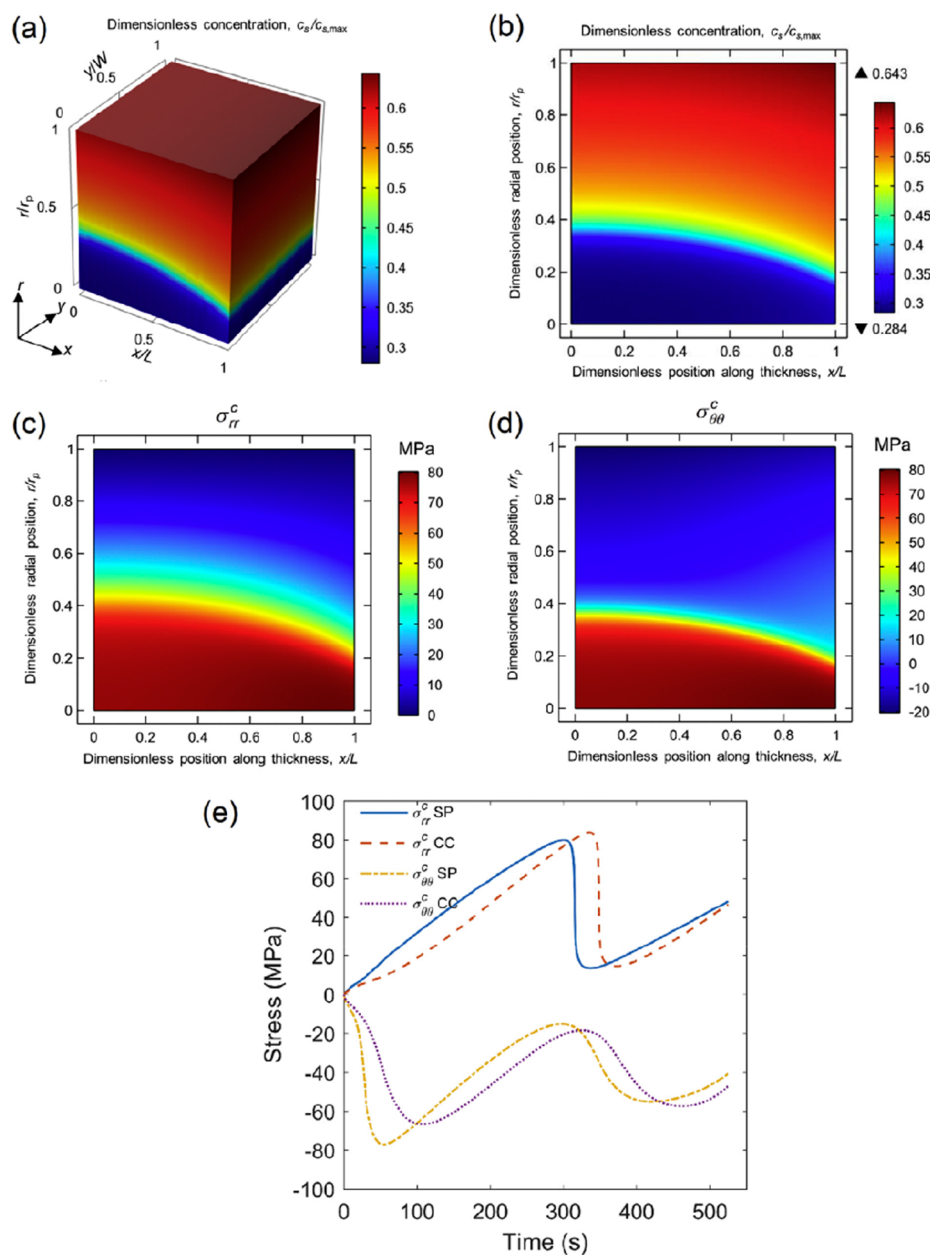
Figure 64. (a) Distribution of lithium concentration inside all particles. Horizontal axes represent particle location in the electrode by the *x* position along the electrode thickness direction and by the *y* position in the plane of the electrode. The vertical axis represents a point in the particle by the radial *r* position. (b) Lithium concentration in particles at *y* = 0. (c) Radial stress distribution in particles. (d) Tangential stress distribution in particles. Results shown are at the instant of 300 s. (e) Temporal profiles of the maximum tensile radial stress and the maximum compressive tangential stress for particles next to the separator (SP) and next to the current collector (CC). Reproduced with permission from ref 430. Copyright 2017 Elsevier Ltd.

provide important insights into degradation in LIBs. In a recent study, Wu et al. considered the effect of electrochemistry on the development of mechanical stress (Figure 64).[430] Note that this particular study was not carried out on the cell level but rather on the electrode as well as on the particle level. The scales are linked through the MSMSL approach, from the particle to cell level. While the stress on the electrode level appeared to be small compared to the one on the particle level, the former could cause severe failure due to interparticle fracture since the bonding between particles is much weaker than the cohesion of atoms inside particles.

In another safety-related study, a model coupling mechanical, electrical, and thermal aspects was used to investigate the short circuit induced by mechanical abuse.[431] Applying quasi-static indentation tests and using a distance-based electrical contact criterion, the model was found to accurately predict the initiation of short circuit due to structural fracture and postshort thermal and electric responses. The maximum current density was detected in the anode active material, whereas a larger indenter size created a larger electrical contact area. For their model implementation, the authors used the commercial finite element software LS-DYNA (tight coupling approach, MSMTC).

8. CONCLUSIONS AND PERSPECTIVES

Mathematical modeling has a promise of both a greater fundamental understanding of existing materials, components,

and cells, and a predictive power for properties and performance of new materials, components, and cells.

Even if battery researchers would agree that mathematical modeling can help at reducing the time-to-market, particularly for the use of rechargeable batteries in the transportation industry, it still has the reputation of (i) complicating the vision of simple phenomena, (ii) not representing reality, (iii) being difficult to understand and implement, and (iv) "predicting" mechanisms, processes, and/or system behaviors already known (and understood) by the experimentalist, thus not very useful.

Mathematical modeling truly merits having this reputation if not used correctly (i.e., if not using the same models as the experimentalists or if not formulating the mathematical equations in terms of concepts, parameters, and variables which are familiar to the experimentalists). Indeed, also experimentalists use mathematical models, more or less intuitively in their daily work, to analyze data, to extract "the" lithium diffusion coefficient in an active material, to determine the conductivity of an electrolyte, or the exchange current density, employing, for example, Fick's "law", Ohm's "law", and the Butler–Volmer "law". These "laws" all relate to theories or mathematical models.

However, are the values extracted by the experiment unique when they depend on the form of the mathematical equation used and thus on the theory under consideration? How about the applicability and the uniqueness of the theories that the experimentalists use? Experimentalists assume these "laws" to be valid for simplicity reasons, and they make assumptions. They, therefore, "isolate" a part of the "reality" in their interpretations. Experimentalists are, indeed, theorists as well.

According to the mathematician and logician Gödel,[432] any formal system which contains mathematics of whole numbers is incomplete and has undecidable statements (i.e., statements which are neither provable nor disprovable) by means of the system itself. Therefore, all theories which crystallize as mathematical models, regardless of their degree of complexity, are essentially incomplete and thus will never represent perfectly the physical system under investigation. Or in other words, both theorists and experimentalists are in trouble. If we, however, accept this premise, it becomes clear that "perfect" models of complex systems like a battery are impossible to achieve: therefore, a model is a more or less lovely imperfect representation of the physical system.

During the past decade, MSM approaches of rechargeable batteries have started to become available. As illustrated in this review, such MSM allow spanning multiple scales and simulating interplays between electrochemistry, transport processes, mechanics, and thermal stress mechanisms. These approaches allow deepening the effect of materials physicochemical properties and the components mesostructure on the overall cell response.

It is also apparent from this review that the MSM battery field is still dominated by sequential linking, MSMSL (Figure 3b), where especially electronic structure calculations serve either (i) as a basis for force field construction for use in MD and/or MC simulations or (ii) to extract parameters needed for continuum model simulations. These linkages are well-established and have developed over several years for both electrode and electrolyte materials. Two conclusions can be drawn. First, the "missing link" is primarily mesoscale modeling, where nonuniformities in the cell, primarily in the composite electrodes or in solid electrolytes, are better represented. Such a mesoscale modeling is needed to truly link molecular level models with cell-scale

modeling approaches. This is an area of MSM requiring larger research efforts including general improvements of modeling tools and softwares, and most likely the proper inclusion of the mesoscale constitutes the major challenge for approaching true MSM of batteries. The proper treatment of the mesoscale is for instance crucial for the development of predictive simulation tools of battery electrodes manufacturing. We also remark that MSMIC approaches (Figure 3c) have been mainly developed within pure continuum paradigms, for instance models coupling a continuum description of the active material particle level with a continuum description of the cell level. Second, there is a need to better develop the MSMIC and MSMTC approaches (Figure 3, panels c and d), where the results obtained from larger scale models (e.g., FEM), on, for example, heat generation in an operating LIB, can be used as input for fine-tuning at smaller scales and for design of materials with better tolerance to induced mechanical stresses.

Altogether, in the studies summarized the above aspects are very rarely covered, but for a true advancement of the MSM methodology, bringing it from myth to reality, focused and long-term efforts are required.

MSM still needs to be improved to even better boost the design and optimization of the next generation of batteries, but there are excellent opportunities for future research actions to overcome some remaining challenges. (i) For some cases of great practical interest, such as NMC active material in LIBs, even the actual charge–discharge mechanism inside active particles has not been established to any sufficient accuracy. To a large extent, this is due to numerous proposed compositions, use of special dopants, etc. This leaves the coupling to higher dimensions (electrode) almost completely open with a lot of basic work to be done. (ii) The exchange current density is one of the most common parameters used in cell models within the Newman approach. It can possibly be predicted from atomistic/molecular simulations, even if challenging, using DFT and AIMD methods to determine the most favorable reaction pathways and activation energies of the associated reaction steps. By employing the transition state theory formalism corrected with an electrochemical double layer model, it is possible to derive a set of reaction rate expressions dependent on the activities of the reactants and products. The zero exchange current can be then derived by assuming equilibrium conditions.[433] This methodology can be particular useful for battery systems dominated by solid/liquid interfacial reactions (e.g., Li-S and Li-air batteries) but has, as far as we know, never been applied. (iii) Conventionally, the parameters for the electrolyte and separator used in basic LIB cell modeling are ion diffusion and conductivity, ion transference numbers, and separator porosity and tortuosity. While the first set of parameters rather easily can be extracted from standard but proper molecular-level MD or MC simulations, the latter are modeled using mesoscale methods. For the former, a higher level of sophistication and accuracy can be obtained by using input from electronic structure calculations, as diffusion of charged species is intimately linked to coordination chemistry and local structure which is better addressed by quantum chemistry methods. Furthermore, also parasitic side-reactions in the electrolyte can be estimated, together with kinetics and influence on both surface layer formation and/or bulk viscosity, if methods like AIMD are used. Molecular-level calculations can also provide input on fluctuations of larger segments and grain boundaries, which in turn are useful input for the mesoscale models. Coupling of these phenomena in MSM of electrolytes
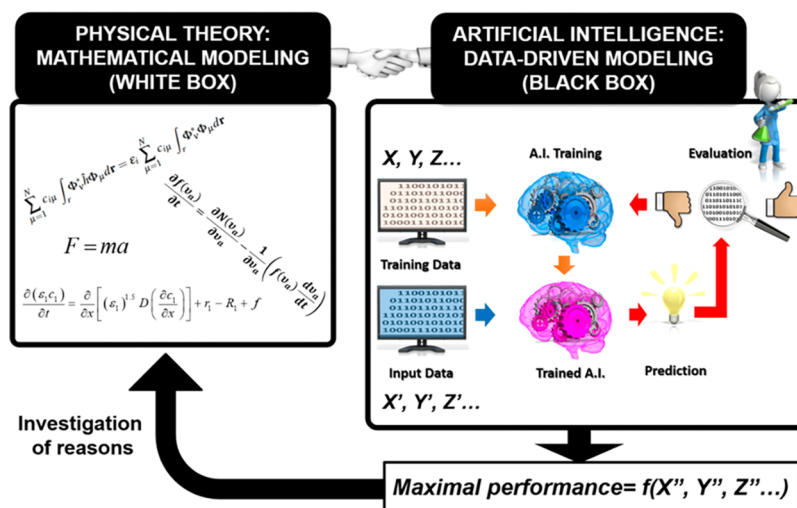
Figure 65. Schematics of an imaginary computational approach combining MSM with machine learning. "X", "Y", and "Z" refer to some characteristics being used as an input in the study (e.g., atomic composition of an active material).[434]

can be foreseen to push the field significantly forward. MSM can itself also bring forth more sophisticated models of the electrolyte by allowing one to incorporate, for example, local temperature and concentration fluctuations and couple this to models of the electrochemistry occurring. Last, for the currently very highlighted field of all solid-state batteries (ASSBs), based on various kind of solid-state electrolytes (SSEs), the MSM of mechanical properties will most likely be of much interest as it is to replace the separator employed in LIBs. (iv) Further development of 3D approaches is needed in order to account for large heterogeneity in transport/reaction, both on larger scale (across the electrode thickness) and locally. This should be based on realistic imaging of actual electrodes but on different scales (usually imaging is carried out on one scale, electrode). New experimental insights should improve the linking from particle-to-electrode scale in terms of structural-morphological features. However, along with that, we need new electrochemical couplings as the validity of the Butler–Volmer equation is limited to rather narrow ranges and conditions. (v) The coupling between electrochemistry and other essential phenomena, such as thermal, mechanical stresses, and side reactions, is still more or less in its infancy. For example, thermal effects extend over all possible scales, from atomic to large cells and even packs. The physics that will link these scales in a realistic way still has to be developed in order to take into account complex microstructures involving different phases which, in turn, undergo certain dynamics, not only due to volumetric changes due to electrochemistry but additionally due to thermal gradients, etc. (vi) Similarly, the coupling of stress development from particle level and electrode level, an essential feature appearing in basically all modern batteries, needs to take into account appropriate interactions between particles. This has yet been poorly explored, and indeed a large amount of data is required to even arrive at relevant models.

Realistically, it may take some time to get satisfactory coupling between the phenomena mentioned above. Luckily, the complexity of battery electrode can be broken down by simplifying various features. Hence, it is expected that progress will be in a step-by-step fashion, *i.e.* starting with state of the art approaches and adding a new level of complexity. Which level will be added will probably largely depend on the experimental insights gained.

Other opportunities and challenges which can be mentioned are as follows. (i) Use MSM to support mathematical reduction techniques for the derivation of models that can be used in diagnosis and prognosis. This is not straightforward if one wants to capture the synergies and competitions between materials and components aging mechanisms: such aging mechanisms' impact on the performance decay are not additive (indeed, some aging mechanisms can cancel each other, and others are reinforced). (ii) Usually models use a code with a particular algorithm to fit the parameters to calculable observables (e.g., potential and capacity). This is performed with a fixed set of physical assumptions. Future MSM will need to include the development of artificial intelligence algorithms for the development, testing, and optimizing multiple (evolutive) generations of models. A master routine would automatically change the physics included in the model, and subroutines optimize each model generation. (iii) Furthermore, three-dimensional immersive visualization tools, based on, for example, virtual reality technology, will be crucial for a better exploitation and understanding, with vast potential also for changing the paradigm of how to communicate results, both between academia and industry as well as toward students. (iv) MSM (which are white box models, as they describe explicity physical mechanisms) should be complimented with machine/deep learning (or black box data-driven) approaches aiming at predicting the influence of experimentally controllable parameters on materials, components, and cell properties (e.g., electrolyte stability and cell electrochemical performance). The most interesting cases "discovered" by the machine/deep learning algorithms can then be analyzed using MSM (Figure 65)

(v) It would be very helpful to combine MSM with online measurement tools of characteristics (such as temperature and voltage) of a wide batch of battery cells in order to refine/improve on-the-fly the parametrization of MSM, as done today for weather forecasting models whose parameters are continuously readjusted from measurements of wind direction and intensity, pressure, and relative humidity. (vi) In order for MSM to boost the transfer of concepts developed at the laboratory scale to the market, it is crucial to work also by coupling with cost-analysis software tools to allow one to evaluate the potential of the technology as a function of the current market.[435]

Today it is clear that the capabilities of modeling techniques in general are attracting a growing interest for gaining fresh insights on existing and new materials. The success stories of MSM presented in this review should not preclude us from focusing on future demands and requirements for improvement. On the basis of the advantage of limited cost, modeling, in general, and MSM, in particular, have strong potential to become an unavoidable driving force to foster innovation.

AUTHOR INFORMATION

Corresponding Author

*E-mail: alejandro.franco@u-picardie.fr.

ORCID

Alejandro A. Franco: 0000-0001-7362-7849
Daniel Brandell: 0000-0002-8019-2801
Miran Gaberscek: 0000-0002-8104-1693
Piotr Jankowski: 0000-0003-0178-8955
Patrik Johansson: 0000-0002-9907-117X

Notes

The authors declare no competing financial interest.

Biographies

Prof. Alejandro A. Franco (born in 1977 in Bahía Blanca, Argentina) received his Ph.D. diploma in 2005 from Université Claude Bernard Lyon 1, France, with his thesis dealing with the multiscale modeling of polymer electrolyte fuel cells. He was a permanent research Engineer at CEA-Grenoble in 2006−2012; since 2013, he has been Full Professor at Université de Picardie Jules Verne in Amiens, France, and since 2016, he has been a Junior Member of the Institut Universitaire de France. He is the leader of the Theory Open Platform at the ALISTORE European Research Institute and the reference person of the computational modeling research topic at the Laboratoire de Réactivité et Chimie des Solides (UMR CNRS 7314), Amiens, France. His current research involves the multiscale modeling and simulation of electrochemical energy devices, such as lithium ion, lithium sulfur, lithium air, and redox flow batteries. He is awardee of an ERC (European Research Council) consolidator grant for his project "ARTISTIC" about the modeling of lithium ion battery fabrication.

Alexis Rucci (born 1985 in Adolfo Gonzales Chaves, Argentina) received his Ph.D. diploma in 2015 from Universidad Nacional del Sur, Argentine, in 2015 with a thesis on Monte Carlo radiation transport for photon beams. Currently, he is doing a postdoc in lithium-ion multiscale modeling under the supervision of Prof. Alejandro A. Franco at Laboratoire de Reactivité et Chimie des Solides (LRCS) within the European Project POROUS4APP.

Daniel Brandell (born 1975) received his Ph.D. at Uppsala University, Sweden, in 2005 with a thesis on MD simulations of polymer electrolytes. After MD studies of ionically conductive membranes as a postdoc at Tartu University, Estonia, and Virginia Tech, Virginia, USA, he returned to Uppsala in 2008 and built a joint experimental-computational research group focusing on soft materials for battery devices. In 2016, he was promoted to Professor in Materials Chemistry.

Christine Frayret (Res. Assistant Professor at Laboratoire de Réactivité des Solides (LRCS), CNRS UMR 7314 Amiens, France) received her Ph.D. degree in the field of Materials Science (Solid Oxide Fuel Cells) under the supervision of Professor Michel Pouchard and Dr. Antoine Villesuzanne at the University of Bordeaux, Institut de Chimie de la Matière Condensée de Bordeaux (ICMCB, France). By calling to computational modelling, especially the methods based on quantum mechanics concepts, and by scrutinizing the electronic structure of

molecules and crystalline materials, her current principal objective is to gain insight on structure−property relationships in order to identify guidelines for the design of energy-related materials.

Miran Gaberscek is the Head of Department for Materials Chemistry at the National Institute of Chemistry, Ljubljana, Slovenia. He is also the Director of Centre of Excellence for Low Carbon Technologies, Slovenia, and Full Professor of Materials Science at the University of Ljubljana. He received his doctoral degree (Dr.Sc.) at the University of Ljubljana in 1994 with part of the experimental work being carried at Technical University of Graz, Austria, where later on he also worked as a research fellow. The primary research field of M. Gaberscek has been novel electrochemical systems for energy storage and conversion (primary and secondary batteries and fuel cells).

Piotr Jankowski (born 1990) studied Chemical Technology at Warsaw University of Technology, where he obtained Bachelor of Engineering (2013) and Master of Science (2014) degrees. After that, he started his Ph.D. studies between Warsaw University of Technology and Chalmers University of Technology within the Alistore-European Research Institute focusing on battery additives.

Patrik Johansson (born 1969, Ph.D. in Inorganic Chemistry at Uppsala University in 1998) is Full Professor in Physics at Chalmers University of Technology, Gothenburg, Sweden. He is also codirector of CNRS FR 3104 ALISTORE-ERI, Europe's largest industry-academia network within the field of modern batteries. His science aims at combining understanding of new materials, mainly electrolytes, at the molecular scale with battery concept development and real battery performance.

REFERENCES

(1) The Latest Bull Case for Electric Cars: The Cheapest Batteries Ever. *Bloomberg.com.* December 5, **2017**.

(2) Blomgren, G. E. The Development and Future of Lithium Ion Batteries. *J. Electrochem. Soc.* **2017**, *164*, A5019−A5025.

(3) Franco, A. *Rechargeable Lithium Batteries: From Fundamentals to Applications*; Elsevier, 2015.

(4) Theory: Definition of theory in English by Oxford Dictionaries. https://en.oxforddictionaries.com/definition/theory (accessed Aug 22, 2018).

(5) Franco, A. A. Multiscale Modelling and Numerical Simulation of Rechargeable Lithium Ion Batteries: Concepts, Methods and Challenges. *RSC Adv.* **2013**, *3*, 13027−13058.

(6) *Physical Multiscale Modeling and Numerical Simulation of Electrochemical Devices for Energy Conversion and Storage: From Theory to Engineering to Practice*; Franco, A. A., Doublet, M. L., Bessler, W. G., Eds.; Green Energy and Technology; Springer-Verlag: London, 2016.

(7) Jain, A.; Shin, Y.; Persson, K. A. Computational Predictions of Energy Materials Using Density Functional Theory. *Nat. Rev. Mater.* **2016**, *1*, 15004.

(8) Effat, M. B.; Wu, C.; Ciucci, F. Modeling Efforts in the Key Areas of Thermal Management and Safety of Lithium Ion Battery Cells: A Mini Review. *Asia-Pac. J. Chem. Eng.* **2016**, *11*, 399−406.

(9) Abada, S.; Marlair, G.; Lecocq, A.; Petit, M.; Sauvant-Moynot, V.; Huet, F. Safety Focused Modeling of Lithium-Ion Batteries: A Review. *J. Power Sources* **2016**, *306*, 178−192.

(10) Fotouhi, A.; Auger, D. J.; Propp, K.; Longo, S.; Wild, M. A Review on Electric Vehicle Battery Modelling: From Lithium-Ion toward Lithium−Sulphur. *Renewable Sustainable Energy Rev.* **2016**, *56*, 1008−1021.

(11) Abraham, A.; Housel, L. M.; Lininger, C. N.; Bock, D. C.; Jou, J.; Wang, F.; West, A. C.; Marschilok, A. C.; Takeuchi, K. J.; Takeuchi, E. S. Investigating the Complex Chemistry of Functional Energy Storage Systems: The Need for an Integrative, Multiscale (Molecular to Mesoscale) Perspective. *ACS Cent. Sci.* **2016**, *2*, 380−387.

(12) Kaj, I.; Konané, V. Modeling Battery Cells under Discharge Using Kinetic and Stochastic Battery Models. *Applied Mathematical Modelling* **2016**, *40*, 7901−7915.

(13) Miranda, D.; Costa, C. M.; Lanceros-Mendez, S. Lithium Ion Rechargeable Batteries: State of the Art and Future Needs of Microscopic Theoretical Models and Simulations. *J. Electroanal. Chem.* **2015**, *739*, 97−110.

(14) Borodin, O.; Olguin, M.; Spear, C. E.; Leiter, K. W.; Knap, J. Towards High Throughput Screening of Electrochemical Stability of Battery Electrolytes. *Nanotechnology* **2015**, *26*, 354003.

(15) Pannala, S.; Turner, J. A.; Allu, S.; Elwasif, W. R.; Kalnaus, S.; Simunovic, S.; Kumar, A.; Billings, J. J.; Wang, H.; Nanda, J. Multiscale Modeling and Characterization for Performance and Safety of Lithium-Ion Batteries. *J. Appl. Phys.* **2015**, *118*, 072017.

(16) Xu, Q.; Zhao, T. S. Fundamental Models for Flow Batteries. *Prog. Energy Combust. Sci.* **2015**, *49*, 40−58.

(17) Llorca, J.; González, C.; Molina Aldareguía, J. M.; Segurado, J.; Seltzer, R.; Sket, F.; Rodríguez, M.; Sádaba, S.; Muñoz, R.; Canal, L. P. Multiscale Modeling of Composite Materials: A Roadmap Towards Virtual Testing. *Adv. Mater.* **2011**, *23*, 5130−5147.

(18) Mukherjee, P. P.; Pannala, S.; Turner, J. A. Modeling and Simulation of Battery Systems. In *Handbook of Battery Materials*; Wiley-Blackwell, 2011; pp 841−875.

(19) Meng, Y. S.; Arroyo-de Dompablo, M. E. First Principles Computational Materials Design for Energy Storage Materials in Lithium Ion Batteries. *Energy Environ. Sci.* **2009**, *2*, 589−609.

(20) Knap, J.; Spear, C. E.; Borodin, O.; Leiter, K. W. Advancing a Distributed Multi-Scale Computing Framework for Large-Scale High-Throughput Discovery in Materials Science. *Nanotechnology* **2015**, *26*, 434004.

(21) de Baas, A. F.. *What Makes a Material Function? Let Me Compute the Ways: Modelling in H2020 LEIT-NMBP Programme Materials and Nanotechnology Projects*; Publications Office: Luxembourg, 2017.

(22) A processed output refers to a model raw output transformed into a parameter or variable which can be "read" by another model. For example, if "activation energy" is the raw output of a DFT calculation then the "kinetic parameter" using this "activation energy" through an Arrhenius law will be the processed output used as an input in a kinetic model.

(23) The European Materials Modelling Council. https://emmc.info/ (accessed Aug 23, 2018).

(24) Frisch, M. J.; Trucks, G. W.; Schlegel, H. B.; Scuseria, G. E.; Robb, M. A.; Cheeseman, J. R.; Scalmani, G.; Barone, V.; Mennucci, B.; Petersson, G. A.; et al. Gaussian, Inc.: Wallingford, CT, 2009.

(25) Gordon Group/GAMESS Homepage. http://www.msg.ameslab.gov/gamess/ (accessed Aug 23, 2018).

(26) SIESTA. https://departments.icmab.es/leem/siesta/ (accessed Aug 23, 2018).

(27) COSMO-RS: predict activity coefficients, logP, VLE from DFT data. https://www.scm.com/product/cosmo-rs/ (accessed Aug 23, 2018).

(28) MATLAB - Le langage du calcul technique. https://fr.mathworks.com/products/matlab.html (accessed Aug 23, 2018).

(29) ANSYS Fluent Software: CFD Simulation. https://www.ansys.com/products/fluids/ansys-fluent (accessed Aug 23, 2018).

(30) COMSOL Multiphysics® Modeling Software. https://www.comsol.com/ (accessed Aug 23, 2018).

(31) Cai, L.; White, R. E. Mathematical Modeling of a Lithium Ion Battery with Thermal Effects in COMSOL Inc. Multiphysics (MP) Software. *J. Power Sources* **2011**, *196*, 5985−5989.

(32) STAR-CCM+ | MDX. https://mdx.plm.automation.siemens.com/star-ccm-plus (accessed Aug 23, 2018).

(33) BEST Battery and Electrochemistry Simulation Tool: Fraunhofer ITWM. https://www.itwm.fraunhofer.de/en/departments/sms/products-services/best-battery-electrochemistry-simulation-tool.html (accessed Sep 10, 2018).

(34) PETSc/Tao: Portable, Extensible Toolkit for Scientific Computation. http://www.mcs.anl.gov/petsc/ (accessed Aug 23, 2018).

(35) Rainald Ehrig Scientific Software: LIMEX Version 4.3. http://www.zib.de/ehrig/software.html (accessed Aug 23, 2018).

(36) Guyer, J. E.; Wheeler, D.; Warren, J. A. FiPy: Partial Differential Equations with Python. *Comput. Sci. Eng.* **2009**, *11*, 6−15.

(37) Kresse, G.; Furthmüller, J. Efficient iterative schemes for ab initio total-energy calculations using a plane-wave basis set. *J. Phys. Rev. B* **1996**, *54*, 11169−11186.

(38) Dovesi, R.; Erba, A.; Orlando, R.; Zicovich-Wilson, C. M.; Civalleri, B.; Maschio, L.; Rérat, M.; Casassa, S.; Baima, J.; Salustro, S.; et al. Quantum-Mechanical Condensed Matter Simulations with CRYSTAL. *Wiley Interdisciplinary Reviews: Computational Molecular Science* **2018**, *8*, No. e1360.

(39) Blaha, P.; Schwarz, K.; Madsen, G. K. H.; Kvasnicka, D. *WIEN2k, An Augmented Plane Wave Plus Local Orbitals Program for Calculating Crystal Properties*. Vienna University of Technology, Vienna, 2001.

(40) SCM Software for Chemistry & Materials. https://www.scm.com/ (accessed Aug 23, 2018).

(41) BigDFT website. http://bigdft.org/Wiki/index.php?title=BigDFT_website (accessed Aug 23, 2018).

(42) Gabriel, M. A.; Genovese, L.; Krosnicki, G.; Lemaire, O.; Deutsch, T.; Franco, A. A. Metallofullerenes as Fuel Cell Electro-catalysts: A Theoretical Investigation of Adsorbates on C59Pt. *Phys. Chem. Chem. Phys.* **2010**, *12*, 9406−9412.

(43) Gabriel, M. A.; Deutsch, T.; Franco, A. A. Fullerene-Based Materials as Catalysts for Fuel Cells. *ECS Trans.* **2009**, *25*, 1−6.

(44) Valiev, M.; Bylaska, E. J.; Govind, N.; Kowalski, K.; Straatsma, T. P.; Van Dam, H. J. J.; Wang, D.; Nieplocha, J.; Apra, E.; Windus, T. L.; et al. NWChem: A Comprehensive and Scalable Open-Source Solution for Large Scale Molecular Simulations. *Comput. Phys. Commun.* **2010**, *181*, 1477−1489.

(45) Gromacs: Fast, Flexible, Free: Gromacs. http://www.gromacs.org/ (accessed Aug 23, 2018).

(46) LAMMPS Molecular Dynamics Simulator https://lammps.sandia.gov/ (accessed Aug 23, 2018).

(47) The Amber Home Page: Tools for Molecular Simulations. http://ambermd.org/ (accessed Aug 23, 2018).

(48) CHARMM: Chemistry at HARvard Macromolecular Mechanics. https://www.charmm.org/charmm/?CFID=b5834392-bccb-42ce-bcc0-2e75e6a4807d&CFTOKEN=0 (accessed Aug 23, 2018).

(49) Science & Technology Facilities Council: Scientific Computing Department: The DL_POLY Molecular Simulation Package. https://www.scd.stfc.ac.uk/Pages/DL_POLY.aspx (accessed Aug 23, 2018).

(50) Bozic, S.; Kondov, I. *Dataflow Management: A Grand Challenge in Multiscale Materials Modelling*; Cunningham, P., Cunningham, M., Eds.; IIMC international Information Management, 2012.

(51) Open for Innovation: KNIME. https://www.knime.com/ (accessed Aug 23, 2018).

(52) AiiDA: Automated Interactive Infrastructure and Database for Computational Science. http://www.aiida.net/ (accessed Aug 23, 2018).

(53) ECCE: Extensible Computational Chemistry Environment http://ecce.emsl.pnl.gov/ (accessed Aug 23, 2018).

(54) UNICORE | Distributed computing and data resources https://www.unicore.eu/ (accessed Aug 23, 2018).

(55) Hager, G.; Wellein, G. *Introduction to High Performance Computing for Scientists and Engineers*; Chapman & Hall/CRC Computational Science Series; CRC Press, 2010.

(56) Elwasif, W. R.; Bernholdt, D. E.; Pannala, S.; Allu, S.; Foley, S. S. Parameter Sweep and Optimization of Loosely Coupled Simulations Using the DAKOTA Toolkit. In *2012 IEEE 15th International Conference on Computational Science and Engineering*; IEEE, 2012; pp 102−110. DOI: 10.1109/ICCSE.2012.24.

(57) Ljung, L. *System Identification: Theory for the User*; Prentice Hall PTR, 1999.

(58) Ljung, L.; Glad, T. On Global Identifiability for Arbitrary Model Parametrizations. *Automatica* **1994**, *30*, 265−276.

(59) Walter, E. *Identifiability of State Space Models: With Applications to Transformation Systems*; Lecture Notes in Biomathematics; Springer-Verlag: Berlin, 1982.

(60) *Identifiability of Parametric Models*; Walter, E., Ed.; Pergamon Press: Oxford, 1987.

(61) Van den Hof, P. M. J.; Van Doren, J. F. M.; Douma, S. G. Identification of Parameters in Large Scale Physical Model Structures, for the Purpose of Model-Based Operations. In *Model-Based Control: Bridging Rigorous Theory and Advanced Technology*; Hof, P. M. J., Scherer, C., Heuberger, P. S. C., Eds.; Springer US: Boston, MA, 2009; pp 125−143.

(62) Santhanagopalan, S.; Guo, Q.; White, R. E. Parameter Estimation and Model Discrimination for a Lithium-Ion Cell. *J. Electrochem. Soc.* **2007**, *154*, A198−A206.

(63) Subramanian, V. R.; Devan, S.; White, R. E. An Approximate Solution for a Pseudocapacitor. *J. Power Sources* **2004**, *135*, 361−367.

(64) Subramanian, V. R.; Tapriyal, D.; White, R. E. A Boundary Condition for Porous Electrodes. *Electrochem. Solid-State Lett.* **2004**, *7*, A259.

(65) Vijayasekaran, B.; Basha, C. A. Shrinking Core Discharge Model for the Negative Electrode of a Lead-Acid Battery. *J. Power Sources* **2006**, *158*, 710−721.

(66) Guo, Q.; Subramanian, V. R.; Weidner, J. W.; White, R. E. Estimation of Diffusion Coefficient of Lithium in Carbon Using AC Impedance Technique. *J. Electrochem. Soc.* **2002**, *149*, A307−A318.

(67) Subramanian, V. R.; Boovaragavan, V.; Potukuchi, K.; Diwakar, V. D.; Guduru, A. A Numeric Symbolic Solution for Impedance Response of Electrochemical Devices I. Introduction of the Method. *Electrochem. Solid-State Lett.* **2007**, *10*, A25−A28.

(68) Boovaragavan, V.; Harinipriya, S.; Subramanian, V. R. Towards Real-Time (Milliseconds) Parameter Estimation of Lithium-Ion Batteries Using Reformulated Physics-Based Models. *J. Power Sources* **2008**, *183*, 361−365.

(69) Hohenberg, P.; Kohn, W. Inhomogeneous Electron Gas. *Phys. Rev.* **1964**, *136* (3B), B864−B871.

(70) Kohn, W.; Sham, L. J. Self-Consistent Equations Including Exchange and Correlation Effects. *Phys. Rev.* **1965**, *140* (4A), A1133−A1138.

(71) Wang, Y.; Perdew, J. P. Correlation Hole of the Spin-Polarized Electron Gas, with Exact Small-Wave-Vector and High-Density Scaling. *Phys. Rev. B: Condens. Matter Mater. Phys.* **1991**, *44*, 13298−13307.

(72) Perdew, J. P.; Burke, K.; Ernzerhof, M. Generalized Gradient Approximation Made Simple. *Phys. Rev. Lett.* **1996**, *77*, 3865−3868.

(73) Wolverton, C.; Zunger, A. Cation and Vacancy Ordering in Li_xCoO_2. *Phys. Rev. B: Condens. Matter Mater. Phys.* **1998**, *57*, 2242−2252.

(74) Aydinol, M. K.; Kohan, A. F.; Ceder, G.; Cho, K.; Joannopoulos, J. Ab Initio Study of Lithium Intercalation in Metal Oxides and Metal Dichalcogenides. *Phys. Rev. B: Condens. Matter Mater. Phys.* **1997**, *56*, 1354−1365.

(75) Zhou, F.; Cococcioni, M.; Marianetti, C. A.; Morgan, D.; Ceder, G. First-Principles Prediction of Redox Potentials in Transition-Metal Compounds with LDA+U. *Phys. Rev. B: Condens. Matter Mater. Phys.* **2004**, *70*, 235121.

(76) Dabo, I.; Ferretti, A.; Poilvert, N.; Li, Y.; Marzari, N.; Cococcioni, M. Koopmans' Condition for Density-Functional Theory. *Phys. Rev. B: Condens. Matter Mater. Phys.* **2010**, *82*, 115121.

(77) Kohn, W.; Meir, Y.; Makarov, D. E. Van Der Waals Energies in Density Functional Theory. *Phys. Rev. Lett.* **1998**, *80*, 4153−4156.

(78) Dobson, J. F.; McLennan, K.; Rubio, A.; Wang, J.; Gould, T.; Le, H. M.; Dinte, B. P. Prediction of Dispersion Forces: Is There a Problem? *Aust. J. Chem.* **2001**, *54*, 513−527.

(79) Mounet, N.; Marzari, N. First-Principles Determination of the Structural, Vibrational and Thermodynamic Properties of Diamond, Graphite, and Derivatives. *Phys. Rev. B: Condens. Matter Mater. Phys.* **2005**, *71*, 205214.

(80) Ooi, N.; Rairkar, A.; Adams, J. B. Density Functional Study of Graphite Bulk and Surface Properties. *Carbon* **2006**, *44*, 231−242.

(81) Grimme, S. Accurate description of van der Waals complexes by density functional theory including empirical corrections. *J. Comput. Chem.* **2004**, *25*, 1463−1473.

(82) Grimme, S.; Antony, J.; Ehrlich, S.; Krieg, H. A Consistent and Accurate Ab Initio Parametrization of Density Functional Dispersion Correction (DFT-D) for the 94 Elements H-Pu. *J. Chem. Phys.* **2010**, *132*, 154104.

(83) Lee, K.; Murray, É. D.; Kong, L.; Lundqvist, B. I.; Langreth, D. C. Higher-Accuracy van Der Waals Density Functional. *Phys. Rev. B: Condens. Matter Mater. Phys.* **2010**, *82*, 081101.

(84) Dion, M.; Rydberg, H.; Schröder, E.; Langreth, D. C.; Lundqvist, B. I. Van Der Waals Density Functional for General Geometries. *Phys. Rev. Lett.* **2004**, *92*, 246401.

(85) von Lilienfeld, O. A.; Tavernelli, I.; Rothlisberger, U.; Sebastiani, D. Optimization of Effective Atom Centered Potentials for London Dispersion Forces in Density Functional Theory. *Phys. Rev. Lett.* **2004**, *93*, 153004.

(86) Tavernelli, I.; Lin, I.-C.; Rothlisberger, U. Multicenter-Type Corrections to Standard DFT Exchange and Correlation Functionals. *Phys. Rev. B: Condens. Matter Mater. Phys.* **2009**, *79*, 045106.

(87) Andersson, Y.; Langreth, D. C.; Lundqvist, B. I. Van Der Waals Interactions in Density-Functional Theory. *Phys. Rev. Lett.* **1996**, *76*, 102−105.

(88) Tkatchenko, A.; Scheffler, M. Accurate Molecular Van Der Waals Interactions from Ground-State Electron Density and Free-Atom Reference Data. *Phys. Rev. Lett.* **2009**, *102*, 073005.

(89) Burdett, J. K. *Chemical Bonding in Solids*; Oxford University Press: New York, 1995.

(90) Bader, R. F. W. A Quantum Theory of Molecular Structure and Its Applications. *Chem. Rev.* **1991**, *91*, 893−928.

(91) Bader, R. F. W. *Atoms in Molecules: A Quantum Theory*; International Series of Monographs on Chemistry; Oxford University Press: Oxford, NY, 1994.

(92) Becke, A. D.; Edgecombe, K. E. A Simple Measure of Electron Localization in Atomic and Molecular Systems. *J. Chem. Phys.* **1990**, *92*, 5397−5403.

(93) Gatti, C. Chemical Bonding in Crystals: New Directions. *Z. Kristallogr. - Cryst. Mater.* **2005**, *220*, 399−457.

(94) Van der Ven, A.; Bhattacharya, J.; Belak, A. A. Understanding Li Diffusion in Li-Intercalation Compounds. *Acc. Chem. Res.* **2013**, *46*, 1216−1225.

(95) Bortz, A. B.; Kalos, M. H.; Lebowitz, J. L. A New Algorithm for Monte Carlo Simulation of Ising Spin Systems. *J. Comput. Phys.* **1975**, *17*, 10−18.

(96) Voter, A. F. Classically Exact Overlayer Dynamics: Diffusion of Rhodium Clusters on Rh(100). *Phys. Rev. B: Condens. Matter Mater. Phys.* **1986**, *34*, 6819−6829.

(97) Maksym, P. A. Fast Monte Carlo Simulation of MBE Growth. *Semicond. Sci. Technol.* **1988**, *3*, 594.

(98) Bulnes, F. M.; Pereyra, V. D.; Riccardo, J. L. Collective Surface Diffusion: n-Fold Way Kinetic Monte Carlo Simulation. *Phys. Rev. E: Stat. Phys., Plasmas, Fluids, Relat. Interdiscip. Top.* **1998**, *58*, 86−92.

(99) Wu, Q.; He, B.; Song, T.; Gao, J.; Shi, S. Cluster Expansion Method and Its Application in Computational Materials Science. *Comput. Mater. Sci.* **2016**, *125*, 243−254.

(100) Sanchez, J. M.; Ducastelle, F.; Gratias, D. Generalized Cluster Description of Multicomponent Systems. *Phys. A* **1984**, *128*, 334−350.

(101) Jonsson, H.; Mills, G.; Jacobsen, K. W. Nudged Elastic Band Method for Finding Minimum Energy Paths of Transitions. In *Classical and Quantum Dynamics in Condensed Phase Simulations*; World Scientific, 1998; pp 385−404.

(102) Shi, S.; Gao, J.; Liu, Y.; Zhao, Y.; Wu, Q.; Ju, W.; Ouyang, C.; Xiao, R. Multi-Scale Computation Methods: Their Applications in Lithium-Ion Battery Research and Development. *Chin. Phys. B* **2016**, *25*, 018212.

(103) Delmas, C.; Braconnier, J.-J.; Hagenmuller, P. A New Variety of $LiCoO_2$ with an Unusual Oxygen Packing Obtained by Exchange Reaction. *Mater. Res. Bull.* **1982**, *17*, 117−123.

(104) Van der Ven, A.; Aydinol, M. K.; Ceder, G.; Kresse, G.; Hafner, J. First-Principles Investigation of Phase Stability in Li_xCoO_2. *Phys. Rev. B: Condens. Matter Mater. Phys.* **1998**, *58*, 2975−2987.

(105) Carlier, D.; Van der Ven, A.; Delmas, C.; Ceder, G. First-Principles Investigation of Phase Stability in the $O2$-$LiCoO_2$ System. *Chem. Mater.* **2003**, *15*, 2651−2660.

(106) Okumura, T.; Yamaguchi, Y.; Shikano, M.; Kobayashi, H. Correlation of Lithium Ion Distribution and X-Ray Absorption near-Edge Structure in O3- and O2-Lithium Cobalt Oxides from First-Principle Calculation. *J. Mater. Chem.* **2012**, *22*, 17340−17348.

(107) Arroyo y de Dompablo, M. E.; Van der Ven, A.; Ceder, G. First-Principles Calculations of Lithium Ordering and Phase Stability on Li_xNiO_2. *Phys. Rev. B: Condens. Matter Mater. Phys.* **2002**, *66*, 064112.

(108) Van der Ven, A.; Ceder, G. Ordering in $Li_x(Ni_{0.5}Mn_{0.5})O_2$ and Its Relation to Charge Capacity and Electrochemical Behavior in Rechargeable Lithium Batteries. *Electrochem. Commun.* **2004**, *6*, 1045−1050.

(109) Hinuma, Y.; Meng, Y. S.; Kang, K.; Ceder, G. Phase Transitions in the $LiNi_{0.5}Mn_{0.5}O_2$ System with Temperature. *Chem. Mater.* **2007**, *19*, 1790−1800.

(110) Van der Ven, A.; Thomas, J. C.; Xu, Q.; Swoboda, B.; Morgan, D. Nondilute Diffusion from First Principles: Li Diffusion in Li_xTiS_2. *Phys. Rev. B: Condens. Matter Mater. Phys.* **2008**, *78*, 104306.

(111) Hinuma, Y.; Meng, Y. S.; Ceder, G. Temperature-Concentration Phase Diagram of $P2$-Na_2CoO_2 from First-Principles Calculations. *Phys. Rev. B: Condens. Matter Mater. Phys.* **2008**, *77*, 224111.

(112) Mo, Y.; Ong, S. P.; Ceder, G. Insights into Diffusion Mechanisms in P2 Layered Oxide Materials by First-Principles Calculations. *Chem. Mater.* **2014**, *26*, 5208−5214.

(113) Mortemard de Boisse, B.; Carlier, D.; Guignard, M.; Delmas, C. Structural and Electrochemical Characterizations of P2 and New O3-$Na_xMn_{1-y}Fe_yO_2$ Phases Prepared by Auto-Combustion Synthesis for Na-Ion Batteries. *J. Electrochem. Soc.* **2013**, *160*, A569−A574.

(114) Du, T.; Xu, B.; Wu, M.; Liu, G.; Ouyang, C. Insight into the Vibrational and Thermodynamic Properties of Layered Lithium Transition-Metal Oxides $LiMO_2$ (M = Co, Ni, Mn): A First-Principles Study. *J. Phys. Chem. C* **2016**, *120*, 5876−5882.

(115) Chang, K.; Hallstedt, B.; Music, D. Thermodynamic and Electrochemical Properties of the Li−Co−O and Li−Ni−O Systems. *Chem. Mater.* **2012**, *24*, 97−105.

(116) Kubaschewski, O.; Alcock, C. B.; Spencer, P. J. *Materials Thermochemistry*, 6th revised ed.; Butterworth-Heinemann Ltd.: Oxford, 1993.

(117) Darling, R.; Newman, J. Dynamic Monte Carlo Simulations of Diffusion in $Li_yMn_2O_4$. *J. Electrochem. Soc.* **1999**, *146*, 3765−3772.

(118) Ouyang, C. Y.; Shi, S. Q.; Wang, Z. X.; Li, H.; Huang, X. J.; Chen, L. Q. Ab Initio Molecular-Dynamics Studies on LixMn2O4 as Cathode Material for Lithium Secondary Batteries. *EPL* **2004**, *67*, 28.

(119) Bhattacharya, J.; Van der Ven, A. Phase Stability and Nondilute Li Diffusion in Spinel $Li_{1+x}Ti_2O_4$. *Phys. Rev. B: Condens. Matter Mater. Phys.* **2010**, *81*, 104304.

(120) Jiang, T.; Rudraraju, S.; Roy, A.; Van der Ven, A.; Garikipati, K.; Falk, M. L. Multiphysics Simulations of Lithiation-Induced Stress in $Li_{1+x}Ti_2O_4$ Electrode Particles. *J. Phys. Chem. C* **2016**, *120*, 27871−27881.

(121) Zhang, W.; Cupid, D. M.; Gotcu, P.; Chang, K.; Li, D.; Du, Y.; Seifert, H. J. High-Throughput Description of Infinite Composition−Structure−Property−Performance Relationships of Lithium−Manganese Oxide Spinel Cathodes. *Chem. Mater.* **2018**, *30*, 2287−2298.

(122) Padhi, A. K.; Nanjundaswamy, K. S.; Goodenough, J. B. Phospho olivines as Positive Electrode Materials for Rechargeable Lithium Batteries. *J. Electrochem. Soc.* **1997**, *144*, 1188−1194.

(123) Masquelier, C.; Croguennec, L. Polyanionic (Phosphates, Silicates, Sulfates) Frameworks as Electrode Materials for Rechargeable Li (or Na) Batteries. *Chem. Rev.* **2013**, *113*, 6552−6591.

(124) Yang, J.; Tse, J. S. Li Ion Diffusion Mechanisms in LiFePO4An Ab Initio Molecular Dynamics Study. *J. Phys. Chem. A* **2011**, *115*, 13045−13049.

(125) Ouyang, C.-Y.; Wang, D.-Y.; Shi, S.-Q.; Wang, Z-X.; Li, H.; Huang, X.-J.; Chen, L.-Q. First Principles Study on $Na_xLi_{1-x}FePO_4$ As Cathode Material for Rechargeable Lithium Batteries. *Chin. Phys. Lett.* **2006**, *23*, 61.

(126) Xiao, P.; Henkelman, G. Kinetic Monte Carlo Study of Li Intercalation in $LiFePO_4$. *ACS Nano* **2018**, *12*, 844−851.

(127) Hin, C. Kinetic Monte Carlo Simulations of Anisotropic Lithium Intercalation into LixFePO4 Electrode Nanocrystals. *Adv. Funct. Mater.* **2011**, *21*, 2477−2487.

(128) Newman, J. S.; Tobias, C. W. Theoretical Analysis of Current Distribution in Porous Electrodes. *J. Electrochem. Soc.* **1962**, *109*, 1183−1191.

(129) Newman, J.; Tiedemann, W. Porous-Electrode Theory with Battery Applications. *AIChE J.* **1975**, *21*, 25−41.

(130) Srinivasan, V.; Newman, J. Discharge Model for the Lithium Iron-Phosphate Electrode. *J. Electrochem. Soc.* **2004**, *151*, A1517−A1529.

(131) Cogswell, D. A.; Bazant, M. Z. Coherency Strain and the Kinetics of Phase Separation in $LiFePO_4$ Nanoparticles. *ACS Nano* **2012**, *6*, 2215−2225.

(132) Bazant, M. Z. Theory of Chemical Kinetics and Charge Transfer Based on Nonequilibrium Thermodynamics. *Acc. Chem. Res.* **2013**, *46*, 1144−1160.

(133) Kang, B.; Ceder, G. Battery Materials for Ultrafast Charging and Discharging. *Nature* **2009**, *458* (7235), 190−193.

(134) Lim, J.; Li, Y.; Alsem, D. H.; So, H.; Lee, S. C.; Bai, P.; Cogswell, D. A.; Liu, X.; Jin, N.; Yu, Y.; et al. Origin and Hysteresis of Lithium Compositional Spatiodynamics within Battery Primary Particles. *Science* **2016**, *353* (6299), 566−571.

(135) Lim, J.-M.; Oh, R.-G.; Cho, W.; Cho, K.; Cho, M.; Park, M.-S. Power Characteristics of Spinel Cathodes Correlated with Elastic Softness and Phase Transformation for High-Power Lithium-Ion Batteries. *J. Mater. Chem. A* **2017**, *5*, 3404−3411.

(136) Ouyang, C. Y.; Shi, S. Q.; Wang, Z. X.; Li, H.; Huang, X. J.; Chen, L. Q. The Effect of Cr Doping on Li Ion Diffusion in $LiFePO_4$ from First Principles Investigations and Monte Carlo Simulations. *J. Phys.: Condens. Matter* **2004**, *16*, 2265.

(137) Recham, N.; Chotard, J.-N.; Dupont, L.; Delacourt, C.; Walker, W.; Armand, M.; Tarascon, J.-M. A 3.6 V Lithium-Based Fluorosulphate Insertion Positive Electrode for Lithium-Ion Batteries. *Nat. Mater.* **2010**, *9*, 68−74.

(138) Frayret, C.; Villesuzanne, A.; Spaldin, N.; Bousquet, E.; Chotard, J.-N.; Recham, N.; Tarascon, J.-M. LiMSO4F (M = Fe, Co and Ni): Promising New Positive Electrode Materials through the DFT Microscope. *Phys. Chem. Chem. Phys.* **2010**, *12*, 15512−15522.

(139) Ramzan, M.; Lebègue, S.; Kang, T. W.; Ahuja, R. Hybrid Density Functional Calculations and Molecular Dynamics Study of Lithium Fluorosulphate, A Cathode Material for Lithium-Ion Batteries. *J. Phys. Chem. C* **2011**, *115*, 2600−2603.

(140) Persson, K.; Hinuma, Y.; Meng, Y. S.; Van der Ven, A.; Ceder, G. Thermodynamic and Kinetic Properties of the Li-Graphite System from First-Principles Calculations. *Phys. Rev. B: Condens. Matter Mater. Phys.* **2010**, *82*, 125416.

(141) Persson, K.; Sethuraman, V. A.; Hardwick, L. J.; Hinuma, Y.; Meng, Y. S.; Van der Ven, A.; Srinivasan, V.; Kostecki, R.; Ceder, G. Lithium Diffusion in Graphitic Carbon. *J. Phys. Chem. Lett.* **2010**, *1*, 1176−1180.

(142) Ganesh, P.; Kim, J.; Park, C.; Yoon, M.; Reboredo, F. A.; Kent, P. R. C. Binding and Diffusion of Lithium in Graphite: Quantum Monte Carlo Benchmarks and Validation of van Der Waals Density Functional Methods. *J. Chem. Theory Comput.* **2014**, *10*, 5318−5323.

(143) Raju, M.; Ganesh, P.; Kent, P. R. C.; van Duin, A. C. T. Reactive Force Field Study of Li/C Systems for Electrical Energy Storage. *J. Chem. Theory Comput.* **2015**, *11*, 2156−2166.

(144) Chou, C.-Y.; Hwang, G. S. Lithiation Behavior of Silicon-Rich Oxide ($SiO_{1/3}$): A First-Principles Study. *Chem. Mater.* **2013**, *25*, 3435−3440.

(145) Schon, T. B.; McAllister, B. T.; Li, P.-F.; Seferos, D. S. The Rise of Organic Electrode Materials for Energy Storage. *Chem. Soc. Rev.* **2016**, *45*, 6345−6404.

(146) Zhao, Q.; Zhu, Z.; Chen, J. Molecular Engineering with Organic Carbonyl Electrode Materials for Advanced Stationary and Redox Flow Rechargeable Batteries. *Adv. Mater.* **2017**, *29*, 1607007.

(147) Armand, M.; Tarascon, J.-M. Building better batteries. *Nature* **2008**, *451*, 652−657.

(148) Poizot, P.; Dolhem, F. Clean Energy New Deal for a Sustainable World: From Non-CO_2 Generating Energy Sources to Greener Electrochemical Storage Devices. *Energy Environ. Sci.* **2011**, *4*, 2003−2019.

(149) Lee, S.; Kwon, G.; Ku, K.; Yoon, K.; Jung, S.-K.; Lim, H.-D.; Kang, K. Recent Progress in Organic Electrodes for Li and Na Rechargeable Batteries. *Adv. Mater.* **2018**, *30*, 1704682.

(150) Beheshti, A.; Norouzi, P.; Ganjali, M. R. A Simple and Robust Model for Predicting the Reduction Potential of Quinones Family; Electrophilicity Index Effect. *Int. J. Electrochem. Sci.* **2012**, *7*, 4811−4821.

(151) Yao, M.; Senoh, H.; Yamazaki, S.; Siroma, Z.; Sakai, T.; Yasuda, K. High-Capacity Organic Positive-Electrode Material Based on a Benzoquinone Derivative for Use in Rechargeable Lithium Batteries. *J. Power Sources* **2010**, *195*, 8336−8340.

(152) Yao, M.; Senoh, H.; Araki, M.; Sakai, T.; Yasuda, K. Organic Positive-Electrode Materials Based on Dialkoxybenzoquinone Derivatives for Use in Rechargeable Lithium Batteries. *ECS Trans.* **2010**, *28*, 3−10.

(153) Zhou, W.; Hernández-Burgos, K.; Burkhardt, S. E.; Qian, H.; Abruña, H. D. Synthesis and Electrochemical and Computational Analysis of Two New Families of Thiophene-Carbonyl Molecules. *J. Phys. Chem. C* **2013**, *117*, 6022−6032.

(154) Chen, Z.; Wannere, C. S.; Corminboeuf, C.; Puchta, R.; Schleyer, P. v. R. Nucleus-Independent Chemical Shifts (NICS) as an Aromaticity Criterion. *Chem. Rev.* **2005**, *105*, 3842−3888.

(155) Kruszewski, J.; Krygowski, T. M. Definition of Aromaticity Basing on the Harmonic Oscillator Model. *Tetrahedron Lett.* **1972**, *13*, 3839−3842.

(156) Fradera, X.; Austen, M. A.; Bader, R. F. W. The Lewis Model and Beyond. *J. Phys. Chem. A* **1999**, *103*, 304−314.

(157) Matito, E.; Duran, M.; Solà, M. The Aromatic Fluctuation Index (FLU): A New Aromaticity Index Based on Electron Delocalization. *J. Chem. Phys.* **2005**, *122*, 014109.

(158) Gatti, C.; Orlando, A. M.; Lo Presti, L. Insights on Spin Polarization through the Spin Density Source Function. *Chem. Sci.* **2015**, *6*, 3845−3852.

(159) Tomerini, D.; Gatti, C.; Frayret, C. Engineering of Unsubstituted Quinoid-like Frameworks Enabling 2 V vs. Li^+/Li

Redox Voltage Tunability and Related Derivatives. *Phys. Chem. Chem. Phys.* **2015**, *17*, 8604−8608.

(160) Tomerini, D.; Gatti, C.; Frayret, C. Playing with Isomerism and N Substitution in Pentalenedione Derivatives for Organic Electrode Batteries: How High Are the Stakes? *Phys. Chem. Chem. Phys.* **2016**, *18*, 2442−2448.

(161) Tomerini, D.; Politano, O.; Gatti, C.; Frayret, C. Electronic Structure and Energy Decomposition Analyses as a Tool to Interpret the Redox Potential Ranking of Naphtho-, Biphenyl- and Biphenylene-Quinone Isomers. *Phys. Chem. Chem. Phys.* **2016**, *18*, 26651−26660.

(162) Ruiz del Árbol, N.; Palacio, I.; Otero Irurueta, G.; Martínez, J. I.; de Andrés, P. L.; Stetsovych, O.; Moro Lagares, M.; Mutombo, P.; Svec, M.; Jelínek, P.; et al. On-Surface Bottom-Up Synthesis of Azine Derivatives Displaying Strong Acceptor Behavior. *Angew. Chem., Int. Ed.* **2018**, *57*, 8582−8586.

(163) Luo, C.; Borodin, O.; Ji, X.; Hou, S.; Gaskell, K. J.; Fan, X.; Chen, J.; Deng, T.; Wang, R.; Jiang, J.; et al. Azo Compounds as a Family of Organic Electrode Materials for Alkali-Ion Batteries. *Proc. Natl. Acad. Sci. U. S. A.* **2018**, *115*, 2004−2009.

(164) Lakraychi, A. E.; Dolhem, F.; Djedaïni-Pilard, F.; Thiam, A.; Frayret, C.; Becuwe, M. Decreasing Redox Voltage of Terephthalate-Based Electrode Material for Li-Ion Battery Using Substituent Effect. *J. Power Sources* **2017**, *359*, 198−204.

(165) Zhao, Q.; Huang, W.; Luo, Z.; Liu, L.; Lu, Y.; Li, Y.; Li, L.; Hu, J.; Ma, H.; Chen, J. High-Capacity Aqueous Zinc Batteries Using Sustainable Quinone Electrodes. *Science Advances* **2018**, *4*, No. eaao1761.

(166) Liu, L.; Miao, L.; Li, L.; Li, F.; Lu, Y.; Shang, Z.; Chen, J. Molecular Electrostatic Potential: A New Tool to Predict the Lithiation Process of Organic Battery Materials. *J. Phys. Chem. Lett.* **2018**, *9*, 3573−3579.

(167) Barrès, A.-L.; Geng, J.; Bonnard, G.; Renault, S.; Gottis, S.; Mentré, O.; Frayret, C.; Dolhem, F.; Poizot, P. High-Potential Reversible Li Deintercalation in a Substituted Tetrahydroxy-p-Benzoquinone Dilithium Salt: An Experimental and Theoretical Study. *Chem. - Eur. J.* **2012**, *18*, 8800−8812.

(168) Bonnard, G.; Barrès, A.-L.; Mentré, O.; Allis, D. G.; Gatti, C.; Poizot, P.; Frayret, C. The Low/Room-Temperature Forms of the Lithiated Salt of 3,6-Dihydroxy-2,5-Dimethoxy-p-Benzoquinone: A Combined Experimental and Dispersion-Corrected Density Functional Study. *CrystEngComm* **2013**, *15*, 2809−2821.

(169) Bonnard, G.; Barrès, A.-L.; Danten, Y.; Allis, D. G.; Mentré, O.; Tomerini, D.; Gatti, C.; Izgorodina, E. I.; Poizot, P.; Frayret, C. Experimental and Theoretical Studies of Tetramethoxy-p-Benzoquinone: Infrared Spectra, Structural and Lithium Insertion Properties. *RSC Adv.* **2013**, *3*, 19081−19096.

(170) Ogihara, N.; Yasuda, T.; Kishida, Y.; Ohsuna, T.; Miyamoto, K.; Ohba, N. Organic Dicarboxylate Negative Electrode Materials with Remarkably Small Strain for High-Voltage Bipolar Batteries. *Angew. Chem.* **2014**, *126*, 11651−11656.

(171) Seo, D.-H.; Kim, H.; Kim, H.; Goddard, W. A.; Kang, K. The Predicted Crystal Structure of $Li_4C_6O_6$ an Organic Cathode Material for Li-Ion Batteries, from First-Principles Multi-Level Computational Methods. *Energy Environ. Sci.* **2011**, *4*, 4938−4941.

(172) Chen, H.; Armand, M.; Demailly, G.; Dolhem, F.; Poizot, P.; Tarascon, J.-M. From Biomass to a Renewable $Li_xC_6O_6$ Organic Electrode for Sustainable Li-Ion Batteries. *ChemSusChem* **2008**, *1*, 348−355.

(173) Yamashita, T.; Momida, H.; Oguchi, T. Crystal Structure Predictions of $Na_xC_6O_6$ for Sodium-Ion Batteries: First-Principles Calculations with an Evolutionary Algorithm. *Electrochim. Acta* **2016**, *195*, 1−8.

(174) Oganov, A. R.; Lyakhov, A. O.; Valle, M. How Evolutionary Crystal Structure Prediction Works—and Why. *Acc. Chem. Res.* **2011**, *44*, 227−237.

(175) Araujo, R. B.; Banerjee, A.; Ahuja, R. Divulging the Hidden Capacity and Sodiation Kinetics of $Na_xC_6Cl_4O_2$A High Voltage Organic Cathode for Sodium Rechargeable Batteries. *J. Phys. Chem. C* **2017**, *121*, 14027−14036.

(176) Chen, Y.; Lüder, J.; Ng, M.-F.; Sullivan, M.; Manzhos, S. Polyaniline and CN-Functionalized Polyaniline as Organic Cathodes for Lithium and Sodium Ion Batteries: A Combined Molecular Dynamics and Density Functional Tight Binding Study in Solid State. *Phys. Chem. Chem. Phys.* **2018**, *20*, 232−237.

(177) Tachikawa, H. Mechanism of Dissolution of a Lithium Salt in an Electrolytic Solvent in a Lithium Ion Secondary Battery: A Direct Ab Initio Molecular Dynamics (AIMD) Study. *ChemPhysChem* **2014**, *15*, 1604−1610.

(178) Bhatt, M. D.; Cho, M.; Cho, K. Density Functional Theory Calculations and Ab Initio Molecular Dynamics Simulations for Diffusion of Li⁺ within Liquid Ethylene Carbonate. *Modell. Simul. Mater. Sci. Eng.* **2012**, *20*, 065004.

(179) Ong, M. T.; Bhatia, H.; Gyulassy, A. G.; Draeger, E. W.; Pascucci, V.; Bremer, P.-T.; Lordi, V.; Pask, J. E. Complex Ion Dynamics in Carbonate Lithium-Ion Battery Electrolytes. *J. Phys. Chem. C* **2017**, *121*, 6589−6595.

(180) Ganesh, P.; Jiang, D.; Kent, P. R. C. Accurate Static and Dynamic Properties of Liquid Electrolytes for Li-Ion Batteries from Ab Initio Molecular Dynamics. *J. Phys. Chem. B* **2011**, *115*, 3085−3090.

(181) Ong, M. T.; Verners, O.; Draeger, E. W.; van Duin, A. C. T.; Lordi, V.; Pask, J. E. Lithium Ion Solvation and Diffusion in Bulk Organic Electrolytes from First-Principles and Classical Reactive Molecular Dynamics. *J. Phys. Chem. B* **2015**, *119*, 1535−1545.

(182) Borodin, O.; Olguin, M.; Ganesh, P.; Kent, P. R. C.; Allen, J. L.; Henderson, W. A. Competitive Lithium Solvation of Linear and Cyclic Carbonates from Quantum Chemistry. *Phys. Chem. Chem. Phys.* **2016**, *18*, 164−175.

(183) Bhatia, H.; Gyulassy, A.; Ong, M.; Lordi, V.; Draeger, E.; Pask, J.; Pascucci, V.; Bremer, P.-T. *Understanding Lithium Solvation and Diffusion through Topological Analysis of First-Principles Molecular Dynamics*; LLNL-TR-704318; Lawrence Livermore National Lab (LLNL): Livermore, CA, 2016.

(184) Tang, Z.-K.; Tse, J. S.; Liu, L.-M. Unusual Li-Ion Transfer Mechanism in Liquid Electrolytes: A First-Principles Study. *J. Phys. Chem. Lett.* **2016**, *7*, 4795−4801.

(185) Chen, J.; Han, K. S.; Henderson, W. A.; Lau, K. C.; Vijayakumar, M.; Dzwiniel, T.; Pan, H.; Curtiss, L. A.; Xiao, J.; Mueller, K. T.; et al. Restricting the Solubility of Polysulfides in Li-S Batteries Via Electrolyte Salt Selection. *Adv. Energy Mater.* **2016**, *6*, 1600160.

(186) Partovi-Azar, P.; Kühne, T. D.; Kaghazchi, P. Evidence for the Existence of Li2S2 Clusters in Lithium−Sulfur Batteries: Ab Initio Raman Spectroscopy Simulation. *Phys. Chem. Chem. Phys.* **2015**, *17*, 22009−22014.

(187) Scheers, J.; Lidberg, D.; Sodeyama, K.; Futera, Z.; Tateyama, Y. Life of Superoxide in Aprotic Li−O₂ Battery Electrolytes: Simulated Solvent and Counter-Ion Effects. *Phys. Chem. Chem. Phys.* **2016**, *18*, 9961−9968.

(188) Ray, P.; Vogl, T.; Balducci, A.; Kirchner, B. Structural Investigations on Lithium-Doped Protic and Aprotic Ionic Liquids. *J. Phys. Chem. B* **2017**, *121*, 5279−5292.

(189) Vicent Luna, J. M.; Ortiz Roldan, J. M.; Hamad, S.; Tena Zaera, R.; Calero, S.; Anta, J. A. Quantum and Classical Molecular Dynamics of Ionic Liquid Electrolytes for Na/Li-Based Batteries: Molecular Origins of the Conductivity Behavior. *ChemPhysChem* **2016**, *17*, 2473−2481.

(190) Haskins, J. B.; Bauschlicher, C. W.; Lawson, J. W. Ab Initio Simulations and Electronic Structure of Lithium-Doped Ionic Liquids: Structure, Transport, and Electrochemical Stability. *J. Phys. Chem. B* **2015**, *119*, 14705−14719.

(191) Umebayashi, Y.; Mitsugi, T.; Fukuda, S.; Fujimori, T.; Fujii, K.; Kanzaki, R.; Takeuchi, M.; Ishiguro, S.-I. Lithium Ion Solvation in Room-Temperature Ionic Liquids Involving Bis-(Trifluoromethanesulfonyl) Imide Anion Studied by Raman Spectroscopy and DFT Calculations. *J. Phys. Chem. B* **2007**, *111*, 13028−13032.

(192) Fujii, K.; Fujimori, T.; Takamuku, T.; Kanzaki, R.; Umebayashi, Y.; Ishiguro, S. Conformational Equilibrium of Bis-(Trifluoromethanesulfonyl) Imide Anion of a Room-Temperature

Ionic Liquid: Raman Spectroscopic Study and DFT Calculations. *J. Phys. Chem. B* **2006**, *110*, 8179−8183.

(193) Haskins, J. B.; Bennett, W. R.; Wu, J. J.; Hernández, D. M.; Borodin, O.; Monk, J. D.; Bauschlicher, C. W.; Lawson, J. W. Computational and Experimental Investigation of Li-Doped Ionic Liquid Electrolytes: [Pyr14][TFSI], [Pyr13][FSI], and [EMIM][BF₄]. *J. Phys. Chem. B* **2014**, *118*, 11295−11309.

(194) Xue, S.; Liu, Y.; Li, Y.; Teeters, D.; Crunkleton, D. W.; Wang, S. Diffusion of Lithium Ions in Amorphous and Crystalline Poly(Ethylene Oxide)3:LiCF₃SO₃ Polymer Electrolytes. *Electrochim. Acta* **2017**, *235*, 122−128.

(195) Miara, L. J.; Suzuki, N.; Richards, W. D.; Wang, Y.; Kim, J. C.; Ceder, G. Li-Ion Conductivity in Li₉S₃N. *J. Mater. Chem. A* **2015**, *3*, 20338−20344.

(196) Ong, S. P.; Mo, Y.; Richards, W. D.; Miara, L.; Lee, H. S.; Ceder, G. Phase Stability, Electrochemical Stability and Ionic Conductivity of the Li₁₀±₁MP₂X₁₂ (M = Ge, Si, Sn, Al or P, and X = O, S or Se) Family of Superionic Conductors. *Energy Environ. Sci.* **2013**, *6*, 148−156.

(197) Zhang, B.; Tan, R.; Yang, L.; Zheng, J.; Zhang, K.; Mo, S.; Lin, Z.; Pan, F. Mechanisms and Properties of Ion-Transport in Inorganic Solid Electrolytes. *Energy Storage Materials* **2018**, *10*, 139−159.

(198) Åvall, G.; Mindemark, J.; Brandell, D.; Johansson, P. Sodium-Ion Battery Electrolytes: Modeling and Simulations. *Adv. Energy Mater.* **2018**, *8*, 1703036.

(199) Deng, Z.; Mo, Y.; Ong, S. P. Computational Studies of Solid-State Alkali Conduction in Rechargeable Alkali-Ion Batteries. *NPG Asia Mater.* **2016**, *8*, No. e254.

(200) Oh, K.; Chang, D.; Lee, B.; Kim, D.-H.; Yoon, G.; Park, I.; Kim, B.; Kang, K. Native Defects in Li₁₀GeP₂S₁₂ and Their Effect on Lithium Diffusion. *Chem. Mater.* **2018**, *30*, 4995−5004.

(201) de Klerk, N. J. J.; Van der Maas, E.; Wagemaker, M. Analysis of Diffusion in Solid-State Electrolytes through MD Simulations, Improvement of the Li-Ion Conductivity in β-Li₃PS₄ as an Example. *ACS Appl. Energy Mater.* **2018**, *1*, 3230−3242.

(202) Chu, I.-H.; Nguyen, H.; Hy, S.; Lin, Y.-C.; Wang, Z.; Xu, Z.; Deng, Z.; Meng, Y. S.; Ong, S. P. Insights into the Performance Limits of the Li₇P₃S₁₁ Superionic Conductor: A Combined First-Principles and Experimental Study. *ACS Appl. Mater. Interfaces* **2016**, *8*, 7843−7853.

(203) Wang, Y.; Richards, W. D.; Bo, S.-H.; Miara, L. J.; Ceder, G. Computational Prediction and Evaluation of Solid-State Sodium Superionic Conductors Na₇P₃X₁₁ (X = O, S, Se). *Chem. Mater.* **2017**, *29*, 7475−7482.

(204) Bo, S.-H.; Wang, Y.; Kim, J. C.; Richards, W. D.; Ceder, G. Computational and Experimental Investigations of Na-Ion Conduction in Cubic Na₃PSe₄. *Chem. Mater.* **2016**, *28*, 252−258.

(205) Zhu, Z.; Chu, I.-H.; Deng, Z.; Ong, S. P. Role of Na⁺ Interstitials and Dopants in Enhancing the Na⁺ Conductivity of the Cubic Na₃PS₄ Superionic Conductor. *Chem. Mater.* **2015**, *27*, 8318−8325.

(206) de Klerk, N. J. J.; Wagemaker, M. Diffusion Mechanism of the Sodium-Ion Solid Electrolyte Na₃PS₄ and Potential Improvements of Halogen Doping. *Chem. Mater.* **2016**, *28*, 3122−3130.

(207) Dawson, J. A.; Attari, T. S.; Chen, H.; Emge, S. P.; Johnston, K. E.; Islam, M. S. Elucidating Lithium-Ion and Proton Dynamics in Anti-Perovskite Solid Electrolytes. *Energy Environ. Sci.* **2018**, *11*, 2993.

(208) Dawson, J. A.; Canepa, P.; Famprikis, T.; Masquelier, C.; Islam, M. S. Atomic-Scale Influence of Grain Boundaries on Li-Ion Conduction in Solid Electrolytes for All-Solid-State Batteries. *J. Am. Chem. Soc.* **2018**, *140*, 362−368.

(209) Chaban, V. Solvation of the Fluorine Containing Anions and Their Lithium Salts in Propylene Carbonate and Dimethoxyethane. *J. Mol. Model.* **2015**, *21*, 172.

(210) Chaban, V. Solvation of Lithium Ion in Dimethoxyethane and Propylene Carbonate. *Chem. Phys. Lett.* **2015**, *631−632*, 1−5.

(211) Chaban, V. V.; Andreeva, N. A. Sodium-Ion Electrolytes Based on Ionic Liquids: A Role of Cation-Anion Hydrogen Bonding. *J. Mol. Model.* **2016**, *22*, 172.

(212) Verners, O.; Van Duin, A. C. T.; Wagemaker, M.; Simone, A. Molecular Dynamics Modeling of Structural Battery Components. In

ICCM 20:20th International Conference on Composite Materials, Copenhagen, Denmark, 19–24 July 2015; Copenhagen, Denmark, 2015.

(213) Verners, O.; Thijsse, B. J.; van Duin, A. C. T.; Simone, A. Salt Concentration Effects on Mechanical Properties of $LiPF_6$/Poly-(Propylene Glycol) Diacrylate Solid Electrolyte: Insights from Reactive Molecular Dynamics Simulations. *Electrochim. Acta* **2016**, *221*, 115–123.

(214) Jorgensen, W. L.; Maxwell, D. S.; Tirado-Rives, J. Development and Testing of the OPLS All-Atom Force Field on Conformational Energetics and Properties of Organic Liquids. *J. Am. Chem. Soc.* **1996**, *118*, 11225–11236.

(215) Jorgensen, W. L.; Ibrahim, M. Structures and Properties of Organic Liquids: N-Alkyl Ethers and Their Conformational Equilibriums. *J. Am. Chem. Soc.* **1981**, *103*, 3976–3985.

(216) Canongia Lopes, J. N.; Pádua, A. A. H. Molecular Force Field for Ionic Liquids Composed of Triflate or Bistriflylimide Anions. *J. Phys. Chem. B* **2004**, *108*, 16893–16898.

(217) Borodin, O.; Smith, G. D. Development of Many−Body Polarizable Force Fields for Li-Battery Applications: 2. LiTFSI-Doped Oligoether, Polyether, and Carbonate-Based Electrolytes. *J. Phys. Chem. B* **2006**, *110*, 6293–6299.

(218) Borodin, O.; Smith, G. D. Development of Many−Body Polarizable Force Fields for Li-Battery Components: 1. Ether, Alkane, and Carbonate-Based Solvents. *J. Phys. Chem. B* **2006**, *110*, 6279–6292.

(219) Borodin, O.; Smith, G. D. Quantum Chemistry and Molecular Dynamics Simulation Study of Dimethyl Carbonate: Ethylene Carbonate Electrolytes Doped with $LiPF_6$. *J. Phys. Chem. B* **2009**, *113*, 1763–1776.

(220) Starovoytov, O. N.; Borodin, O.; Bedrov, D.; Smith, G. D. Development of a Polarizable Force Field for Molecular Dynamics Simulations of Poly (Ethylene Oxide) in Aqueous Solution. *J. Chem. Theory Comput.* **2011**, *7*, 1902–1915.

(221) Lee, S.; Park, S. S. Dielectric Constants of Binary Mixtures of Propylene Carbonate with Dimethyl Carbonate and Ethylene Carbonate from Molecular Dynamics Simulation: Comparison between Non-Polarizable and Polarizable Force Fields. *Mol. Phys.* **2013**, *111*, 277–285.

(222) Kumar, N.; Seminario, J. M. Lithium-Ion Model Behavior in an Ethylene Carbonate Electrolyte Using Molecular Dynamics. *J. Phys. Chem. C* **2016**, *120*, 16322–16332.

(223) Borodin, O.; Smith, G. D. LiTFSI Structure and Transport in Ethylene Carbonate from Molecular Dynamics Simulations. *J. Phys. Chem. B* **2006**, *110*, 4971–4977.

(224) Arslanargin, A.; Powers, A.; Beck, T. L.; Rick, S. W. Models of Ion Solvation Thermodynamics in Ethylene Carbonate and Propylene Carbonate. *J. Phys. Chem. B* **2016**, *120*, 1497–1508.

(225) Vatamanu, J.; Borodin, O.; Smith, G. D. Molecular Dynamics Simulation Studies of the Structure of a Mixed Carbonate/$LiPF_6$ Electrolyte near Graphite Surface as a Function of Electrode Potential. *J. Phys. Chem. C* **2012**, *116*, 1114–1121.

(226) Soetens, J.-C.; Millot, C.; Maigret, B. Molecular Dynamics Simulation of $Li^+BF_4^-$ in Ethylene Carbonate, Propylene Carbonate, and Dimethyl Carbonate Solvents. *J. Phys. Chem. A* **1998**, *102*, 1055–1061.

(227) Park, C.; Kanduč, M.; Chudoba, R.; Ronneburg, A.; Risse, S.; Ballauff, M.; Dzubiella, J. Molecular Simulations of Electrolyte Structure and Dynamics in Lithium−Sulfur Battery Solvents. *J. Power Sources* **2018**, *373*, 70–78.

(228) Jankowski, P.; Dranka, M.; Wieczorek, W.; Johansson, P. TFSI and TDI Anions: Probes for Solvate Ionic Liquid and Disproportionation-Based Lithium Battery Electrolytes. *J. Phys. Chem. Lett.* **2017**, *8*, 3678–3682.

(229) Wahlers, J.; Fulfer, K. D.; Harding, D. P.; Kuroda, D. G.; Kumar, R.; Jorn, R. Solvation Structure and Concentration in Glyme-Based Sodium Electrolytes: A Combined Spectroscopic and Computational Study. *J. Phys. Chem. C* **2016**, *120*, 17949–17959.

(230) Lapidus, S. H.; Rajput, N. N.; Qu, X.; Chapman, K. W.; Persson, K. A.; Chupas, P. J. Solvation Structure and Energetics of Electrolytes for Multivalent Energy Storage. *Phys. Chem. Chem. Phys.* **2014**, *16*, 21941−21945.

(231) Shimizu, K.; Freitas, A. A.; Atkin, R.; Warr, G. G.; FitzGerald, P. A.; Doi, H.; Saito, S.; Ueno, K.; Umebayashi, Y.; Watanabe, M.; et al. Structural and Aggregate Analyses of (Li Salt + Glyme) Mixtures: The Complex Nature of Solvate Ionic Liquids. *Phys. Chem. Chem. Phys.* **2015**, *17*, 22321−22335.

(232) Murphy, T. K.; Callear, S.; Yepuri, N.; Shimizu, K.; Watanabe, M.; Canongia Lopes, J. N.; Darwish, T. G.; Warr, G.; Atkin, R. Bulk Nanostructure of the Prototypical 'Good' and 'Poor' Solvate Ionic Liquids [Li(G4)][TFSI] and [Li(G4)][NO_3]. *Phys. Chem. Chem. Phys.* **2016**, *18*, 17224−17236.

(233) Tsuzuki, S.; Shinoda, W.; Matsugami, M.; Umebayashi, Y.; Ueno, K.; Mandai, T.; Seki, S.; Dokko, K.; Watanabe, M. Structures of [Li(Glyme)]$^+$ Complexes and Their Interactions with Anions in Equimolar Mixtures of Glymes and Li[TFSA]: Analysis by Molecular Dynamics Simulations. *Phys. Chem. Chem. Phys.* **2015**, *17*, 126−129.

(234) Coles, S. W.; Mishin, M.; Perkin, S.; Fedorov, M. V.; Ivaništšev, V. B. The Nanostructure of a Lithium Glyme Solvate Ionic Liquid at Electrified Interfaces. *Phys. Chem. Chem. Phys.* **2017**, *19*, 11004−11010.

(235) Kuritz, N.; Murat, M.; Balaish, M.; Ein-Eli, Y.; Natan, A. PFC and Triglyme for Li−Air Batteries: A Molecular Dynamics Study. *J. Phys. Chem. B* **2016**, *120*, 3370−3377.

(236) Samuel, D.; Steinhauser, C.; Smith, J. G.; Kaufman, A.; Radin, M. D.; Naruse, J.; Hiramatsu, H.; Siegel, D. J. Ion Pairing and Diffusion in Magnesium Electrolytes Based on Magnesium Borohydride. *ACS Appl. Mater. Interfaces* **2017**, *9*, 43755−43766.

(237) Saito, S.; Watanabe, H.; Ueno, K.; Mandai, T.; Seki, S.; Tsuzuki, S.; Kameda, Y.; Dokko, K.; Watanabe, M.; Umebayashi, Y. Li^+ Local Structure in Hydrofluoroether Diluted Li-Glyme Solvate Ionic Liquid. *J. Phys. Chem. B* **2016**, *120*, 3378−3387.

(238) Seo, D. M.; Borodin, O.; Han, S.-D.; Boyle, P. D.; Henderson, W. A. Electrolyte Solvation and Ionic Association II. Acetonitrile-Lithium Salt Mixtures: Highly Dissociated Salts. *J. Electrochem. Soc.* **2012**, *159*, A1489−A1500.

(239) Seo, D. M.; Borodin, O.; Balogh, D.; O'Connell, M.; Ly, Q.; Han, S.-D.; Passerini, S.; Henderson, W. A. Electrolyte Solvation and Ionic Association III. Acetonitrile-Lithium Salt Mixtures−Transport Properties. *J. Electrochem. Soc.* **2013**, *160*, A1061−A1070.

(240) Fujii, K.; Hamano, H.; Doi, H.; Song, X.; Tsuzuki, S.; Hayamizu, K.; Seki, S.; Kameda, Y.; Dokko, K.; Watanabe, M.; et al. Unusual Li^+ Ion Solvation Structure in Bis(Fluorosulfonyl)Amide Based Ionic Liquid. *J. Phys. Chem. C* **2013**, *117*, 19314−19324.

(241) Kubisiak, P.; Eilmes, A. Molecular Dynamics Simulations of Ionic Liquid Based Electrolytes for Na-Ion Batteries: Effects of Force Field. *J. Phys. Chem. B* **2017**, *121*, 9957−9968.

(242) Umebayashi, Y.; Hamano, H.; Seki, S.; Minofar, B.; Fujii, K.; Hayamizu, K.; Tsuzuki, S.; Kameda, Y.; Kohara, S.; Watanabe, M. Liquid Structure of and Li^+ Ion Solvation in Bis-(Trifluoromethanesulfonyl)Amide Based Ionic Liquids Composed of 1-Ethyl-3-Methylimidazolium and N-Methyl-N-Propylpyrrolidinium Cations. *J. Phys. Chem. B* **2011**, *115*, 12179−12191.

(243) Eilmes, A.; Kubisiak, P. Quantum-Chemical and Molecular Dynamics Study of M+[TOTO]− (M = Li, Na, K) Ionic Liquids. *J. Phys. Chem. B* **2013**, *117*, 12583−12592.

(244) Haskins, J. B.; Wu, J. J.; Lawson, J. W. Computational and Experimental Study of Li-Doped Ionic Liquids at Electrified Interfaces. *J. Phys. Chem. C* **2016**, *120*, 11993−12011.

(245) Solano, C. J. F.; Jeremias, S.; Paillard, E.; Beljonne, D.; Lazzaroni, R. A Joint Theoretical/Experimental Study of the Structure, Dynamics, and Li^+ Transport in Bis([Tri]Fluoro[Methane]Sulfonyl)-Imide [T]FSI-Based Ionic Liquids. *J. Chem. Phys.* **2013**, *139*, 034502.

(246) Vatamanu, J.; Vatamanu, M.; Borodin, O.; Bedrov, D. A Comparative Study of Room Temperature Ionic Liquids and Their Organic Solvent Mixtures near Charged Electrodes. *J. Phys.: Condens. Matter* **2016**, *28*, 464002.

(247) Li, Z.; Borodin, O.; Smith, G. D.; Bedrov, D. Effect of Organic Solvents on Li^+ Ion Solvation and Transport in Ionic Liquid

Electrolytes: A Molecular Dynamics Simulation Study. *J. Phys. Chem. B* **2015**, *119*, 3085−3096.

(248) Sun, B.; Mindemark, J.; Morozov, E. V.; Costa, L. T.; Bergman, M.; Johansson, P.; Fang, Y.; Furó, I.; Brandell, D. Ion Transport in Polycarbonate Based Solid Polymer Electrolytes: Experimental and Computational Investigations. *Phys. Chem. Chem. Phys.* **2016**, *18*, 9504−9513.

(249) Savoie, B. M.; Webb, M. A.; Miller, T. F. Enhancing Cation Diffusion and Suppressing Anion Diffusion via Lewis-Acidic Polymer Electrolytes. *J. Phys. Chem. Lett.* **2017**, *8*, 641−646.

(250) Wheatle, B. K.; Keith, J. R.; Mogurampelly, S.; Lynd, N. A.; Ganesan, V. Influence of Dielectric Constant on Ionic Transport in Polyether-Based Electrolytes. *ACS Macro Lett.* **2017**, *6*, 1362−1367.

(251) Shao, Y.; Rajput, N. N.; Hu, J.; Hu, M.; Liu, T.; Wei, Z.; Gu, M.; Deng, X.; Xu, S.; Han, K. S.; et al. Nanocomposite Polymer Electrolyte for Rechargeable Magnesium Batteries. *Nano Energy* **2015**, *12*, 750−759.

(252) Ebadi, M.; Costa, L. T.; Araujo, C. M.; Brandell, D. Modelling the Polymer Electrolyte/Li-Metal Interface by Molecular Dynamics Simulations. *Electrochim. Acta* **2017**, *234*, 43−51.

(253) Diddens, D.; Heuer, A. Lithium Ion Transport Mechanism in Ternary Polymer Electrolyte-Ionic Liquid Mixtures: A Molecular Dynamics Simulation Study. *ACS Macro Lett.* **2013**, *2*, 322−326.

(254) Diddens, D.; Paillard, E.; Heuer, A. Improving the Lithium Ion Transport in Polymer Electrolytes by Functionalized Ionic-Liquid Additives: Simulations and Modeling. *J. Electrochem. Soc.* **2017**, *164*, E3225−E3231.

(255) Chattoraj, J.; Knappe, M.; Heuer, A. Dependence of Ion Dynamics on the Polymer Chain Length in Poly(Ethylene Oxide)-Based Polymer Electrolytes. *J. Phys. Chem. B* **2015**, *119*, 6786−6791.

(256) Diddens, D.; Heuer, A. Simulation Study of the Lithium Ion Transport Mechanism in Ternary Polymer Electrolytes: The Critical Role of the Segmental Mobility. *J. Phys. Chem. B* **2014**, *118*, 1113−1125.

(257) Müller Plathe, F.; van Gunsteren, W. F. Computer Simulation of a Polymer Electrolyte: Lithium Iodide in Amorphous Poly(Ethylene Oxide). *J. Chem. Phys.* **1995**, *103*, 4745−4756.

(258) Borodin, O.; Smith, G. D. Molecular Dynamics Simulations of Poly(Ethylene Oxide)/LiI Melts. 2. Dynamic Properties. *Macromolecules* **2000**, *33*, 2273−2283.

(259) Borodin, O.; Smith, G. D. Mechanism of Ion Transport in Amorphous Poly(Ethylene Oxide)/LiTFSI from Molecular Dynamics Simulations. *Macromolecules* **2006**, *39*, 1620−1629.

(260) Diddens, D.; Heuer, A.; Borodin, O. Understanding the Lithium Transport within a Rouse-Based Model for a PEO/LiTFSI Polymer Electrolyte. *Macromolecules* **2010**, *43*, 2028−2036.

(261) Rajput, N. N.; Murugesan, V.; Shin, Y.; Han, K. S.; Lau, K. C.; Chen, J.; Liu, J.; Curtiss, L. A.; Mueller, K. T.; Persson, K. A. Elucidating the Solvation Structure and Dynamics of Lithium Polysulfides Resulting from Competitive Salt and Solvent Interactions. *Chem. Mater.* **2017**, *29*, 3375−3379.

(262) Wang, F.; Borodin, O.; Gao, T.; Fan, X.; Sun, W.; Han, F.; Faraone, A.; Dura, J. A.; Xu, K.; Wang, C. Highly Reversible Zinc Metal Anode for Aqueous Batteries. *Nat. Mater.* **2018**, *17*, 543−549.

(263) Borodin, O. Polarizable Force Field Development and Molecular Dynamics Simulations of Ionic Liquids. *J. Phys. Chem. B* **2009**, *113*, 11463−11478.

(264) Morrow, T. I.; Maginn, E. J. Molecular Dynamics Study of the Ionic Liquid 1-n-Butyl-3-Methylimidazolium Hexafluorophosphate. *J. Phys. Chem. B* **2002**, *106*, 12807−12813.

(265) Chaban, V. Polarizability versus Mobility: Atomistic Force Field for Ionic Liquids. *Phys. Chem. Chem. Phys.* **2011**, *13*, 16055−16062.

(266) Köddermann, T.; Reith, D.; Ludwig, R. Comparison of Force Fields on the Basis of Various Model Approaches—How To Design the Best Model for the [CnMIM][NTf2] Family of Ionic Liquids. *ChemPhysChem* **2013**, *14*, 3368−3374.

(267) Lassègues, J.-C.; Grondin, J.; Aupetit, C.; Johansson, P. Spectroscopic Identification of the Lithium Ion Transporting Species in LiTFSI-Doped Ionic Liquids. *J. Phys. Chem. A* **2009**, *113*, 305−314.

(268) Aabloo, A.; Thomas, J. Molecular Dynamics Simulation of Lithium Ion Mobility in a PEO Surface. *Solid State Ionics* **2001**, *143*, 83−87.

(269) Brandell, D.; Liivat, A.; Kasemägi, H.; Aabloo, A.; Thomas, J. O. Molecular Dynamics Simulation of the LiPF6·PEO6 Structure. *J. Mater. Chem.* **2005**, *15*, 1422−1428.

(270) Hektor, A.; Klintenberg, M. K.; Aabloo, A.; Thomas, J. O. Molecular Dynamics Simulation of the Effect of a Side Chain on the Dynamics of the Amorphous LiPF6−PEO System. *J. Mater. Chem.* **2003**, *13*, 214−218.

(271) Karo, J.; Brandell, D. A Molecular Dynamics Study of the Influence of Side-Chain Length and Spacing on Lithium Mobility in Non-Crystalline LiPF6·PEOx; X = 10 and 30. *Solid State Ionics* **2009**, *180*, 1272−1284.

(272) Borodin, O.; Smith, G. D. Molecular Dynamics Simulations of Poly(Ethylene Oxide)/LiI Melts. 1. Structural and Conformational Properties. *Macromolecules* **1998**, *31*, 8396−8406.

(273) Brandell, D.; Liivat, A.; Aabloo, A.; Thomas, J. O. Molecular Dynamics Simulation of the Crystalline Short-Chain Polymer System LiPF6·PEO6 (Mw ∼ 1000). *J. Mater. Chem.* **2005**, *15*, 4338−4345.

(274) Balbuena, P. B.; Lamas, E. J.; Wang, Y. Molecular Modeling Studies of Polymer Electrolytes for Power Sources. *Electrochim. Acta* **2005**, *50*, 3788−3795.

(275) Jinnouchi, R.; Okazaki, K. Molecular Dynamics Study of Transport Phenomena in Perfluorosulfonate Ionomer Membranes for Polymer Electrolyte Fuel Cells. *J. Electrochem. Soc.* **2003**, *150*, E66−E73.

(276) Borodin, O.; Smith, G. D.; Jaffe, R. L. Ab Initio Quantum Chemistry and Molecular Dynamics Simulations Studies of LiPF6/Poly(Ethylene Oxide) Interactions. *J. Comput. Chem.* **2001**, *22*, 641−654.

(277) Siqueira, L. J. A.; Ribeiro, M. C. C. Molecular Dynamics Simulation of the Polymer Electrolyte Poly(Ethyleneoxide)/LiClO4. I. Structural Properties. *J. Chem. Phys.* **2005**, *122*, 194911.

(278) Duan, Y.; Halley, J. W.; Curtiss, L.; Redfern, P. Mechanisms of Lithium Transport in Amorphous Polyethylene Oxide. *J. Chem. Phys.* **2005**, *122*, 054702.

(279) Borodin, O.; Smith, G. D. Molecular Dynamics Simulation Study of LiI-Doped Diglyme and Poly(Ethylene Oxide) Solutions. *J. Phys. Chem. B* **2000**, *104*, 8017−8022.

(280) Palma, A.; Pasquarello, A.; Ciccotti, G.; Car, R. Cu++ and Li+ Interaction with Polyethylene Oxide by Ab Initio Molecular Dynamics. *J. Chem. Phys.* **1998**, *108*, 9933−9936.

(281) Dixon, B. G.; Scott Morris, R. Computational Chemistry: Design and Experimental Verification of Pre-Designed Heteropolymer Electrolytes for Rechargeable Lithium Batteries. *J. Power Sources* **2003**, *119−121*, 856−858.

(282) Brandell, D.; Kasemägi, H.; Tamm, T.; Aabloo, A. Molecular Dynamics Modeling the Li-PolystyreneTFSI/PEO Blend. *Solid State Ionics* **2014**, *262*, 769−773.

(283) Kasemägi, H.; Klintenberg, M.; Aabloo, A.; Thomas, J. O. Molecular Dynamics Simulation of the Effect of Adding an Al2O3 Nanoparticle to PEO−LiCl/LiBr/LiI Systems. *J. Mater. Chem.* **2001**, *11*, 3191−3196.

(284) Lu, K.; Rudzinski, J. F.; Noid, W. G.; Milner, S. T.; Maranas, J. K. Scaling Behavior and Local Structure of Ion Aggregates in Single-Ion Conductors. *Soft Matter* **2014**, *10*, 978−989.

(285) Mullinax, J. W.; Noid, W. G. Generalized Yvon-Born-Green Theory for Molecular Systems. *Phys. Rev. Lett.* **2009**, *103*, 198104.

(286) Hall, L. M.; Stevens, M. J.; Frischknecht, A. L. Effect of Polymer Architecture and Ionic Aggregation on the Scattering Peak in Model Ionomers. *Phys. Rev. Lett.* **2011**, *106*, 127801.

(287) Hall, L. M.; Seitz, M. E.; Winey, K. I.; Opper, K. L.; Wagener, K. B.; Stevens, M. J.; Frischknecht, A. L. Ionic Aggregate Structure in Ionomer Melts: Effect of Molecular Architecture on Aggregates and the Ionomer Peak. *J. Am. Chem. Soc.* **2012**, *134*, 574−587.

(288) Hall, L. M.; Stevens, M. J.; Frischknecht, A. L. Dynamics of Model Ionomer Melts of Various Architectures. *Macromolecules* **2012**, *45*, 8097−8108.

(289) Lu, K.; Maranas, J. K.; Milner, S. T. Ion-Mediated Charge Transport in Ionomeric Electrolytes. *Soft Matter* **2016**, *12*, 3943−3954.

(290) Ting, C. L.; Stevens, M. J.; Frischknecht, A. L. Structure and Dynamics of Coarse-Grained Ionomer Melts in an External Electric Field. *Macromolecules* **2015**, *48*, 809−818.

(291) Brandell, D.; Liivat, A.; Aabloo, A.; Thomas, J. O. Conduction Mechanisms in Crystalline LiPF6·PEO6 Doped with SiF62- and SF6. *Chem. Mater.* **2005**, *17*, 3673−3680.

(292) Qin, J.; de Pablo, J. J. Ordering Transition in Salt-Doped Diblock Copolymers. *Macromolecules* **2016**, *49*, 3630−3638.

(293) Nitzan, A.; Ratner, M. A. Conduction in Polymers: Dynamic Disorder Transport. *J. Phys. Chem.* **1994**, *98*, 1765−1775.

(294) Snyder, J. F.; Ratner, M. A.; Shriver, D. F. Polymer Electrolytes and Polyelectrolytes: Monte Carlo Simulations of Thermal Effects on Conduction. *Solid State Ionics* **2002**, *147*, 249−257.

(295) Maitra, A.; Heuer, A. Cation Transport in Polymer Electrolytes: A Microscopic Approach. *Phys. Rev. Lett.* **2007**, *98*, 227802.

(296) Borodin, O.; Smith, G. D.; Geiculescu, O.; Creager, S. E.; Hallac, B.; DesMarteau, D. Li$^+$ Transport in Lithium Sulfonylimide−Oligo(Ethylene Oxide) Ionic Liquids and Oligo(Ethylene Oxide) Doped with LiTFSI. *J. Phys. Chem. B* **2006**, *110*, 24266−24274.

(297) Hanson, B.; Pryamitsyn, V.; Ganesan, V. Mechanisms Underlying Ionic Mobilities in Nanocomposite Polymer Electrolytes. *ACS Macro Lett.* **2013**, *2*, 1001−1005.

(298) Mogurampelly, S.; Ganesan, V. Effect of Nanoparticles on Ion Transport in Polymer Electrolytes. *Macromolecules* **2015**, *48*, 2773−2786.

(299) Webb, M. A.; Savoie, B. M.; Wang, Z.-G.; Miller, T. F., III Chemically Specific Dynamic Bond Percolation Model for Ion Transport in Polymer Electrolytes. *Macromolecules* **2015**, *48*, 7346−7358.

(300) Husch, T.; Yilmazer, N. D.; Balducci, A.; Korth, M. Large-Scale Virtual High-Throughput Screening for the Identification of New Battery Electrolyte Solvents: Computing Infrastructure and Collective Properties. *Phys. Chem. Chem. Phys.* **2015**, *17*, 3394−3401.

(301) Brox, S.; Röser, S.; Husch, T.; Hildebrand, S.; Fromm, O.; Korth, M.; Winter, M.; Cekic Laskovic, I. Alternative Single-Solvent Electrolytes Based on Cyanoesters for Safer Lithium-Ion Batteries. *ChemSusChem* **2016**, *9*, 1704−1711.

(302) Korth, M. Large-Scale Virtual High-Throughput Screening for the Identification of New Battery Electrolyte Solvents: Evaluation of Electronic Structure Theory Methods. *Phys. Chem. Chem. Phys.* **2014**, *16*, 7919−7926.

(303) Husch, T.; Korth, M. Charting the Known Chemical Space for Non-Aqueous Lithium−Air Battery Electrolyte Solvents. *Phys. Chem. Chem. Phys.* **2015**, *17*, 22596−22603.

(304) Jeschke, S.; Johansson, P. Predicting the Solubility of Sulfur: A COSMO-RS-Based Approach to Investigate Electrolytes for Li−S Batteries. *Chem. - Eur. J.* **2017**, *23*, 9130−9136.

(305) Ganesh, P.; Kent, P. R. C.; Jiang, D. Solid−Electrolyte Interphase Formation and Electrolyte Reduction at Li-Ion Battery Graphite Anodes: Insights from First-Principles Molecular Dynamics. *J. Phys. Chem. C* **2012**, *116*, 24476−24481.

(306) Leung, K.; Budzien, J. L. Ab Initio Molecular Dynamics Simulations of the Initial Stages of Solid−Electrolyte Interphase Formation on Lithium Ion Battery Graphitic Anodes. *Phys. Chem. Chem. Phys.* **2010**, *12*, 6583−6586.

(307) Brennan, M. D.; Breedon, M.; Best, A. S.; Morishita, T.; Spencer, M. J. S. Surface Reactions of Ethylene Carbonate and Propylene Carbonate on the Li(001) Surface. *Electrochim. Acta* **2017**, *243*, 320−330.

(308) Leung, K.; Qi, Y.; Zavadil, K. R.; Jung, Y. S.; Dillon, A. C.; Cavanagh, A. S.; Lee, S.-H.; George, S. M. Using Atomic Layer Deposition to Hinder Solvent Decomposition in Lithium Ion Batteries: First-Principles Modeling and Experimental Studies. *J. Am. Chem. Soc.* **2011**, *133*, 14741−14754.

(309) Yu, J.; Balbuena, P. B.; Budzien, J.; Leung, K. Hybrid DFT Functional-Based Static and Molecular Dynamics Studies of Excess Electron in Liquid Ethylene Carbonate. *J. Electrochem. Soc.* **2011**, *158*, A400−A410.

(310) Martinez de la Hoz, J. M.; Leung, K.; Balbuena, P. B. Reduction Mechanisms of Ethylene Carbonate on Si Anodes of Lithium-Ion Batteries: Effects of Degree of Lithiation and Nature of Exposed Surface. *ACS Appl. Mater. Interfaces* **2013**, *5*, 13457−13465.

(311) Moradabadi, A.; Bakhtiari, M.; Kaghazchi, P. Effect of Anode Composition on Solid Electrolyte Interphase Formation. *Electrochim. Acta* **2016**, *213*, 8−13.

(312) McCreery, R. L. Advanced Carbon Electrode Materials for Molecular Electrochemistry. *Chem. Rev.* **2008**, *108*, 2646−2687.

(313) Aurbach, D.; Ein Eli, Y.; Markovsky, B.; Zaban, A.; Luski, S.; Carmeli, Y.; Yamin, H. The Study of Electrolyte Solutions Based on Ethylene and Diethyl Carbonates for Rechargeable Li Batteries II. Graphite Electrodes. *J. Electrochem. Soc.* **1995**, *142*, 2882−2890.

(314) Chen, X.; Hou, T.-Z.; Li, B.; Yan, C.; Zhu, L.; Guan, C.; Cheng, X.-B.; Peng, H.-J.; Huang, J.-Q.; Zhang, Q. Towards Stable Lithium-Sulfur Batteries: Mechanistic Insights into Electrolyte Decomposition on Lithium Metal Anode. *Energy Storage Materials* **2017**, *8*, 194−201.

(315) Camacho-Forero, L. E.; Smith, T. W.; Bertolini, S.; Balbuena, P. B. Reactivity at the Lithium−Metal Anode Surface of Lithium−Sulfur Batteries. *J. Phys. Chem. C* **2015**, *119*, 26828−26839.

(316) Camacho-Forero, L. E.; Smith, T. W.; Balbuena, P. B. Effects of High and Low Salt Concentration in Electrolytes at Lithium−Metal Anode Surfaces. *J. Phys. Chem. C* **2017**, *121*, 182−194.

(317) Sodeyama, K.; Yamada, Y.; Aikawa, K.; Yamada, A.; Tateyama, Y. Sacrificial Anion Reduction Mechanism for Electrochemical Stability Improvement in Highly Concentrated Li-Salt Electrolyte. *J. Phys. Chem. C* **2014**, *118*, 14091−14097.

(318) Piper, D. M.; Evans, T.; Leung, K.; Watkins, T.; Olson, J.; Kim, S. C.; Han, S. S.; Bhat, V.; Oh, K. H.; Buttry, D. A.; et al. Stable Silicon-Ionic Liquid Interface for next-Generation Lithium-Ion Batteries. *Nat. Commun.* **2015**, *6*, 6230.

(319) Yildirim, H.; Haskins, J. B.; Bauschlicher, C. W.; Lawson, J. W. Decomposition of Ionic Liquids at Lithium Interfaces. 1. Ab Initio Molecular Dynamics Simulations. *J. Phys. Chem. C* **2017**, *121*, 28214−28234.

(320) Budi, A.; Basile, A.; Opletal, G.; Hollenkamp, A. F.; Best, A. S.; Rees, R. J.; Bhatt, A. I.; O'Mullane, A. P.; Russo, S. P. Study of the Initial Stage of Solid Electrolyte Interphase Formation upon Chemical Reaction of Lithium Metal and N-Methyl-N-Propyl-Pyrrolidinium-Bis(Fluorosulfonyl)Imide. *J. Phys. Chem. C* **2012**, *116*, 19789−19797.

(321) Bedrov, D.; Smith, G. D.; van Duin, A. C. T. Reactions of Singly-Reduced Ethylene Carbonate in Lithium Battery Electrolytes: A Molecular Dynamics Simulation Study Using the ReaxFF. *J. Phys. Chem. A* **2012**, *116*, 2978−2985.

(322) Islam, M. M.; van Duin, A. C. T. Reductive Decomposition Reactions of Ethylene Carbonate by Explicit Electron Transfer from Lithium: An EReaxFF Molecular Dynamics Study. *J. Phys. Chem. C* **2016**, *120*, 27128−27134.

(323) Yun, K.-S.; Pai, S. J.; Yeo, B. C.; Lee, K.-R.; Kim, S.-J.; Han, S. S. Simulation Protocol for Prediction of a Solid-Electrolyte Interphase on the Silicon-Based Anodes of a Lithium-Ion Battery: ReaxFF Reactive Force Field. *J. Phys. Chem. Lett.* **2017**, *8*, 2812−2818.

(324) Guk, H.; Kim, D.; Choi, S.-H.; Chung, D. H.; Han, S. S. Thermostable Artificial Solid-Electrolyte Interface Layer Covalently Linked to Graphite for Lithium Ion Battery: Molecular Dynamics Simulations. *J. Electrochem. Soc.* **2016**, *163*, A917−A922.

(325) Kim, S.-P.; van Duin, A. C. T.; Shenoy, V. B. Effect of Electrolytes on the Structure and Evolution of the Solid Electrolyte Interphase (SEI) in Li-Ion Batteries: A Molecular Dynamics Study. *J. Power Sources* **2011**, *196*, 8590−8597.

(326) Islam, M. M.; Bryantsev, V. S.; van Duin, A. C. T. ReaxFF Reactive Force Field Simulations on the Influence of Teflon on Electrolyte Decomposition during Li/SWCNT Anode Discharge in Lithium-Sulfur Batteries. *J. Electrochem. Soc.* **2014**, *161*, E3009−E3014.

(327) Pereira-Nabais, C.; Światowska, J.; Chagnes, A.; Ozanam, F.; Gohier, A.; Tran-Van, P.; Cojocaru, C.-S.; Cassir, M.; Marcus, P.

Interphase Chemistry of Si Electrodes Used as Anodes in Li-Ion Batteries. *Appl. Surf. Sci.* **2013**, *266*, 5−16.

(328) Edström, K.; Herstedt, M.; Abraham, D. P. A New Look at the Solid Electrolyte Interphase on Graphite Anodes in Li-Ion Batteries. *J. Power Sources* **2006**, *153*, 380−384.

(329) Peled, E.; Bar Tow, D.; Merson, A.; Gladkich, A.; Burstein, L.; Golodnitsky, D. Composition, Depth Profiles and Lateral Distribution of Materials in the SEI Built on HOPG-TOF SIMS and XPS Studies. *J. Power Sources* **2001**, *97−98*, 52−57.

(330) Lu, M.; Cheng, H.; Yang, Y. A Comparison of Solid Electrolyte Interphase (SEI) on the Artificial Graphite Anode of the Aged and Cycled Commercial Lithium Ion Cells. *Electrochim. Acta* **2008**, *53*, 3539−3546.

(331) Senftle, T. P.; Hong, S.; Islam, M. M.; Kylasa, S. B.; Zheng, Y.; Shin, Y. K.; Junkermeier, C.; Engel-Herbert, R.; Janik, M. J.; Aktulga, H. M.; et al. The ReaxFF Reactive Force-Field: Development, Applications and Future Directions. *npj Comput. Mater.* **2016**, *2*, 15011.

(332) Islam, M. M.; Kolesov, G.; Verstraelen, T.; Kaxiras, E.; van Duin, A. C. T. EReaxFF: A Pseudoclassical Treatment of Explicit Electrons within Reactive Force Field Simulations. *J. Chem. Theory Comput.* **2016**, *12*, 3463−3472.

(333) Cheng, T.; Merinov, B. V.; Morozov, S.; Goddard, W. A. Quantum Mechanics Reactive Dynamics Study of Solid Li-Electrode/Li6PS5Cl-Electrolyte Interface. *ACS Energy Lett.* **2017**, *2*, 1454−1459.

(334) Borodin, O.; Zhuang, G. V.; Ross, P. N.; Xu, K. Molecular Dynamics Simulations and Experimental Study of Lithium Ion Transport in Dilithium Ethylene Dicarbonate. *J. Phys. Chem. C* **2013**, *117*, 7433−7444.

(335) Borodin, O.; Bedrov, D. Interfacial Structure and Dynamics of the Lithium Alkyl Dicarbonate SEI Components in Contact with the Lithium Battery Electrolyte. *J. Phys. Chem. C* **2014**, *118*, 18362−18371.

(336) Bedrov, D.; Borodin, O.; Hooper, J. B. Li$^+$ Transport and Mechanical Properties of Model Solid Electrolyte Interphases (SEI): Insight from Atomistic Molecular Dynamics Simulations. *J. Phys. Chem. C* **2017**, *121*, 16098−16109.

(337) Tasaki, K. Solvent Decompositions and Physical Properties of Decomposition Compounds in Li-Ion Battery Electrolytes Studied by DFT Calculations and Molecular Dynamics Simulations. *J. Phys. Chem. B* **2005**, *109*, 2920−2933.

(338) Abe, T.; Kawabata, N.; Mizutani, Y.; Inaba, M.; Ogumi, Z. Correlation Between Cointercalation of Solvents and Electrochemical Intercalation of Lithium into Graphite in Propylene Carbonate Solution. *J. Electrochem. Soc.* **2003**, *150*, A257−A261.

(339) Jeong, S.-K.; Inaba, M.; Mogi, R.; Iriyama, Y.; Abe, T.; Ogumi, Z. Surface Film Formation on a Graphite Negative Electrode in Lithium-Ion Batteries: Atomic Force Microscopy Study on the Effects of Film-Forming Additives in Propylene Carbonate Solutions. *Langmuir* **2001**, *17*, 8281−8286.

(340) Jeong, S.-K.; Inaba, M.; Iriyama, Y.; Abe, T.; Ogumi, Z. AFM Study of Surface Film Formation on a Composite Graphite Electrode in Lithium-Ion Batteries. *J. Power Sources* **2003**, *119−121*, 555−560.

(341) Jorn, R.; Kumar, R.; Abraham, D. P.; Voth, G. A. Atomistic Modeling of the Electrode−Electrolyte Interface in Li-Ion Energy Storage Systems: Electrolyte Structuring. *J. Phys. Chem. C* **2013**, *117*, 3747−3761.

(342) Takenaka, N.; Suzuki, Y.; Sakai, H.; Nagaoka, M. On Electrolyte-Dependent Formation of Solid Electrolyte Interphase Film in Lithium-Ion Batteries: Strong Sensitivity to Small Structural Difference of Electrolyte Molecules. *J. Phys. Chem. C* **2014**, *118*, 10874−10882.

(343) Takenaka, N.; Sakai, H.; Suzuki, Y.; Uppula, P.; Nagaoka, M. A Computational Chemical Insight into Microscopic Additive Effect on Solid Electrolyte Interphase Film Formation in Sodium-Ion Batteries: Suppression of Unstable Film Growth by Intact Fluoroethylene Carbonate. *J. Phys. Chem. C* **2015**, *119*, 18046−18055.

(344) Methekar, R. N.; Northrop, P. W. C.; Chen, K.; Braatz, R. D.; Subramanian, V. R. Kinetic Monte Carlo Simulation of Surface Heterogeneity in Graphite Anodes for Lithium-Ion Batteries: Passive Layer Formation. *J. Electrochem. Soc.* **2011**, *158*, A363−A370.

(345) Hao, F.; Liu, Z.; Balbuena, P. B.; Mukherjee, P. P. Mesoscale Elucidation of Solid Electrolyte Interphase Layer Formation in Li-Ion Battery Anode. *J. Phys. Chem. C* **2017**, *121*, 26233−26240.

(346) Röder, F.; Braatz, R. D.; Krewer, U. Multi-Scale Simulation of Heterogeneous Surface Film Growth Mechanisms in Lithium-Ion Batteries. *J. Electrochem. Soc.* **2017**, *164*, E3335−E3344.

(347) Shinagawa, C.; Ushiyama, H.; Yamashita, K. Multiscale Simulations for Lithium-Ion Batteries: SEI Film Growth and Capacity Fading. *J. Electrochem. Soc.* **2017**, *164*, A3018−A3024.

(348) Colclasure, A. M.; Smith, K. A.; Kee, R. J. Modeling Detailed Chemistry and Transport for Solid-Electrolyte-Interface (SEI) Films in Li−Ion Batteries. *Electrochim. Acta* **2011**, *58*, 33−43.

(349) Christensen, J.; Newman, J. A Mathematical Model for the Lithium-Ion Negative Electrode Solid Electrolyte Interphase. *J. Electrochem. Soc.* **2004**, *151*, A1977−A1988.

(350) Legrand, N.; Raël, S.; Knosp, B.; Hinaje, M.; Desprez, P.; Lapicque, F. Including Double-Layer Capacitance in Lithium-Ion Battery Mathematical Models. *J. Power Sources* **2014**, *251*, 370−378.

(351) Srivastav, S.; Xu, C.; Edström, K.; Gustafsson, T.; Brandell, D. Modelling the Morphological Background to Capacity Fade in Si-Based Lithium-Ion Batteries. *Electrochim. Acta* **2017**, *258*, 755−763.

(352) Pinson, M. B.; Bazant, M. Z. Theory of SEI Formation in Rechargeable Batteries: Capacity Fade, Accelerated Aging and Lifetime Prediction. *J. Electrochem. Soc.* **2013**, *160*, A243−A250.

(353) Lawder, M. T.; Northrop, P. W. C.; Subramanian, V. R. Model-Based SEI Layer Growth and Capacity Fade Analysis for EV and PHEV Batteries and Drive Cycles. *J. Electrochem. Soc.* **2014**, *161*, A2099−A2108.

(354) Spotnitz, R. Simulation of Capacity Fade in Lithium-Ion Batteries. *J. Power Sources* **2003**, *113*, 72−80.

(355) Ramadass, P.; Haran, B.; White, R.; Popov, B. N. Mathematical Modeling of the Capacity Fade of Li-Ion Cells. *J. Power Sources* **2003**, *123*, 230−240.

(356) Liaw, B. Y.; Jungst, R. G.; Nagasubramanian, G.; Case, H. L.; Doughty, D. H. Modeling Capacity Fade in Lithium-Ion Cells. *J. Power Sources* **2005**, *140*, 157−161.

(357) Ning, G.; Popov, B. N. Cycle Life Modeling of Lithium-Ion Batteries. *J. Electrochem. Soc.* **2004**, *151*, A1584−A1591.

(358) Safari, M.; Morcrette, M.; Teyssot, A.; Delacourt, C. Multimodal Physics-Based Aging Model for Life Prediction of Li-Ion Batteries. *J. Electrochem. Soc.* **2009**, *156*, A145−A153.

(359) Trask, S. E.; Li, Y.; Kubal, J. J.; Bettge, M.; Polzin, B. J.; Zhu, Y.; Jansen, A. N.; Abraham, D. P. From Coin Cells to 400 MAh Pouch Cells: Enhancing Performance of High-Capacity Lithium-Ion Cells via Modifications in Electrode Constitution and Fabrication. *J. Power Sources* **2014**, *259*, 233−244.

(360) Dargaville, S.; Farrell, T. W. Predicting Active Material Utilization in LiFePO$_4$ Electrodes Using a Multiscale Mathematical Model. *J. Electrochem. Soc.* **2010**, *157*, A830−A840.

(361) Song, J.; Bazant, M. Z. Effects of Nanoparticle Geometry and Size Distribution on Diffusion Impedance of Battery Electrodes. *J. Electrochem. Soc.* **2013**, *160*, A15−A24.

(362) Hutzenlaub, T.; Thiele, S.; Paust, N.; Spotnitz, R.; Zengerle, R.; Walchshofer, C. Three-Dimensional Electrochemical Li-Ion Battery Modelling Featuring a Focused Ion-Beam/Scanning Electron Microscopy Based Three-Phase Reconstruction of a LiCoO$_2$ Cathode. *Electrochim. Acta* **2014**, *115*, 131−139.

(363) Newman, J.; Thomas-Alyea, K. E. *Electrochemical Systems*, 3rd ed.; Wiley-Interscience: Hoboken, N.J, 2004.

(364) Allain, H.; Van Weelderen, R.; Baudouy, B.; Quintard, M.; Prat, M.; Soulaine, C. Investigation of Suitability of the Method of Volume Averaging for the Study of Heat Transfer in Superconducting Accelerator Magnet Cooled by Superfluid Helium. *Cryogenics* **2013**, *53*, 128−134.

(365) Lai, W.; Ciucci, F. Mathematical Modeling of Porous Battery Electrodes—Revisit of Newman's Model. *Electrochim. Acta* **2011**, *56*, 4369−4377.

(366) Huang, J.; Li, Z.; Zhang, J.; Song, S.; Lou, Z.; Wu, N. An Analytical Three-Scale Impedance Model for Porous Electrode with

Agglomerates in Lithium-Ion Batteries. *J. Electrochem. Soc.* **2015**, *162*, A585–A595.

(367) Knehr, K. W.; Brady, N. W.; Lininger, C. N.; Cama, C. A.; Bock, D. C.; Lin, Z.; Marschilok, A. C.; Takeuchi, K. J.; Takeuchi, E. S.; West, A. C. Mesoscale Transport in Magnetite Electrodes for Lithium-Ion Batteries. *ECS Trans.* **2015**, *69*, 7–19.

(368) Chadha, T. S.; Suthar, B.; Rife, D.; Subramanian, V. R.; Biswas, P. Model Based Analysis of One-Dimensional Oriented Lithium-Ion Battery Electrodes. *J. Electrochem. Soc.* **2017**, *164*, E3114–E3121.

(369) Gully, A.; Liu, H.; Srinivasan, S.; Sethurajan, A. K.; Schougaard, S.; Protas, B. Effective Transport Properties of Porous Electrochemical Materials — A Homogenization Approach. *J. Electrochem. Soc.* **2014**, *161*, E3066–E3077.

(370) Gupta, A.; Seo, J. H.; Zhang, X.; Du, W.; Sastry, A. M.; Shyy, W. Effective Transport Properties of LiMn2O4 Electrode via Particle-Scale Modeling. *J. Electrochem. Soc.* **2011**, *158*, A487–A497.

(371) Stephenson, D. E.; Walker, B. C.; Skelton, C. B.; Gorzkowski, E. P.; Rowenhorst, D. J.; Wheeler, D. R. Modeling 3D Microstructure and Ion Transport in Porous Li-Ion Battery Electrodes. *J. Electrochem. Soc.* **2011**, *158*, A781–A789.

(372) Lee, S.; Sastry, A. M.; Park, J. Study on Microstructures of Electrodes in Lithium-Ion Batteries Using Variational Multi-Scale Enrichment. *J. Power Sources* **2016**, *315*, 96–110.

(373) Thangavel, V.; Xue, K.-H.; Mammeri, Y.; Quiroga, M.; Mastouri, A.; Guéry, C.; Johansson, P.; Morcrette, M.; Franco, A. A. A Microstructurally Resolved Model for Li-S Batteries Assessing the Impact of the Cathode Design on the Discharge Performance. *J. Electrochem. Soc.* **2016**, *163*, A2817–A2829.

(374) Franco, A. A.; Xue, K.-H. Carbon-Based Electrodes for Lithium Air Batteries: Scientific and Technological Challenges from a Modeling Perspective. *ECS J. Solid State Sci. Technol.* **2013**, *2*, M3084–M3100.

(375) Albertus, P.; Girishkumar, G.; McCloskey, B.; Sánchez-Carrera, R. S.; Kozinsky, B.; Christensen, J.; Luntz, A. C. Identifying Capacity Limitations in the Li/Oxygen Battery Using Experiments and Modeling. *J. Electrochem. Soc.* **2011**, *158*, A343–A351.

(376) Sandhu, S. S.; Fellner, J. P.; Brutchen, G. W. Diffusion-Limited Model for a Lithium/Air Battery with an Organic Electrolyte. *J. Power Sources* **2007**, *164*, 365–371.

(377) Andrei, P.; Zheng, J. P.; Hendrickson, M.; Plichta, E. J. Some Possible Approaches for Improving the Energy Density of Li-Air Batteries. *J. Electrochem. Soc.* **2010**, *157*, A1287–A1295.

(378) Wang, Y. Modeling Discharge Deposit Formation and Its Effect on Lithium-Air Battery Performance. *Electrochim. Acta* **2012**, *75*, 239–246.

(379) Li, X.; Faghri, A. Optimization of the Cathode Structure of Lithium-Air Batteries Based on a Two-Dimensional, Transient, Non-Isothermal Model. *J. Electrochem. Soc.* **2012**, *159*, A1747–A1754.

(380) Neidhardt, J. P.; Fronczek, D. N.; Jahnke, T.; Danner, T.; Horstmann, B.; Bessler, W. G. A Flexible Framework for Modeling Multiple Solid, Liquid and Gaseous Phases in Batteries and Fuel Cells. *J. Electrochem. Soc.* **2012**, *159*, A1528–A1542.

(381) Nimon, V. Y.; Visco, S. J.; De Jonghe, L. C.; Volfkovich, Y. M.; Bograchev, D. A. Modeling and Experimental Study of Porous Carbon Cathodes in Li-O₂ Cells with Non-Aqueous Electrolyte. *ECS Electrochem. Lett.* **2013**, *2*, A33–A35.

(382) Xue, K.-H.; Nguyen, T.-K.; Franco, A. A. Impact of the Cathode Microstructure on the Discharge Performance of Lithium Air Batteries: A Multiscale Model. *J. Electrochem. Soc.* **2014**, *161*, E3028–E3035.

(383) Bevara, V.; Andrei, P. Changing the Cathode Microstructure to Improve the Capacity of Li-Air Batteries: Theoretical Predictions. *J. Electrochem. Soc.* **2014**, *161*, A2068–A2079.

(384) Olivares-Marín, M.; Palomino, P.; Enciso, E.; Tonti, D. Simple Method to Relate Experimental Pore Size Distribution and Discharge Capacity in Cathodes for Li/O₂ Batteries. *J. Phys. Chem. C* **2014**, *118*, 20772–20783.

(385) Xue, K.-H.; McTurk, E.; Johnson, L.; Bruce, P. G.; Franco, A. A. A Comprehensive Model for Non-Aqueous Lithium Air Batteries Involving Different Reaction Mechanisms. *J. Electrochem. Soc.* **2015**, *162*, A614–A621.

(386) Du, W.; Xue, N.; Shyy, W.; Martins, J. R. R. A. A Surrogate-Based Multi-Scale Model for Mass Transport and Electrochemical Kinetics in Lithium-Ion Battery Electrodes. *J. Electrochem. Soc.* **2014**, *161*, E3086–E3096.

(387) Salvadori, A.; Bosco, E.; Grazioli, D. A Computational Homogenization Approach for Li-Ion Battery Cells: Part 1 — Formulation. *J. Mech. Phys. Solids* **2014**, *65*, 114–137.

(388) Salvadori, A.; Grazioli, D.; Geers, M. G. D. Governing Equations for a Two-Scale Analysis of Li-Ion Battery Cells. *Int. J. Solids Struct.* **2015**, *59*, 90–109.

(389) Wieser, C.; Prill, T.; Schladitz, K. Multiscale Simulation Process and Application to Additives in Porous Composite Battery Electrodes. *J. Power Sources* **2015**, *277*, 64–75.

(390) Wiedemann, A. H.; Goldin, G. M.; Barnett, S. A.; Zhu, H.; Kee, R. J. Effects of Three-Dimensional Cathode Microstructure on the Performance of Lithium-Ion Battery Cathodes. *Electrochim. Acta* **2013**, *88*, 580–588.

(391) Danner, T.; Singh, M.; Hein, S.; Kaiser, J.; Hahn, H.; Latz, A. Thick Electrodes for Li-Ion Batteries: A Model Based Analysis. *J. Power Sources* **2016**, *334*, 191–201.

(392) GeoDict. https://www.math2market.com/ (accessed Sept 18, 2018).

(393) Dysart, A. D.; Burgos, J. C.; Mistry, A.; Chen, C.-F.; Liu, Z.; Hong, C. N.; Balbuena, P. B.; Mukherjee, P. P.; Pol, V. G. Towards Next Generation Lithium-Sulfur Batteries: Non-Conventional Carbon Compartments/Sulfur Electrodes and Multi-Scale Analysis. *J. Electrochem. Soc.* **2016**, *163*, A730–A741.

(394) Barai, P.; Mistry, A.; Mukherjee, P. P. Poromechanical Effect in the Lithium—Sulfur Battery Cathode. *Extreme Mech. Lett.* **2016**, *9*, 359–370.

(395) Chen, C.-F.; Mistry, A.; Mukherjee, P. P. Probing Impedance and Microstructure Evolution in Lithium—Sulfur Battery Electrodes. *J. Phys. Chem. C* **2017**, *121*, 21206–21216.

(396) Bao, J.; Xu, W.; Bhattacharya, P.; Stewart, M.; Zhang, J.-G.; Pan, W. Discharge Performance of Li—O₂ Batteries Using a Multiscale Modeling Approach. *J. Phys. Chem. C* **2015**, *119*, 14851–14860.

(397) Torayev, A.; Rucci, A.; Magusin, P. C. M. M.; Demortière, A.; De Andrade, V.; Grey, C. P.; Merlet, C.; Franco, A. A. Stochasticity of Pores Interconnectivity in Li—O₂ Batteries and Its Impact on the Variations in Electrochemical Performance. *J. Phys. Chem. Lett.* **2018**, *9*, 791–797.

(398) Silin, D.; Patzek, T. Pore Space Morphology Analysis Using Maximal Inscribed Spheres. *Phys. A* **2006**, *371*, 336–360.

(399) Shim, J.; Striebel, K. A. Effect of Electrode Density on Cycle Performance and Irreversible Capacity Loss for Natural Graphite Anode in Lithium-Ion Batteries. *J. Power Sources* **2003**, *119–121*, 934–937.

(400) Zhu, M.; Park, J.; Sastry, A. M. Particle Interaction and Aggregation in Cathode Material of Li-Ion Batteries: A Numerical Study. *J. Electrochem. Soc.* **2011**, *158*, A1155–A1159.

(401) Cerbelaud, M.; Lestriez, B.; Guyomard, D.; Videcoq, A.; Ferrando, R. Brownian Dynamics Simulations of Colloidal Suspensions Containing Polymers as Precursors of Composite Electrodes for Lithium Batteries. *Langmuir* **2012**, *28*, 10713–10724.

(402) Cerbelaud, M.; Lestriez, B.; Ferrando, R.; Videcoq, A.; Richard-Plouet, M.; Teresa Caldes, M.; Guyomard, D. Numerical and Experimental Study of Suspensions Containing Carbon Blacks Used as Conductive Additives in Composite Electrodes for Lithium Batteries. *Langmuir* **2014**, *30*, 2660–2669.

(403) Cerbelaud, M.; Lestriez, B.; Videcoq, A.; Ferrando, R.; Guyomard, D. Understanding the Structure of Electrodes in Li-Ion Batteries: A Numerical Study. *J. Electrochem. Soc.* **2015**, *162*, A1485–A1492.

(404) Smith, K. C.; Mukherjee, P. P.; Fisher, T. S. Columnar Order in Jammed LiFePO₄ Cathodes: Ion Transport Catastrophe and Its Mitigation. *Phys. Chem. Chem. Phys.* **2012**, *14*, 7040–7050.

(405) Liu, Z.; Mukherjee, P. P. Microstructure Evolution in Lithium-Ion Battery Electrode Processing. *J. Electrochem. Soc.* **2014**, *161*, E3248–E3258.

(406) Stershic, A. J.; Simunovic, S.; Nanda, J. Modeling the Evolution of Lithium-Ion Particle Contact Distributions Using a Fabric Tensor Approach. *J. Power Sources* **2015**, *297*, 540−550.

(407) Forouzan, M. M.; Chao, C.-W.; Bustamante, D.; Mazzeo, B. A.; Wheeler, D. R. Experiment and Simulation of the Fabrication Process of Lithium-Ion Battery Cathodes for Determining Microstructure and Mechanical Properties. *J. Power Sources* **2016**, *312*, 172−183.

(408) Nelson, G. J.; Ausderau, L. J.; Shin, S.; Buckley, J. R.; Mistry, A.; Mukherjee, P. P.; De Andrade, V. Transport-Geometry Interactions in Li-Ion Cathode Materials Imaged Using X-Ray Nanotomography. *J. Electrochem. Soc.* **2017**, *164*, A1412−A1424.

(409) Ngandjong, A. C.; Rucci, A.; Maiza, M.; Shukla, G.; Vazquez-Arenas, J.; Franco, A. A. Multiscale Simulation Platform Linking Lithium Ion Battery Electrode Fabrication Process with Performance at the Cell Level. *J. Phys. Chem. Lett.* **2017**, *8*, 5966−5972.

(410) Bruggeman, D. a. G. Berechnung verschiedener physikalischer Konstanten von heterogenen Substanzen. I. Dielektrizitätskonstanten und Leitfähigkeiten der Mischkörper aus isotropen Substanzen. *Ann. Phys.* **1935**, *416*, 636−664.

(411) Miranda, D.; Costa, C. M.; Almeida, A. M.; Lanceros-Méndez, S. Modeling Separator Membranes Physical Characteristics for Optimized Lithium Ion Battery Performance. *Solid State Ionics* **2015**, *278*, 78−84.

(412) Xiao, X.; Wu, W.; Huang, X. A Multi-Scale Approach for the Stress Analysis of Polymeric Separators in a Lithium-Ion Battery. *J. Power Sources* **2010**, *195*, 7649−7660.

(413) Shi, D.; Xiao, X.; Huang, X.; Kia, H. Modeling Stresses in the Separator of a Pouch Lithium-Ion Cell. *J. Power Sources* **2011**, *196*, 8129−8139.

(414) Bernardi, D.; Pawlikowski, E.; Newman, J. A General Energy Balance for Battery Systems. *J. Electrochem. Soc.* **1985**, *132*, 5−12.

(415) Guo, M.; White, R. E. A Distributed Thermal Model for a Li-Ion Electrode Plate Pair. *J. Power Sources* **2013**, *221*, 334−344.

(416) Saw, L. H.; Ye, Y.; Tay, A. A. O. Electrochemical−Thermal Analysis of 18650 Lithium Iron Phosphate Cell. *Energy Convers. Manage.* **2013**, *75*, 162−174.

(417) McCleary, D. A. H.; Meyers, J. P.; Kim, B. Three-Dimensional Modeling of Electrochemical Performance and Heat Generation of Spirally and Prismatically Wound Lithium-Ion Batteries. *J. Electrochem. Soc.* **2013**, *160*, A1931−A1943.

(418) Christensen, J.; Cook, D.; Albertus, P. An Efficient Parallelizable 3D Thermoelectrochemical Model of a Li-Ion Cell. *J. Electrochem. Soc.* **2013**, *160*, A2258−A2267.

(419) Tourani, A.; White, P.; Ivey, P. A Multi Scale Multi-Dimensional Thermo Electrochemical Modelling of High Capacity Lithium-Ion Cells. *J. Power Sources* **2014**, *255*, 360−367.

(420) Kim, G.-H.; Smith, K.; Lawrence-Simon, J.; Yang, C. Efficient and Extensible Quasi-Explicit Modular Nonlinear Multiscale Battery Model: GH-MSMD. *J. Electrochem. Soc.* **2017**, *164*, A1076−A1088.

(421) Fan, G.; Pan, K.; Storti, G. L.; Canova, M.; Marcicki, J.; Yang, X. G. A Reduced-Order Multi-Scale, Multi-Dimensional Model for Performance Prediction of Large-Format Li-Ion Cells. *J. Electrochem. Soc.* **2017**, *164*, A252−A264.

(422) Mortazavi, B.; Yang, H.; Mohebbi, F.; Cuniberti, G.; Rabczuk, T. Graphene or H-BN Paraffin Composite Structures for the Thermal Management of Li-Ion Batteries: A Multiscale Investigation. *Appl. Energy* **2017**, *202*, 323−334.

(423) Allu, S.; Kalnaus, S.; Elwasif, W.; Simunovic, S.; Turner, J. A.; Pannala, S. A New Open Computational Framework for Highly-Resolved Coupled Three-Dimensional Multiphysics Simulations of Li-Ion Cells. *J. Power Sources* **2014**, *246*, 876−886.

(424) Turner, J.; Allu, S.; Berrill, M.; Elwasif, W.; Kalnaus, S.; Kumar, A.; Lebrun-Grandie, D.; Pannala, S.; Simunovic, S. Safer Batteries through Coupled Multiscale Modeling. *Procedia Comput. Sci.* **2015**, *51*, 1168−1177.

(425) Latz, A.; Zausch, J. Multiscale Modeling of Lithium Ion Batteries: Thermal Aspects. *Beilstein J. Nanotechnol.* **2015**, *6*, 987−1007.

(426) Ohlberger, M.; Rave, S.; Schindler, F. Model Reduction for Multiscale Lithium-Ion Battery Simulation. In *Numerical Mathematics and Advanced Applications ENUMATH 2015*; Karasözen, B., Manguoğlu, M., Tezer-Sezgin, M., Göktepe, S., Uğur, Ö., Eds.; Lecture Notes in Computational Science and Engineering; Springer International Publishing, 2016; pp 317−331.

(427) Zhao, W.; Luo, G.; Wang, C.-Y. Modeling Nail Penetration Process in Large-Format Li-Ion Cells. *J. Electrochem. Soc.* **2015**, *162*, A207−A217.

(428) Priimägi, P.; Kasemägi, H.; Aabloo, A.; Brandell, D.; Zadin, V. Thermal Simulations of Polymer Electrolyte 3D Li-Microbatteries. *Electrochim. Acta* **2017**, *244*, 129−138.

(429) Kupper, C.; Bessler, W. G. Multi-Scale Thermo-Electrochemical Modeling of Performance and Aging of a LiFePO$_4$/Graphite Lithium-Ion Cell. *J. Electrochem. Soc.* **2017**, *164*, A304−A320.

(430) Wu, B.; Lu, W. A Battery Model That Fully Couples Mechanics and Electrochemistry at Both Particle and Electrode Levels by Incorporation of Particle Interaction. *J. Power Sources* **2017**, *360*, 360−372.

(431) Zhang, C.; Santhanagopalan, S.; Sprague, M. A.; Pesaran, A. A. A Representative-Sandwich Model for Simultaneously Coupled Mechanical-Electrical-Thermal Simulation of a Lithium-Ion Cell under Quasi-Static Indentation Tests. *J. Power Sources* **2015**, *298*, 309−321.

(432) Gödel, K. Über formal unentscheidbare Sätze der Principia Mathematica und verwandter Systeme I. *Monatsh. f. Mathematik und Physik* **1931**, *38*, 173−198.

(433) Quiroga, M. A.; Xue, K.-H.; Nguyen, T.-K.; Tułodziecki, M.; Huang, H.; Franco, A. A. A Multiscale Model of Electrochemical Double Layers in Energy Conversion and Storage Devices. *J. Electrochem. Soc.* **2014**, *161*, E3302−E3310.

(434) Franco, A. A. HELIS European Project. *Progress meeting presentation*, Bordeaux, France, February 6, 2018.

(435) Malek, K.; Maine, E.; McCarthy, I. P. A Typology of Clean Technology Commercialization Accelerators. *J. Eng. Technol. Manage.* **2014**, *32*, 26−39.